INTERFACIAL PROPERTIES AND PHASE BEHAVIOUR OF AN IONIC MICROEMULSION SYSTEM

Grenslaag eigenschappen en fasegedrag van een ionisch micro-emulsie systeem

(met een samenvatting in het Nederlands)

PROEFSCHRIFT

Ter verkrijging van de graad van doctor aan de Universiteit Utrecht, op gezag van de Rector Magnificus prof.dr. J.A. van Ginkel, in gevolge het besluit van het College van Dekanen in het openbaar te verdedigen op maandag 22 november 1993 des middags te 4.15 uur.

door

Willem Kornelis Kegel
Geboren op 17 januari 1961 te Hilversum

promotor: prof. dr. H.N.W.Lekkerkerker
Hoogleraar Fysische Scheikunde aan de Universiteit Utrecht

The investigations described in this thesis are part of the research program of the Netherlands Foundation for Chemical Research (SON), with financial support from the Netherlands Organization for Scientific Research (NWO).

CIP-GEGEVENS KONINKLIJKE BIBLIOTHEEK, DEN HAAG

Kegel, Willem Kornelis

Interfacial properties and phase behaviour of an ionic microemulsion system / Willem Kornelis Kegel, - Utrecht;
Universiteit Utrecht, Faculteit Scheikunde
Proefschrift Universiteit Utrecht. - Met samenvatting in het Nederlands.
ISBN 90-393-0199-9
Trefw.: emulsies ; fasegedrag / oppervlakchemie.

Een kentering. Loerend, angstig, vol hoop sluipt het antwoord om de vraag heen, zoekt wanhopig in haar ontoegankelijk gezicht, volgt haar op de onzinnigste, dat wil zeggen zich van het antwoord zo ver mogelijk verwijderende wegen.

Franz Kafka, Huwelijksvoorbereidingen op het land.

-Chapter 2 is reprinted from *Langmuir* **9**, 252, (1993).

-Part of Chapter 5 is published in *Colloids and Surfaces* **A76**, 241 (1993).

-Chapter 5 is accepted for publication in *The Journal of Physical Chemistry*.

-Chapter 6 is submitted to *Europhysics Letters*.

-Chapters 3 and 4 will be submitted.

Contents

CHAPTER 1

GENERAL INTRODUCTION

1.1 Introduction.

Mixtures of water and a hydrocarbon fluid ('oil') are not thermodynamically stable. Although they may be dispersed into one another leading to course emulsions, the system sooner or later seperates into the constituent liquids. The underlying reason for this instability is the large positive interfacial free energy of the dispersed system which decreases by reduction of the interfacial area. Hoar and Schulman [1] in 1943 for the first time described dispersions of water in oil and oil in water forming spontaneously upon the addition of surface active agents (surfactants or amphiphiles). These dispersions are slightly opalescent (blue) indicating the presence of structures with length scales that are considerably larger than molecular dimensions but much smaller than the wavelength of visible light. Because of these length scales, these systems are nowadays commonly referred to as microemulsions. It is generally accepted that the stability of microemulsions is due to the adsorption of surfactant(s) at the extensive oil-water interface so that the interfacial tension γ is reduced several orders of magnitude. Under this condition the (still positive) interfacial free energy γA (with A the area of the interface) is compensated by the negative free energy of mixing being of order k_BT (k_B is Boltzmann's constant and T is the absolute temperature) per microemulsion droplet. For a system of spherical droplets with radius R

$$4\pi R^2\gamma \cong k_BT \qquad (1).$$

Experimentally it is found that R is of order 10nm implying that γ is of order 0.01mN/m. This is indeed very small compared to the interfacial tension of oil and water without added surfactant being approximately 50mN/m.

In many cases the critical micelle concentration or the solubility limit of a surfactant is reached before the interfacial tension is low enough to permit microemulsion formation. Addition of a cosurfactant of a different nature (usually an alcohol) then lowers the interfacial tension further.

Water-oil-surfactant(s) systems do not only form isotropic dispersions of droplets. Many other structures are encountered experimentally, depending on the concentrations of the constituent parts and the temperature (for reviews see e.g. [6,7]). These structures range from bicontinuous at low surfactant concentrations (up to a few weight percent) to hexagonal, cubic and lamellar liquid crystalline at higher concentrations.

1.2 Theories of microemulsion phase behaviour.

In the last decade considerable progress has been made in understanding the surprisingly rich phase behaviour of oil-water-surfactant systems. Three different approaches to this problem can be distinguished that differ in their choice of the basic length and energy scales [8]: microscopic theories, Ginzburg-Landau theories and phenomenological models. We briefly discuss them below.

In microscopic models [9-14] the oil, water and amphiphile molecules are described by statistical objects with little or no internal structure. Interactions are quantified by microscopic parameters. In these microscopic theories either the language of an Ising model or of a lattice model of an oil-water-amphiphile solution is used. Interactions are attractive between polar entities (water and the amphiphilic head group) and between non-polar entities (oil and the surfactant tails) and repulsive between polar and non-polar objects. Although many details are different in these models, they all allow to study bulk phase behaviour, the structure of the interfaces, their tensions and the associated wetting properties. Moreover structure factors can be calculated and the real space structure of various phases can be examined by Monte Carlo simulation. As this approach starts from the molecular level, it is possible to study the progression from 'weak' to 'strong' amphiphilic systems (i.e. systems in which the affinity of the amphiphile for the oil-water interface is weak and strong, respectively) and to observe the above mentioned properties.

In Ginzburg-Landau theories the starting point is an expansion of the free energy in powers of order parameters. This free energy is usually obtained from symmetry arguments once the choice of order parameters to be employed to describe the system has been made [15,16]. The basic variables in Ginzburg-Landau theories (the spatially varying order parameter fields) are defined at some mesoscopic length scale being large compared to a molecular

scale and small compared to macroscopic lengths. These models depend upon (unknown) coefficients in the free energy expansion rather than microscopic interaction parameters. The advantage of this approach is that largely analytical analysis is permitted.

As shown by Teubner and Strey [17] the structure factor of a microemulsion is easily calculated from a single order parameter expansion of the free energy. This structure factor depends upon 3 expansion parameters and describes experimental Small Angle Neutron Scattering and Small Angle X-ray Scattering results very well. In order to describe generic phase behaviour and to distinguish ordered- from disordered phases, an expansion of the free energy in three order parameters is required [8].

In phenomenological theories monolayers at the oil water interface are considered as incompressible 2 dimensional fluids. This is probably a good approximation for 'strong' amphiphilic systems where the surfactant concentration in solution becomes extremely small and the monolayers are saturated. These kind of systems are hard to handle with the above mentioned approaches as the calculation of very large concentration differences is required. Moreover the relevant energy scale (i.e. the scale at which fluctuation effects can be observed) is certainly not the molecular scale as the free energy to remove a surfactant molecule from a monolayer in these systems is much larger than the thermal energy. The basic energy scale as used in this approach is the energy required to deform a surfactant sheet. The local curvature free energy per unit area arising from this deformation is written as an expansion in powers of the local curvatures. The integrated curvature free energy depends upon the expansion parameters being the bending elastic moduli and the spontaneous curvature [18]. The analysis of a very simple 'random surface model' based upon a Hamiltonian arising from the curvature free energy only, already leads to several distinct phases [19]. In other phenomenological models, the total free energy of the system is written as the sum of the curvature free energy and the entropy of mixing of oil and water domains [20-22]. The basic length scale, the persistence length, exponentially depends on the bending elastic modulus [23].

For droplet type microemulsions coexisting with an excess phase this approach can be formulated quite rigorous. This leads to the prediction of detailed properties such as droplet size distributions and interfacial tensions [24,25].

1.3 Outline of the thesis.

In the work presented in this thesis predictions following from phenomenological theories are tested. This is done by studying a model system composed of brine (aqueous salt solution), cyclohexane, the ionic surfactant Sodium Dodecyl sulfate (SDS) and the cosurfactant pentanol and/or hexanol. These different cosurfactants are expected to give rise to different monolayer properties.

Chapter 2 and 3 deal with properties of the mixed SDS-cosurfactant monolayer at the planar cyclohexane- brine interface. In Chapter 2 the influence of the different cosurfactants upon the adsorption densities of SDS and cosurfactant is studied. In Chapter 3 the bending elastic modulus of the mixed monolayer as a function of the cosurfactant chain length is determined. A combination of the results presented in these chapters allow a qualitative comparison with a molecular theory.

In Chapter 4 a thermodynamic theory of droplet type microemulsions in equilibrium with an excess phase is described. Predicted volume fraction dependence of the (mean) droplet radius, interfacial tensions of the planar cyclohexane- brine interface and polydispersities of the droplet radius are tested experimentally. From the measured droplet radius dependence and the results presented in chapter 3 the value of the Gaussian bending elastic modulus as a function of the cosurfactant chainlength is estimated.

Chapter 5 starts with a summary of phenomenological theories. The phase behaviour of the system as a function of the hexanol fraction in a pentanol/hexanol mixture as cosurfactant is presented. A special attention to microemulsion- lamellar liquid crystal phase competition is given. In order to understand this competition, we show that variations of the Gaussian bending elastic modulus should be taken into account.

In Chapter 6 a Small Angle X-ray Scattering study of both single- and multiphasic lamellar systems is presented. From the results it is concluded that even at large interlamellar spacing and high salt concentrations electrostatic interactions still play a role in these systems.

References.

[1] Hoar,T.P. and Schulman,J.H., Nature **152**, 102, (1943).

[2] Volmer,M., Z.Physik.Chem. **124**, 151, (1927); **155**, 281, (1931); **206**, 181,

(1957), **207**, 307, (1957).

[3] Kochanova,L.A., Fedoseeva, N.P., Kuchumova, V.M., Pertsov,A.V. and Rebinder,P.A., Coll.J.USSR **35**, 779, (1973].

[4] Reiss,H., J.Colloid Interface Sci. **53**, 61, (1975)

[5] Reiss,H., Adv.Colloid Interface Sci. **7**, 1, (1977).

[6] Bellocq,A.M., Biais,J., Bothorel,P., Clin,B. Fourche, G., Lalanne,P., Lemaire,B., Lemanceau,B., and Roux,D., Adv.Colloid Interface Sci. **20**, 167, (1984).

[7] Kahlweit,M., Strey,R., and Busse,G., J.Phys.Chem.**94**, 3881, (1990).

[8] Gompper,G. and Schick,M., to appear in *Phase Transitions and Critical Phenomena*, C.Domb and J.Lebowitz (eds.).

[9] Widom,B., J.Chem.Phys.**84**, 6943, (1986).

[10] Dawson,K.A., Lipkin,M.D., and Widom,B., J.Chem.Phys.**88**, 5149, (1988).

[11] Stockfish,T.P., and Wheeler,J.C., J.Phys.Chem.**92**, 3292, (1988).

[12] Schick,M., and Wei-Heng Shih, Phys.Rev.Lett.**59**, 1205, (1987)..

[13] Gompper,G. and schick,M., Phys.Rev.Lett.**62**, 1647, (1989).

[14] Schick,M., Physica A **172**, 200, (1991).

[15] Gompper,G. and Schick,M., Phys.Rev.Lett.**65**, 1116, (1990).

[16] Chen,K., Jayaprakash,C., Pandit,R. and Wenzel,W., Phys.Rev.Lett.**65**, 2736, (1990).

[17] Teubner,M. and Strey,R., J.Chem.Phys. **87**, 3195, (1987).

[18] Helfrich,W., Z.Naturforsch.**28c**, 693, (1973).

[19] Huse,D.A. and Leibler.S., J.Phys. (France) **49**, 605, (1988).

[20] Andelman,D., Cates,M.E., Roux,D., and Safran,S.A., J.Chem.Phys.**87**, 7229, (1987).

[21] Cates,M.E., Andelman,D., Safran,S.A., and Roux,D., Langmuir **4**, 802, (1988).

[22] Golubovic,L. and Lubensky,T.C., Phys.Rev.A**41**, 4343, (1990).

[23] De Gennes,P.G. and Taupin,C., J.Phys.Chem.**86**, 2294, (1982).

[24] Overbeek, J.Th.G., Verhoeckx, G.J., De Bruyn,P.L., and Lekkerkerker, H.N.W., J.Colloid Interface Sci. **119**, 422, (1987).

[25] Overbeek, J.Th.G., Progr.Colloid Polym.Sci. **83**, 1, (1990).

CHAPTER 2

Adsorption of Sodium Dodecyl Sulfate and Cosurfactant at the Planar Cyclohexane–Brine Interface. Validity of the Saturation Adsorption Approximation and Effects of the Cosurfactant Chain Length

W. K. Kegel, G. A. van Aken,† M. N. Bouts, H. N. W. Lekkerkerker,*
J. Th. G. Overbeek, and P. L. de Bruyn

Van't Hoff Laboratory, University of Utrecht, Padualaan 8, 3584 CH Utrecht, The Netherlands

Received April 22, 1992. In Final Form: September 8, 1992

The interfacial excess concentrations of sodium dodecyl sulfate (SDS) and two different cosurfactants (pentanol and hexanol) in mixed monolayers at the interface between water (with 0.2 M NaCl) and an oil phase consisting of cyclohexane and cosurfactant are determined from surface tension measurements using the Gibbs adsorption equation. The data are analyzed in two ways: assuming saturation adsorption and fitting the data to the Szyszkowski equation. This analysis reveals that a constant interfacial concentration in the vicinity of the critical micelle concentration is a good approximation even though the cosurfactant interfacial concentration does not reach its saturation value in the experimental cosurfactant concentration range. For both pentanol and hexanol, at low concentrations a strong competition between cosurfactant and SDS is observed, whereas at higher concentrations the composition of the interface remains practically constant. Under these conditions a high packing density in the mixed monolayer is observed.

Introduction

The area of the interface water–oil is an important quantity in microemulsion theory.[1-4] This area is generated and stabilized by the adsorption of surfactant (and cosurfactant, if applicable). Therefore it is important to know the interfacial concentrations of the surfactant.

We have studied a model system composed of brine (aqueous salt solution), cyclohexane, ionic surfactant (sodium dodecyl sulfate, SDS) and a nonionic cosurfactant (an alcohol). By variation of the salt and cosurfactant concentration and the chain length of the cosurfactant, we can regulate some properties of the interface which serve as input parameters in the above mentioned theories.

Examination of the phase behavior using equal volumes of brine and oil for the two alcohols pentanol and hexanol revealed some large differences. Details are reported in ref 5. In this article, we report the determination of the interfacial concentrations of SDS and the alcohols as a function of SDS and cosurfactant activities at constant salt concentration. We also address the question whether or not the apparently different interfacial properties are accompanied by a difference in composition of the interface.

For systems containing pentanol, the interfacial excess concentrations have been determined by Verhoeckx et al.[6] Since this work we have obtained better numbers based on improved techniques and improved interpretation.

We have determined the interfacial excess concentration, Γ_i, by using the Gibbs adsorption equation

$$\left(\frac{\partial\gamma}{\partial \ln (a_i)}\right)_{a_{j\neq i,k,l},T,P} = -RT\Gamma_i \qquad (1)$$

on measurements of the interfacial tension γ between water and oil obtained with the spinning drop method. In eq 1 a_i and Γ_i are the activity and the interfacial concentration of component i, respectively, a_k and a_l are the activities of two reference components (e.g. water and cyclohexane), and R, T, and P have their usual meaning. Since the interfacial tension of water–oil is very low under conditions where microemulsions can be formed, the measurements from which the slope of γ vs ln (a_i) is determined must be carried out at low to very low interfacial tensions.

From (1) it follows that in order to determine the interfacial concentration, we need to know the interfacial tensions as a function of the activities in a bulk phase $\gamma(\ln (a_i))$. In the case of systems containing only one surface-active solute, saturation adsorption is often found in the vicinity of the cmc and the interfacial concentration is obtained by fitting the data points to a straight line. In this paper, a system containing two surface-active components is studied. Interfacial tensions of this kind of systems are often also interpreted as if saturation adsorption occurs in the neighborhood of the cmc.[6-8] Here we will avoid this assumption by fitting the data to the Szyszkowski equation and compare the results with the assumption of saturation adsorption. The equation

$$\gamma_0 - \gamma = B \ln\left(\frac{c_i}{A} + 1\right) \qquad (2)$$

in which γ_0 is the interfacial tension at which $c_i = 0$, $B = RT\Gamma_{i,\infty}$, and $\Gamma_{i,\infty}$ is the saturation adsorption, was originally stated by Szyszkowski[9] on purely empirical grounds and its validity appears to be quite broad.[10,11] As shown by Rosen and Aronson,[10] (2) appears to fit data points

* Author to whom correspondence should be addressed.
† Present address: Department of Biophysical Chemistry. Netherlands Institute for Diary Research (NIZO), P.O. Box 20, 6710 BA Ede, The Netherlands.

(1) Overbeek, J. Th. G.; Verhoeckx, G. J.; de Bruyn, P. L.; Lekkerkerker, H. N. W. *J. Colloid Interface Sci.* **1987**, *119*, 422.
(2) Andelman, D.; Cates, M. E.; Roux, D.; Safran, S. A. *J. Chem. Phys.* **1987**, *87*, 7229.
(3) Widom, B. *Langmuir* **1987**, *3*, 12.
(4) Golubovic, L.; Lubensky, T. C. **1990**, *Phys. Rev. A* **41**, 4343.
(5) Chapter 5 of this thesis.
(6) Verhoeckx, G. J.; de Bruyn, P. L.; Overbeek, J. Th. G. *J. Colloid Interface Sci.* **1987**, *119*, 409.
(7) Aveyard, R.; Binks, B. P.; Mead, J. *J. Chem. Soc. Faraday Trans. 1* **1987**, *83*, 2347.
(8) Zhou, J. S.; Dupeyrat, M. *J. Colloid Interface Sci.* **1990**, *134*, 320.
(9) von Szyszkowski, B. *Z. Phys. Chem.* **1908**, *64*, 385.
(10) Rosen, M. J.; Aronson, S. *Colloids Surf.* **1981**, *3*, 201.
(11) Van Hunsel, J.; Joos, P. *Langmuir* **1987**, *3*, 1069. Joos, P.; Vollhardt, D.; Vermeulen, M. *Langmuir* **1990**, *6*, 524.

reasonably well as long as the surface pressure exceeds 20 mN/m and $c/A \gg 1$.

As already shown independently by Frumkin and Haber[12] in the 1920s, (2) is easily derived by combining the Langmuir adsorption equation

$$\Gamma(c_i) = \Gamma_{i,\infty} \frac{c_i}{A + c_i} \tag{3}$$

with the Gibbs equation (1). The "fitparameter" A can thus be regarded as the ratio of the desorption and adsorption rate constants.

Several attempts have been made[13-15] to derive (2) from more fundamental concepts, which will not be discussed here.

Experimental Section

Materials. Sodium dodecyl sulfate (SDS) was "specially pure" grade from BDH. It was purified by recrystallization in ethanol (2 times) and was stored in a vacuum desiccator over silica gel. Immediately before use, it was dissolved in water and filtered through a C18-silica column (SEP-pak cartridge, Millipore, prewetted with methanol and water).

Cyclohexane, 1-pentanol, 1-hexanol, and NaCl were Baker "analyzed" reagents and were used without further purification. Deionized water was distilled 3 times before use.

Sample Preparation. An 8.00-g portion of initial oil phase was carefully poured on 10.00 g of initial water phase in 25-mL glass tubes with Teflon-sealed screw caps. The initial oil phase was a solution of 1-pentanol or 1-hexanol in cyclohexane, with different initial mass fractions, and the water phase was a 0.20 M NaCl solution containing various amounts of SDS. Equilibrium was attained by gently rolling the samples on a roller bench (ca. 1 rev/min). Shaking or rolling too fast promotes the formation of unstable coarse emulsions or liquid crystalline phases that may persist for quite a long period of time.[16]

Analysis of the Equilibrated Phases. Pentanol and hexanol concentrations in the oil and water phase were measured with a Packard Model 433 gas chromatograph equipped with a flame ionization detector and a glass column packed with cross-linked polystyrene resin. The SDS concentration in the water phase was determined colorimetrically[17,18] for every sample. An excess quantity of methylene-blue was added to a water sample containing SDS. The equimolar complex was extracted with chloroform and the extinction was measured at 652 nm using a Bausch and Lomb/Shimadzu Spectronic 200-UV spectrophotometer. The detection limit is approximately 10^{-7} M in the original water phase. The possible presence of (a small amount of) water and SDS in the oil phase does not have any influence on the analysis.

Interfacial Tensions. Interfacial tensions between the water and oil phases were measured by the use of the spinning drop technique. The apparatus was built in our laboratory.[16] It enables one to measure interfacial tensions between approximately 10^{-4} and 10^2 mN/m. A precision glass tube (internal diameter 4 mm, length 95 mm, Teflon sealed) is rotated at high speed (up to 12 000 rpm). Inside the tube, a small drop of the less dense phase is introduced into the denser phase. Drop dimensions were measured by moving a microscope with cross-threads fixed to the eye piece by means of a pair of calibrated translators. Correction for refraction of light was carried out. The glass tube was thermostated because of the heat produced by the friction of the ball bearings. The interfacial tension was calculated from the length, l, and the maximum diameter, d, of the rotating drop (see Figure 1).

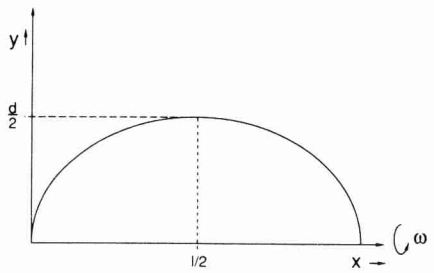

Figure 1. Coordinate system for a drop in the spinning drop tensiometer.

By equating the pressure difference inside and outside a drop in a centrifugal field to the capillary pressure across the interface, Princen et al.[19] find the following differential equation for the shape

$$\frac{dX}{dY} = \frac{Y(1 - \alpha Y^2/4)}{(1 - Y^2(1 - \alpha Y^2/4)^2)^{1/2}} \tag{4}$$

Here the dimensionless variables X and Y are defined in units of r_o, the radius of curvature at ($x = 0$, $y = 0$)

$$X = x/r_o;\ Y = y/r_o \tag{5}$$

Further the dimensionless shape parameter

$$\alpha = \frac{\Delta\rho\omega^2 r_o^3}{2\gamma} \tag{6}$$

where $\Delta\rho$ is the density difference between the two phases, ω the angular velocity of rotation, and γ the interfacial tension. Now (4) can be solved numerically to yield $X_o = l/2r_o$ and $Y_o = d/2r_o$ for any α. We used a numerical procedure to obtain α corresponding to the experimentally observed ratio $Y_o/X_o = l/d$. From the corresponding X_o and Y_o, r_o can immediately be calculated and γ follows from (6). The interfacial tensions obtained in this way were compared to literature values and showed good agreement.[16]

Fitting Data to the Szyszkowski Equation. A Levenberg–Marquardt algorithm was used[20] and convergence was usually reached within less than 10 iterations.

Determination of Cosurfactant Activities from Their Distribution between the Oil and Water Phase. At equilibrium the distribution constant K^ϕ and the experimentally accessible distribution coefficient K are related by

$$K = \frac{x^o}{x^w} = K^\phi \frac{f^w}{f^o} \tag{7}$$

where the superscripts w and o refer to the water and oil phase, respectively, and x and f are the fractions (mass, mole, or whatever) and the activity coefficients of the cosurfactant. Measurement of K as a function of the cosurfactant fraction in the oil phase revealed that the data could be well described by

$$K = D + E \frac{x^o}{1 + x^o} \tag{8}$$

Results for pentanol and hexanol are presented in Figure 2.

Since salt is hardly soluble in the oil phase, we assume that the activity of the cosurfactant in the oil phase is independent of the salt concentration in the water phase and further that $f^w = 1$ at $c^w_{NaCl} = 0$, at the low cosurfactant concentrations such as occur in the water phase. At finite salt concentrations, f^w appears to be larger than 1; the cosurfactant is salted out. As $x^o \to 0$, $f^o \to 1$ and thus

(12) Freundlich, H. *Kapillarchemie*; Akademische Verlagsgesellschaft m.b.h.: Leipzig, 1930; Band I, Vierte Auflage, pp 77–79.
(13) Defay, R.; Prigogine, I. *Surface Tension and Adsorption*: Longmans: London, 1966; p 167.
(14) van den Tempel, M.; Lucassen, J.; Lucassen-Reynders, E. H. *J. Phys. Chem.* **1965**, *69*, 1798.
(15) Ross, S.; Morrison, I. D. *J. Colloid Interface Sci.* **1983**, *91*, 244.
(16) van Aken, G. A. Thesis Rijksuniversiteit Utrecht, 1990.
(17) Fossil Energy, U.S. Department of Energy, BC/20009-8, C9 (1980).
(18) Reid, V. W.; Longmans, G. F.; Heinert, E. *Tenside* **1967**, *4*, 292.
(19) Princen, H. M.; Zia, I. Y. Z.; Mason, S. G. *J. Colloid Interface Sci.* **1967**, *23*, 99.
(20) Press, W. H., Flannery, B. P., Teukolsky, S. A. and Vetterling, W. T. *Numerical Recipes*: Cambridge University Press: Cambridge, 1987; Chapter 14.

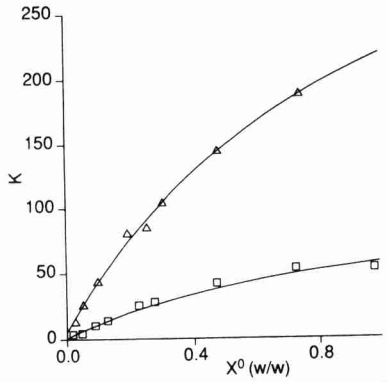

Figure 2. Distribution coefficient K of pentanol (□) and hexanol (△) between cyclohexane and brine at an NaCl concentration of 0.20 M. x^o is the mass fraction in the oil phase after equilibration. Drawn lines represent the least-squares fit according to eq 8.

$$\lim_{x^o \to 0} K = K^\theta f^w = D \tag{9}$$

Dividing (8) on both sides by D we immediately obtain the activity coefficient of the cosurfactant in the oil phase

$$\frac{1}{f^o} = 1 + \frac{E}{D}\frac{x^o}{1 + x^o} \tag{10}$$

which is enough for the determination of the surface excess as the activities can now be calculated. The activity coefficient in the water phase can also be determined. In Figure 3 results of K as a function of the salt concentration are given. Figure 3 shows a linear dependence of K on the salt concentration. We therefore define a salting out constant k^w which will be the only quantity which takes into account the nonideality of the cosurfactant in the water phase

$$f^w = 1 + k^w c^w{}_{NaCl} \tag{11}$$

In ref 16 the validity of (11) was verified by measuring the interfacial tension of a system containing cosurfactant, water, and salt as a function of the salt concentration. By use of the measured value of k^w (Table I), the cosurfactant interfacial concentration agreed with the one obtained by variation of the cosurfactant concentration. Equilibrium cosurfactant activities were calculated from the initial fractions in oil iteratively by (8), (7), and (11) and mass conservation within the experimental error range. Values for the coefficients D, E, and k^w are presented in Table I. The value of k^w in the pentanol system (0.62 ± 0.03) is in good agreement with the one obtained in a system containing dodecane instead of cyclohexane (0.616).[21]

Activity coefficients have also been obtained by IR spectroscopy and by osmometry.[22] Comparison with our results reveals that these appear to be weakly dependent on the alcohol chain length and the nature of the hydrocarbon. For example at an alcohol concentration of 0.05 mol/dm³ the activity coefficients are 0.700 for pentanol in cyclohexane (this work), 0.735 for hexanol in cyclohexane (this work), 0.811 for octanol in n-octane,[22] and 0.792 for dodecanol in n-octane.[22] The strongest nonideality in the above series occurs for pentanol which is a reflection of its more polar character.

From Table I and (10) it follows that the tendency of the cosurfactant to reside into the oil phase is strongly influenced by the amount of cosurfactant already present, an indication of a multiassociation equilibrium. In the limit of small concentrations, pentanol has a slight preference for the water phase but hexanol is already nearly 5 times more soluble in the oil phase.

(21) Aveyard, R.; Heselden, R. *J. Chem. Soc., Faraday Discuss.* **1975**, *71*, 312.

(22) Aveyard, R.; Briscoe, R. J.; Chapman, J. *Trans. Faraday Soc.* **1973**, *69*, 1772.

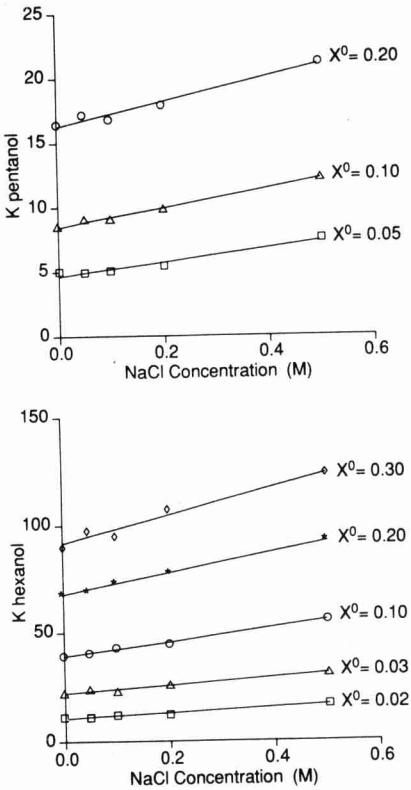

Figure 3. Distribution coefficient K as a function of the salt concentration for a few equilibrium pentanol (a, top) and hexanol (b, bottom) mass fractions in the oil phase. Mass fractions are indicated in the figures.

Table I. Values for the Distribution Coefficients of the Cosurfactants Pentanol and Hexanol[a]

	pentanol	hexanol
D	0.86	4.9
E	104.9	433.1
k^w/(mol/L)	0.62 ± 0.03	0.72 ± 0.02

[a] D and E (eq 8) were determined at 0.2 M NaCl and k^w is the mean value obtained for initial weight fractions of cosurfactant in cyclohexane between 0.02 and 0.30.

Results and Analysis

Parts a and b of Figure 4 show the interfacial tensions as a function of the logarithm of the SDS concentration in the aqueous phase at different initial weight fractions of pentanol and hexanol, respectively. Because of the low SDS concentration in the water phase, the SDS activity coefficient at concentrations below the cmc was assumed not to vary with the SDS concentration.

Except for the isotherm representing the initial pentanol weight fraction of 20%, the Szyszkowski equation appears to fit the data points quite well. In the case of low initial cosurfactant concentrations (≤7.5%), a good fit was obtained over the whole range of SDS concentrations used, even when $C_{SDS} = 0$ is taken into account. At higher concentrations the shape of the isotherm apparently becomes more "curved", indicating a stronger adsorption gradient in a comparable SDS concentration range, and

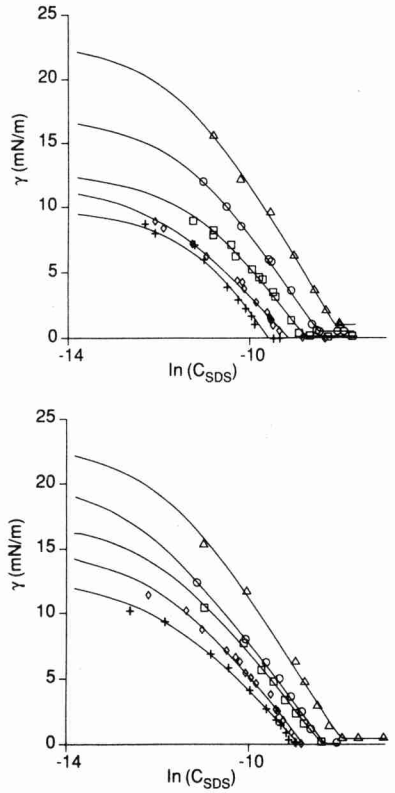

Figure 4. Interfacial tensions between oil and water in the presence of SDS, salt, and pentanol (a, top) or hexanol (b, bottom) as a function of the SDS concentration in the water phase. Symbols △, ○, □, ◇, and + correspond to initial mass fractions of 0.01, 0.02 (a) or 0.03 (b), 0.05, 0.10, and 0.20 (w/w), respectively. The isotherm corresponding to 0.075 (w/w) hexanol is not shown. The salt concentration in the water phase is 0.20 M. Solid lines correspond to Szyszkowski fits (as long as c_{SDS} < cmc).

a good fit could only be obtained without the point (C_{SDS} = 0, γ_o). The reason for this is not understood.

The shape of the adsorption isotherm corresponding to 10% pentanol in the oil phase (Figure 4a) is somewhat deviating compared to the other ones. Comparing the results with those reported in ref 16 shows that this behavior at this particular pentanol concentration is reproducible. Comparing parts a and b of Figure 4 reveals that systems containing pentanol apparently form micelles or microemulsions at significantly lower SDS concentrations in water over the whole range of initial cosurfactant concentrations than the systems containing the same concentrations of hexanol in the oil phase. The cmc's as well as the cosurfactant activities in the water phase are listed in Table II. From Table II it is clear that at equal concentrations of pentanol and hexanol in the oil phase pentanol has a larger effect on the value of the cmc of SDS because of its higher activity in the water phase.

In Table III single component adsorptions are given and a comparison is made between the SDS adsorptions assuming saturation adsorption in the vicinity of the cmc (i.e. fitting those data points to a straight line) and calculating the interfacial concentrations at the cmc using the coefficients from the Szyszkowski fit according to (2). The number of points in Figure 4 used for the linear fits

Table II. cmc Values of SDS and Cosurfactant Activities in the Water Phase (0.2 M NaCl) as a Function of Initial Weight Fractions of Cosurfactant in the Oil Phase

initial	pentanol		hexanol	
mass fraction	cmc (mmol/L)	a (mol/L)	cmc (mmol/L)	a (mol/L)
0.00	0.605	0.000	0.605	0.000
0.01	0.283	0.043	0.310	0.011
0.02	0.201	0.067		
0.03			0.227	0.018
0.05	0.139	0.092	0.208	0.022
0.075			0.173	0.024
0.100	0.098	0.107	0.146	0.025
0.200	0.068	0.124	0.125	0.029

Table III. SDS Interfacial Excess Concentrations Assuming Saturation Adsorption (Γ_{lin}^{SDS}), Number of Points at SDS Concentrations in the Water Phase Lower Than the cmc Used for the Linear Fit (no. of points), Interfacial Concentrations at the cmc (Γ_{szys}^{SDS}), and Saturation Interfacial Concentrations ($\Gamma_{SDS,\infty}$) Resulting from Fitting Data to Equation 2 as a Function of Initial Cosurfactant Weight Fractions in Cyclohexane (x^o_{init})[a]

x^o_{init} (w/w)	Γ_{lin}^{SDS}	no. of points	Γ_{szys}^{SDS}	$\Gamma_{SDS,\infty}$
		Pentanol		
0.01	2.54 ± 0.02	4	2.44 ± 0.20	2.52 ± 0.07
0.02	2.10 ± 0.05	5	2.12 ± 0.06	2.24 ± 0.03
0.05	2.01 ± 0.07	6	1.90 ± 0.12	2.10 ± 0.07
0.10	1.81 ± 0.07	8	1.65 ± 0.21	1.66 ± 0.08
0.20	1.76 ± 0.03	7	1.60 ± 0.17[b]	1.76 ± 0.06[b]
		Hexanol		
0.01	2.70 ± 0.10	4	2.27 ± 0.19	2.34 ± 0.07
0.03	2.17 ± 0.06	5	1.92 ± 0.11	1.95 ± 0.03
0.05	1.81 ± 0.07	5	1.83 ± 0.12	1.88 ± 0.04
0.075	1.85 ± 0.05	6	1.91 ± 0.15	1.91 ± 0.06
0.10	1.86 ± 0.03	8	1.79 ± 0.15	1.87 ± 0.05
0.20	1.71 ± 0.05	7	1.58 ± 0.10	1.60 ± 0.04
pure SDS	(3.62 ± 0.04)		3.44 ± 0.19	3.45 ± 0.05

Pure pentanol: Γ_p = 4.71 ± 0.12[c]

Pure hexanol: Γ_h = 4.65 ± 0.14[c]

[a] The NaCl concentrations in the water phase is 0.2 M. All interfacial concentrations are an μmol/L. [b] Only the data points in the vicinity of the cmc were fit. [c] No Szyszkowsky fit was carried out; a plot of γ versus ln (a_{co}) with a_{co} ranging from 0.01 to 0.05 M in water yields a straight line, indicating that saturation adsorption is already attained at very low cosurfactant concentrations.

is also indicated. It is clear that these results are highly comparable. Although strictly speaking the deviation from saturation adsorption (the value B/RT) at the cmc is not significant, the trend is about 2–5% lower. From Table III it follows that the interfacial concentration of SDS as a function of cosurfactant concentration at cosurfactant weight fractions higher than about 0.05 is almost constant, which implies, using a Maxwell relation emerging from (1)

$$\left(\frac{\partial \Gamma_{co}}{\partial \ln (a_{sds})}\right)_{a_{co}} = \left(\frac{\partial \Gamma_{sds}}{\partial \ln (a_{co})}\right)_{a_{SDS}} \qquad (12)$$

that the cosurfactant interfacial concentration as a function of the SDS concentration is also constant. The cosurfactant interfacial concentrations are obtained by interpolating the γ–ln (C_{SDS}) curves at several SDS concentrations and fitting the data to the Szyszkowski equation (2) where the cosurfactant activity instead of its concentration in the water phase c_i was used.

Results for the highest SDS concentration at which no cmc is exceeded (0.065 mol/L for systems with pentanol and 0.123 mol/L for systems with hexanol) are shown in Figure 5.

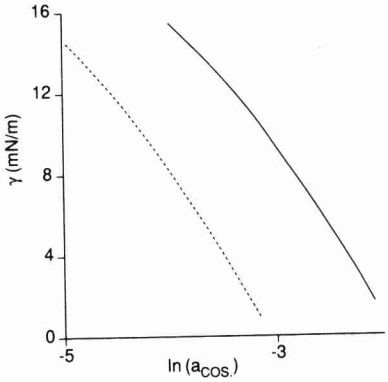

Figure 5. Interfacial tension between oil and water in the presence of SDS, salt, and pentanol (solid line) or hexanol (dashed line) as a function of the logarithm of the cosurfactant activity (mol/L).

Table IV. Parameter Values for Cosurfactant Interfacial Excess Concentration According to Equations 2 and 3

	pentanol	hexanol
$\Gamma_{co,\infty}$ (μmol/m²)	4.44 ± 0.06	4.46 ± 0.10
A (mol/m³)	24.72 ± 0.81	7.80 ± 0.29

Table V. Cosurfactant Interfacial Excess Concentrations (Γ_{co}, μmol/m²), Adsorption Ratios (Γ_{co}/Γ_{SDS}, mol/mol), Total Interfacial Excess Concentrations ($\Gamma_{co} + \Gamma_{sds}$, μmol/m²) and Mean Molecular Areas (σ_{mean}, nm²)[a]

x°_{init}	Γ_{co}	Γ_{co}/Γ_{SDS}	$\Gamma_{co} + \Gamma_{SDS}$	σ_{mean}
		Pentanol		
0.00	0.00	0.00	3.62	0.46
0.01	2.85 ± 0.09	1.12	5.39	0.31
0.02	3.26 ± 0.13	1.55	5.36	0.31
0.05	3.55 ± 0.15	1.77	5.56	0.30
0.10	3.64 ± 0.15	2.01	5.45	0.30
0.20	3.73 ± 0.15	2.12	5.49	0.30
1.00	4.7	-	4.7	0.35
		Hexanol		
0.00	0.00	0.00	3.62	0.46
0.01	2.62 ± 0.16	0.97	5.32	0.31
0.03	3.15 ± 0.19	1.45	5.32	0.31
0.05	3.30 ± 0.20	1.82	5.11	0.32
0.075	3.38 ± 0.20	1.83	5.23	0.31
0.10	3.40 ± 0.20	1.83	5.26	0.31
0.20	3.51 ± 0.21	2.05	5.22	0.32
1.00	4.7		4.7	0.35

[a] Γ_{lin}^{SDS} from Table I was used.

For the highest SDS concentrations at which no cmc is exceeded, values for $\Gamma_{co,\infty}$ and A in (2) are presented in Table IV. From (2) and Table IV we deduce that at initial weight fractions cosurfactant higher than about 0.05 (corresponding to a pentanol activity of 9.20×10^{-2} mol/L and a hexanol activity of 2.16×10^{-2} mol/L in the water phase) the cosurfactant interfacial concentration does not increase significantly although its saturation value as obtained from the Szyszkowski equation (2) is markedly higher. Table V gives some values of the cosurfactant interfacial concentration obtained from (2) and Table IV and a comparison of the adsorption ratios and packing densities of the two cosurfactants.

From these results it follows that the molecular composition of the interface is independent of the cosurfactant used and the behavior of the interfacial composition as a function of the cosurfactant concentration is highly comparable: at low cosurfactant concentrations (initial weight fraction <0.05) a strong pushing out effect is observed, i.e. the area per SDS molecule increases dramatically from 0.46 nm² to about 1 nm². At higher concentrations, the composition of the interface remains nearly constant and a high packing density of the mixed monolayer compared to single component adsorptions is observed.

Discussion and Conclusion

In this work, one of the questions we addressed is whether or not the composition of the interface changes if two slightly different cosurfactants are used. The answer appears to be very simple: it does not change significantly so the difference in phase behavior of the microemulsion systems observed must be due to a more subtle effect than just a difference in surface composition. A discussion in terms of differences in the values of the bending elastic moduli and natural radii of the interface is presented in ref 5.

It is proved that the approximation of saturation adsorption in the vicinity of the cmc gives rise to comparable interfacial concentrations to those obtained by the application of the Szyszkowsky equation over a broader range. From the application of the Szyszkowsky equation, it is however found that the SDS interfacial concentrations do not significantly differ from their saturation values but the cosurfactant interfacial concentrations definitely do. Even at the highest cosurfactant concentrations, the saturation value is significantly higher than the interfacial concentration close to the cmc.

The constancy of the interfacial composition as a function of the cosurfactant concentration is not in agreement with observations in other systems. Zhou and Dupeyrat[8] find, using lower cosurfactant concentrations (butanol, pentanol, and benzyl alcohol up to 0.10 (w/w)) and a rather high salt concentration (0.43 M), a strong competition effect over the whole range of cosurfactant concentrations in dodecane: in the pentanol system, the molecular area of SDS increases from 0.46 up to 1.8 nm². As a consequence, a much higher cosurfactant/SDS ratio is found: $\Gamma_{co}/\Gamma_{SDS} = 4.9$. These results are qualitatively in agreement with calculations by Ruckenstein et al.[23] on systems in which the chain length of the linear alkane, the surfactant, and the cosurfactant are varied. Aveyard et al.[7] find an even higher cosurfactant SDS ratio ($\Gamma_{co}/\Gamma_{SDS} = 5.5$) in a system containing octanol (up to 5% (w/w)), cyclohexane, and 0.3 M NaCl at 30 °C. As pointed out in ref 16, the pentanol interfacial concentration used by Verhoeckx et al.[6] is too high because of their assumption that the pentanol interfacial concentration in the mixed monolayer should be equal to its saturation adsorption value without SDS. This is in contradiction with (12) and the observation that Γ_{SDS} for mixed adsorption is different from the value without pentanol.

It is interesting to note that in all cases discussed above, the mean area per molecule in the mixed monolayer is constant and equals approximately 0.30 nm², significantly lower than the values for single-component adsorption.

Acknowledgment. The authors are indebted to Jacques Suurmond for his contribution to the experimental work and to Tibor den Ouden for providing the fit procedure.

(23) Ruckenstein, E.; Rao, I. V., *J. Colloid Interface Sci.* **1987**, *117*, 104.

CHAPTER 3

DETERMINATION OF THE BENDING ELASTIC MODULUS OF MIXED SURFACTANT - COSURFACTANT MONOLAYERS AT THE PLANAR CYCLOHEXANE - BRINE INTERFACE BY POLARIZATION MODULATION ELLIPSOMETRY.

Willem K.Kegel and Henk N.W.Lekkerkerker.

Abstract

The bending elastic modulus K of mixed surfactant (SDS)- cosurfactant monolayers at the cyclohexane - brine interface is deduced from polarization modulation ellipsometry measurements. It is shown that K increases with order $0.1k_BT$ upon replacing pentanol by hexanol as a cosurfactant. Taking into account the compositions of the mixed monolayer as reported earlier it is concluded that the increase is in qualitative agreement with the results of model calculations presented by Szleifer et al. [I.Szleifer, D.Kramer, A.Ben-Shaul, W.M.Gelbart and S.A.Safran, J.Chem.Phys.**92**,6800,(1990)].

3.1. Introduction.

Liquid-liquid or liquid-gas interfaces being macroscopically flat are more or less rough at smaller lengthscales. This roughness, caused by thermal motion and referred to as surface corrugations (or ripples), can be demonstrated by optical techniques such as surface light scattering, reflectometry and ellipsometry. These techniques are effectively sensitive for the fluctuating dielectric constant (or refractive index) profile but they are not equally sensitive for all wavelengths of the corrugations. Corrugations with wavelengths of the order of the wavelength of light cause a laser beam reflected at the surface to scatter significantly in all directions [1-3]. For small lengthscales, ellipsometry is the most sensitive technique [4-6]. Ellipsometry allows to measure the polarization state of light reflected from an interface between two materials. The polarization state is determined by properties of the dielectric constant profile being composed of a structural variation and a fluctuation contribution caused by corrugations. In the case of a liquid-liquid interface covered with a surfactant monolayer this fluctuation contribution is expected to dominate as the restoring forces of the thermal fluctuations are small [5]. Meunier [5] obtained the ellipsometric coefficient at the Brewster angle as a function of the bending elastic modulus K and the surface tension γ by a proper summation over the thermal modes. Therefore K can be obtained by measuring the ellipsometric coefficient at the Brewster angle.

In this paper we present values of K in systems composed of SDS, brine, cyclohexane and 2 different alcohols: pentanol and hexanol. We will first describe how K can be obtained from ellipsometric measurements. This is performed in two steps: in section 3.2.1 a statistical analysis of surface corrugations is given and after that (section 3.2.2) we give the relation between the mean squared amplitudes of the corrugations and the ellipsometric coefficient. In section 3.2.3 the optical arrangement of the ellipsometer built in our laboratory is described. The experimental set up is described in section 3.3 after which the results are presented in section 3.4. In section 3.5 a short discussion is given.

3.2.Theory

3.2.1 Statistical analysis of surface corrugations.

The mean position of the interface is taken in the x-y plane and the

deviation from this mean position is defined by a function $\zeta=\zeta(x,y)$. This function is expanded in a Fourier series in a square with length L ($-L/2<x,y<L/2$).

$$\zeta(x,y)= \sum_{q_x,q_y} \zeta_{q_x,q_y} \exp[i(q_x x + q_y y)] \ , \qquad (1)$$

with

$$q_x=n_x\frac{2\pi}{L} \ ; \ \ q_y=n_y\frac{2\pi}{L} \ , \qquad (2)$$

and $n_x,n_y=\pm1, \pm2,...$

ζ_{q_x,q_y} are the Fourier coefficients with the complex conjugate $\zeta^*_{q_x,q_y}=\zeta_{-q_x,-q_y}$. As will be shown later (cf eq.(16)) the ellipsometric coefficient is related to the averages $<|\zeta_{q_x,q_y}|^2>$. These averages were calculated by Mandelstam [2] by analysing the free energy required to create each mode. Here we follow the same analysis but with the curvature free energy as an additional contribution which was first performed by Meunier [5].

The free energy ΔF to create a corrugation is the the sum of the gravitational free energy ΔF_g, the capillary free energy ΔF_{cap} and the curvature free energy ΔF_{curv}. The gravitational free energy is

$$\Delta F_g=\frac{1}{2}\Delta\rho g\int_{-L/2}^{+L/2}\int [\zeta(x,y)]^2 dxdy = \frac{1}{2}\Delta\rho g \sum_{q_x,q_y} |\zeta_{q_x,q_y}|^2 L^2 \ , \qquad (3)$$

where $\Delta\rho$ denotes the density difference between the two phases and g is the gravity constant. The free energy contribution due to increasing the area with ΔA

$$\Delta F_{cap}=\gamma\Delta A \ , \qquad (4)$$

with γ the interfacial tension. An infinitesimal area dA spanned by the

surface above a rectangle dxdy is

$$dA= \left(1 + \left(\frac{\partial\zeta}{\partial x}\right)^2 + \left(\frac{\partial\zeta}{\partial y}\right)^2 \right)^{1/2} dxdy \quad , \tag{5}$$

assuming that the gradients of the corrugations are small we may write

$$\Delta F_{cap} \cong \frac{\gamma}{2} \int_{-L/2}^{+L/2} \int dxdy \left(\left(\frac{\partial\zeta}{\partial x}\right)^2 + \left(\frac{\partial\zeta}{\partial y}\right)^2 \right) \quad . \tag{6}$$

Introducing

$$q=(q_x^2 + q_y^2)^{1/2} \tag{7}$$

we find by applying eq.(1)

$$\Delta F_{cap}= \frac{\gamma}{2} \sum_{q_x,q_y} q^2 |\zeta_{q_x,q_y}|^2 L^2 \quad . \tag{8}$$

The work required to bend the interface is given by the curvature free energy calculated by Helfrich [7]

$$\Delta F_{curv}= \frac{K}{2} \int_{-L/2}^{+L/2} \int dxdy \left(\frac{1}{R_1} + \frac{1}{R_2} \right)^2 \quad , \tag{9}$$

where K denotes the bending elastic modulus and $1/R_1$ and $1/R_2$ are the principal curvatures. A second term proportional to $1/R_1R_2$ appearing in Helfrich's expression of the free energy is absent in (9). This is due to the fact that the integral over this term only depends on the topology of the surface (Gauss-Bonnet theorem) being unchanged by corrugations. Again assuming small corrugation gradients we may write

$$\frac{1}{R_1} + \frac{1}{R_2} = \frac{\partial^2\zeta}{\partial x^2} + \frac{\partial^2\zeta}{\partial y^2} \quad , \tag{10}$$

so that

$$\Delta F_{curv}=\frac{K}{2}\sum_{q_x,q_y} q^4 |\zeta_{q_x,q_y}|^2 L^2 \quad . \tag{11}$$

Application of the equipartition theorem stating that the work necessary to create each mode is equal to $\frac{1}{2}k_BT$ or

$$<|\zeta_{q_x,q_y}|^2>[\Delta\rho g + \gamma q^2 + Kq^4] L^2/2 = \frac{1}{2}k_BT \quad ,$$

thus

$$<|\zeta_{q_x,q_y}|^2>= \frac{k_BT}{L^2(\Delta\rho g + \gamma q^2 + Kq^4)} \quad . \tag{12}$$

By taking into account higher order terms in eqs.(6) and (10) Meunier [6] deduced a coupled mode theory leading to a q dependence of both γ and K. We will further assume independent modes as implicit in eqs.(6) and (10).

3.2.2.Contribution of surface corrugations to the ellipsometric coefficient.
The ellipsometric coefficient r is a complex number defined by

$$r=\frac{r_p}{r_s} = \rho e^{i\Delta} \tag{13}$$

with r_p and r_s the reflectivity amplitudes of the electric field for p (parallel to the plane of incidence) and s (perpendicular) polarized light. $\Delta=\delta_p-\delta_s$ with $\delta_p(\delta_s)$ the phase shift experienced upon reflection of light polarized parallel (perpendicular) to the plane of incidence. The Brewster angle θ_B is defined as $\Delta(\theta_B)=\pi/2$. In case of a perfect interface (i.e. the dielectric constant profile changes discontinuously at the interface to the bulk values of the materials) where Fresnel's equations apply, r_p and hence r is zero at this angle. A finite value of r at the Brewster angle is therefore caused by deviations from the Fresnel dielectric constant profile. From now on we will only consider the ellipsometric coefficient at the Brewster angle:

$r \equiv r(\theta_B)$.

Drude [8] obtained a general relation between η, which depends upon interfacial properties, and ρ

$$\eta = \frac{\lambda}{\pi} \frac{n_1^2 - n_2^2}{(n_1^2 + n_2^2)^{1/2}} \rho \quad , \tag{14}$$

with λ the wavelength of light and n_1 and n_2 the refractive indices of the two phases. η can be expressed as the sum of a 'structural' term η_s and a 'roughness' term η_r caused by the surface corrugations

$$\eta = \eta_s + \eta_r \quad . \tag{15}$$

The structural term η_s is model dependent and will not be specified. The roughness term can be shown to be [6,10,11]

$$\eta_r = -\frac{3}{2} \frac{(n_1^2 - n_2^2)^2}{n_1^2 + n_2^2} \sum_{q_x, q_y} q \langle |\zeta_{q_x,q_y}|^2 \rangle \quad . \tag{16}$$

Replacing the summation by an integration we obtain

$$\sum_{q_x, q_y} q \langle |\zeta_{q_x,q_y}|^2 \rangle = \left(\frac{L}{2\pi}\right)^2 \int_{-\infty}^{+\infty} \int q \langle |\zeta_{q_x,q_y}|^2 \rangle dq_x dq_y$$

$$= \left(\frac{L}{2\pi}\right)^2 \int_0^{+\infty} q \frac{k_B T}{L^2(\Delta\rho g + \gamma q^2 + K q^4)} 2\pi q dq = \frac{k_B T}{4(K\gamma)^{1/2}} \quad . \tag{17}$$

In writing down the final result we have used that the gravity term in eq.(12) is very small compared to the other contributions. Combination of this expression with eq.(16) gives

$$\eta_r = -\frac{3k_B T}{8} \frac{(n_1^2 - n_2^2)^2}{(n_1^2 + n_2^2)} (\gamma K)^{-1/2} \quad . \tag{18}$$

In a microemulsion system one may vary γ by e.g. varying the salt concentration. It is expected that this does not significantly influences K as long as the salt concentration is not too low and the range over which it is varied is not too broad [12]. By plotting η obtained from ellipsometry (eq.14) against $\gamma^{-1/2}$, K is obtained from the slope and η_s from the intercept (eqs.(15) and (18)).

3.2.3. Polarization Modulation Ellipsometry.

Measurements on liquid-gas [4] and liquid-liquid [5,6] interfaces reveal that the magnitude of the ellipsometric coefficient $|r|$ is very small at the Brewster angle. This may cause large errors when classical ellipsometric techniques are used [13]. Therefore we used a polarization modulation technique [14].

The ellipsometer is based upon the design of Meunier [15] who used the optical arrangement as reported by Jasperson and Schnatterly [14] and Beaglehole [4]. It is mounted vertically to reflect off the horizontal liquid/liquid interface. The optical arrangement is shown in fig.1.

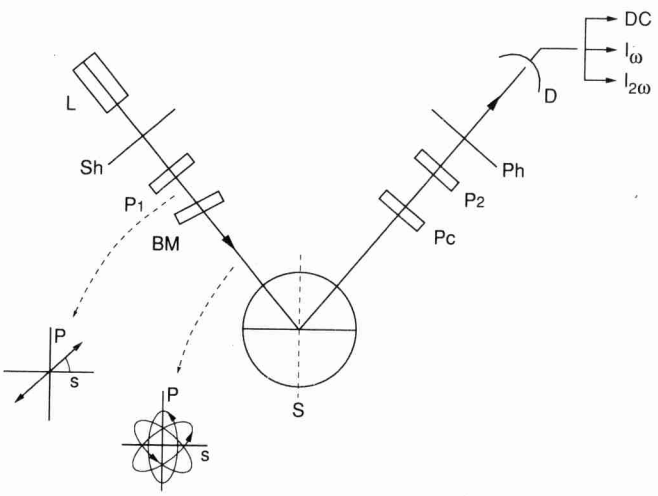

Fig.1. Schematic representation of the optical arrangement of the ellipsometer. L, Sh, P1, BM, S, PC, P2, Ph and D denote the Laser, Shutter, Glen thomson polarizer, Birefringent Modulator, Sample, Pockels cel, Polarizer, Pinhole and photodiode Detector.

A laser beam is passed through a Polarizer (P1) oriented at 45° relative to the plane of incidence so that it has equal s and p amplitudes. The Birefringent Modulator BM is a fused quartz rod which is modulated by a piezoelectric transducer in such a way that it has an ω=50 kHz fundamental longitudonal resonance. The laserbeam is then transmitted with a time dependent phase shift between the s and p amplitudes $\delta=\delta_0\sin(\omega t)$ with t the time and δ_0 the relative phase amplitude being effectively a function of the peak to peak voltage applied to the transducer. This light is reflected from the (liquid-liquid) surface and passes through a Pockels Cel (PC) which operates in such a way as to cause a retardation between the s and p components of either 0 or $\lambda/2$ where λ denote the wavelength of the light. The Polarizer P2 is oriented parallel to P1 so that the combination of the Pockels Cel and Polarizer P2 acts as an analyser oriented perpendicular or parallel to P1. By switching between these orthogonal positions at low frequency (order 1/10 Hz) one compensates for small residual signals associated with imperfections of the modulator and static birefringence of the sample cell windows [4]. Then the light passes through a pinhole to the detector. The detector signal is composed of a DC signal, a fundamental and higher harmonic components to be measured with a low pass filter and lock-in amplifiers. The signal R_ω measured with a lock-in amplifier at frequency ω, normalised by the DC signal is

$$R_\omega = \mp \frac{4\rho \sin(\Delta) J_1(\delta_0)}{1 + \rho^2 \mp 2\rho\cos(\Delta) J_0(\delta_0)} \qquad (19)$$

and that at frequency 2ω

$$R_{2\omega} = \mp \frac{4\rho \cos(\Delta) J_2(\delta_0)}{1 + \rho^2 \mp 2\rho\cos(\Delta) J_0(\delta_0)} \qquad (20)$$

where J_0, J_1, J_2 are Bessel functions and $\rho = \frac{r_p}{r_s} e^{-i\Delta} = re^{-i\Delta} = tg\Psi$. The $\mp$ sign refers to the 0 and $\lambda/2$ mode of the Pockels cel. The derivation of (19) and (20) from the optical configuration schematically depicted in fig.1 is presented in the Appendix. Now δ_0 can be adjusted until $J_0(\delta_0)=0$. The Brewster Angle is defined as the angle of incidence where $\Delta=\pi/2$. From eq.(20) it

follows that at this angle $R_{2\omega}=0$ and ρ follows from eq.(19). At the Brewster Angle $\rho<<1$ and therefore it is possible to approximate

$$R_{\omega}=\pm 4\rho J_1(\delta_0) \qquad (21).$$

3.3. Experimental

Materials.

Sodium dodecyl sulphate (SDS) was 'specially pure' grade purchased from BDH. It was further purified by recrystallisation in ethanol (2 times) and was stored in a vacuum desiccator over silica gel. Cyclohexane, n-pentanol, n-hexanol and NaCl (Baker) were 'analysed' grade and were used without further purification. Deionized water was doubly distilled before use.

Preparation of the samples.

Equal volumes of initial water phase (various concentrations of NaCl and 0.07% (w/w) SDS being of order 10 times the critical micelle concentration [16]) and oil phase (15% (w/w) pentanol or 8% (w/w) hexanol in cyclohexane) were carefully mixed in glass tubes with teflon screw caps. Equilibrium was attained by gently rolling the samples on a roller bench (ca. 1 rev/min) for several days.

Experimental setup of the ellipsometer

The ellipsometer consists of two arms which could rotate by moving over a steel wheel in the middle of which the sample cel is located. The arms could be positioned above and below the liquid surface thus allowing the light to be incident from the upper phase and from the lower phase. The optical components, a 2mw He-Ne laser (λ=632.8nm), a shutter, a Glen-Thomson polarizer and a birefringent modulator on the incidence side and a Pockels cel, a polarizer, a pinhole and a photodiode detector on the reflectance side (see fig.1) are mounted on the arms. The angles of incidence and of reflectance could be adjusted roughly by pinning the arms into equidistant holes (every 4 degrees) in the steel wheel. Fine adjustment was performed by using micrometers.

The birefringent modulator was tilted over a few degrees in order to avoid multiple reflections. The sample cell, a cylindrical ampule filled with equal volumes of water and oil phase, was placed horizontally into a sample holder.

The sample holder was filled with water running slowly through a circuit with a thermostated bath. Light was incident and reflected through windows which can be rotated in the vertical plane. The sample cell could be moved in the plane perpendicular to the plane of incidence. This allowed us to perform measurements at different positions of the interface.

The system is aligned as follows. (1) The s and p direction of the polarizers p1 and p2 are found using a simple and effective method as reported in [17]. First, in the straight through position of the arms, the azimuth angles of p1 and p2 at which intensity minima occur are determined. The same is done after a sample is placed (in this case optical glass) and the arms positioned near the Brewster angle. The intersection of the lines is the deepest minimum and correspond to the s and p positions of the polarizers with an accuracy of a few minutes. (2) Back in the straight through position, p1 is set in the p direction and the birefringence modulator operating at an arbitrary peak to peak voltage is oriented so that no fundamental or 2ω signals are measured. This is most accurately done at a p2 position of $\pm 45^{\circ}$. (3) p1 and p2 are oriented at $+45^{\circ}$. The Pockels cel, operating at a Bias voltage not too far from the one corresponding to a $\lambda/2$ phase retardation, is oriented so that a minimum intensity is obtained. The absolute minimum is iteratively found by varying the position and the Bias voltage. In this configuration the optical axis of the Pockels cel is oriented at -45° and the Bias voltage corresponds to $\lambda/2$ phase retardation. Then the Bias voltage corresponding to zero retardation is found at maximal intensity. The configuration is verified by orienting p2 at -45° but now the minimum intensity should correspond to zero- and the maximum one to $\lambda/2$ phase retardation. (4) With p1 and p2 oriented at 45° the peak to peak voltage of the photoelastic modulator is adjusted until equal DC intensities are obtained in the 0 and $\lambda/2$ mode of the Pockels cel. This voltage corresponds to the relative phase amplitude δ_0 where $J_0(\delta_0)=0$, as is clear from eq.(A9) in the Appendix. (5) J_2 is found by measuring $R_{2\omega}$ (eq.(20)) and J_1 by inserting a quarter wave plate ($\Delta=\pi/2$) and measuring R_{ω} (eq.(19)).

With this alignment we measured ρ and Δ of (optical) glass at several angles and compared it with literature values. In an incident angle range of $30\text{-}70^{\circ}$ the agreement was excellent. Moreover we verified the value of K for an AOT- dodecane- brine system as reported in [18]. These measurements (as well as the measurements on the SDS, alcohol,brine, cyclohexane systems) were

carried out at a temperature of 25 °C. After transfer to the sample holder the samples were permitted to regain equilibrium. Measurements were started as soon as the reflected DC intensity (at arbitrary angle) was constant in time which took a few ours to several days.

Interfacial tensions.

The interfacial tensions were measured with a spinning drop tensiometer (Krüss, Hamburg, SITE 04) at a temperature of 25 °C. The measurements were complicated by the formation of liquid crystals in the droplets. This effect could be avoided (though not in all cases) by very slowly introducing the less dense phase into the denser phase.

3.4. Results

In fig.2 the interfacial tensions as a function of the salt concentration are presented. The salt concentration range where excess oil and water phase are present (corresponding to a preferred curvature of the mixed monolayer of about 0) are also indicated in the figure.

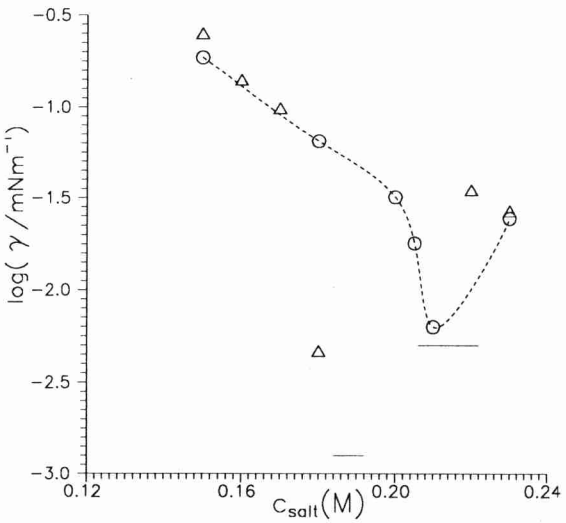

Fig.2. Interfacial tensions between water and oil phase as a function of the salt concentration of the pentanol system (circles) and the hexanol system (triangles). The the 3 phase (brine-microemulsion-oil) regions are indicated by the bars. The (dashed) line is a guide to the eye.

Fig.3 shows the ellipsometric coefficient η (calculated from the measured ρ with eq.(14)) as a function of the salt concentration and in fig.4 we plotted η against $(n_1^2-n_2^2)^2/[(n_1^2+n_2^2)\gamma^{1/2}]$. The slope of the lines gives K being $(0.9\pm0.1)k_BT$ for the pentanol system and $(1.1\pm0.1)k_BT$ for the hexanol system.

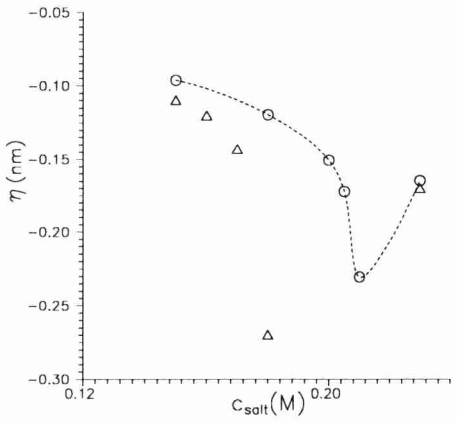

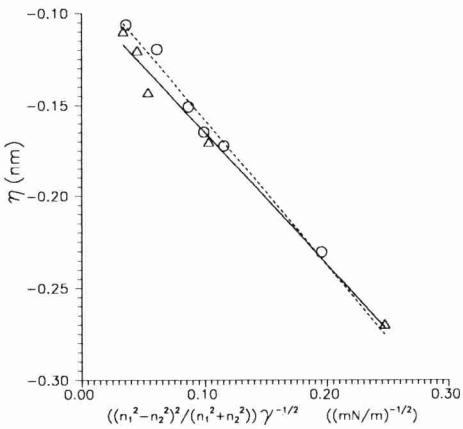

Fig.3, left. The ellipsometric coefficient η as a function of the salt concentration. Symbols the same as in fig.2.

Fig.4, right. The ellipsometric coefficient η as a function of $(n_1^2-n_2^2)/[(n_1^2+n_2^2)\gamma^{1/2}]$. Symbols the same as in fig.2. The lines (dashed for pentanol and solid for hexanol systems) are linear best fit lines.

3.5. Discussion and Conclusion.

We note that the difference of K between the pentanol and the hexanol system is of order $0.1k_BT$. The area per surfactant molecule ($0.93nm^2$) as well as the alcohol/surfactant ratio (2 alcohol molecules/SDS molecule) in the (planar) mixed SDS cosurfactant monolayer is the same for the pentanol and hexanol systems [16]. Furthermore from the work of Verhoeckx et al. [19] and van Aken [20] it is expected that these quantities are approximately constant within the salt concentration range studied here. Thus the observed difference in K is caused by 2 methyl groups per nm^2 in the mixed monolayer between brine

and cyclohexane.

By calculating the lateral pressure profile at the chainside of a surfactant monolayer Szleifer et al. [21] showed that K reduces from 10's of k_BT to k_BT upon replacing long chain molecules (C_{12}) by short chain ones (C_6). Our results indicate that this trend is still observable when C_5 is replaced by C_6.

Acknowledgements.

The authors thank Gerard Harder and Marco van Amerongen for skillfully constructing the ellipsometer and to Carel van der Werf for doing the computer interfacing. Jan Dhont is thanked for his useful suggestions during the construction of the ellipsometer. We are grateful to Jacques Meunier for his kind hospitality during the visit of one of us (WK) at the ENS, Paris, and to Jacques Meunier and Hamid Kellay for interesting discussions. WK likes to express his gratitude to Bob Aveyard for his kind permission to perform the spinning drop measurements at the University of Hull and to Agnes Peels for her help with the measurements. A.Vrij, Jan Dhont and Ger Koper are thanked for useful comments on the manuscript.

Appendix.

A. Derivation of eqs.(19) and (20) from the optical arrangement fig.1.

To obtain the reflected intensity we calculate the electric field using the Jones vector formulation [13]. Any optical component changing the components of the electric field can be represented by a 2×2 matrix (called the Jones matrix) describing the action that it performs on the light beam. For the optical configuration schematically depicted in fig.1 we have

$$\begin{pmatrix} E_p \\ E_s \end{pmatrix} = \mathbf{M}_a.\mathbf{R}(\alpha_a).\mathbf{M}_s.\mathbf{R}(-\alpha_{BM}).\mathbf{M}_{BM}.\mathbf{R}(\alpha_{BM}).\mathbf{R}(-\alpha_{p1}).\mathbf{M}_{p1}.\mathbf{R}(\alpha_{p1}).\mathbf{E}_0 \quad ,(A1)$$

where $\mathbf{M}_a$, $\mathbf{M}_s$, $\mathbf{M}_{BM}$, and $\mathbf{M}_p$ denote the Jones matrices of the Pockels cel plus polarizer P2 acting as an analyser, the sample, the birefringent modulator and the polarizer P1. $\mathbf{E}_0$ is the incident electric field. $\mathbf{R}(\alpha_i)$ denote rotation transformation matrices around an angle α being the orientation relative to the plane of incidence of the components i indicated by the subscripts. Performing the matrix multiplication (A1) using

$$\mathbf{M}_a=\mathbf{M}_{p1}=\begin{pmatrix}1 & 0\\ 0 & 0\end{pmatrix} \quad , \qquad \text{(A2)}$$

$$\mathbf{M}_s=\begin{pmatrix}r_p & 0\\ 0 & r_s\end{pmatrix}=\begin{pmatrix}\rho e^{i\Delta} & 0\\ 0 & 1\end{pmatrix} \quad , \qquad \text{(A3)}$$

$$\mathbf{M}_{BM}=\begin{pmatrix}e^{i\delta} & 0\\ 0 & 1\end{pmatrix} \quad , \qquad \text{(A4)}$$

$$\mathbf{R}(\alpha)=\begin{pmatrix}\cos(\alpha) & \sin(\alpha)\\ -\sin(\alpha) & \cos(\alpha)\end{pmatrix} \quad , \qquad \text{(A5)}$$

and the optical configuration $\alpha_a=\pm\pi/4$, $\alpha_{BM}=0$, and $\alpha_{P1}=\pi/4$ gives for the intensity at the detector $I=\mathbf{E}^*.\mathbf{E}$ with $\mathbf{E}^*$ the complex conjugate of the electric field

$$I=\frac{I_0}{4}(\rho^2 \mp 2\rho\cos(\Delta-\delta)+1) \quad , \qquad \text{(A6)}$$

where the $\mp$ sign again refers to the two modes of the Pockels cel. I_0 denotes the intensity of the laser beam. As $\delta=\delta_0\sin(\omega t)$ it can be seen from (A6) that the detector signal contains quite complicated harmonic contents. The strength of each harmonic can be found by using the expansion in Bessel functions [14]

$$\sin(\delta_0\sin(\omega t))=2\sum_{m=0}^{\infty} J_{2m+1}(\delta_0)\sin[(2m+1)\omega t] \quad , \qquad \text{(A7)}$$

$$\cos(\delta_0\sin(\omega t))=2\sum_{m=0}^{\infty} J_{2m}(\delta_0)\cos(2m\omega t) \quad . \qquad \text{(A8)}$$

It turns out to be convenient to use terms up to 2ω. Inserting (A7) and (A8) into (A6) leads to the following expressions for the DC, fundamental and second harmonic signals I_{DC}, I_ω and $I_{2\omega}$

$$I_{DC} = \frac{I_0}{4}(\rho^2 \mp 2\rho J_0(\delta_0)\cos\Delta + 1) \quad , \qquad \text{(A9)}$$

$$I_{\omega} = \frac{I_0}{4}(\mp 4\rho J_1(\delta_0)\sin(\omega t)\sin\Delta) \quad , \qquad \text{(A10)}$$

$$I_{2\omega} = \frac{I_0}{4}(\mp 4\rho J_2(\delta_0)\cos(2\omega t)\cos\Delta) \quad . \qquad \text{(A11)}$$

and with $R_{m\omega}=I_{m\omega}/I_{DC}$, eqs.(19) and (20) follow directly.

References.

[1] Smoluchowski, M. von, Ann.Physik **25**, 225, (1908).

[2] Mandelstam, L., Ann.Physik **41**, 609, (1913).

[3] Vrij, A., Advan.Colloid Interface Sci. **2**, 39, (1968).

[4] Beaglehole, D., Physica **100B**, 163, (1980).

[5] Meunier, J., J.Phys.Lett. (France) **46**, L-1005, (1985).

[6] Meunier,J., J.Phys. (France) **48**, 1819, (1987).

[7] Helfrich, W., Z.Naturforsch. **28c**, 693, (1973).

[8] Drude, P., 'The Theory of Optics' (Dover, New York) (1959).

[9] Groce,P., J.Opt.(Paris) **8**, 127, (1977).

[10] Zielinska, B.J.A., Bedeaux, D. and Vlieger,J., Physica A **107**, 91, (1981).

[11] Blokhuis, E.M. and Bedeaux, D., Physica A **164**, 515, (1990).

[12] Lekkerkerker, H.N.W., Physica A **159**, 319, (1989).

[13] Azzam, R.M.A., and Bashara, N.M., 'Ellipsometry and polarized light', (Amsterdam 1977).

[14] Jasperson, S.N. and Schnatterly, S.E., Rev.Sci.Instr. **40**, 761, (1969).

[15] Meunier,J. Personal communications during a visit of one of us (W.K.) at the E.N.S. Paris.

[16] Kegel, W.K., Aken, G.A. van, Bouts, M.N., Lekkerkerker, H.N.W., Overbeek, J.Th.G., and de Bruyn, P.L., Langmuir **9**, 252, (1993); Chapter 2 of this thesis.

[17] McCrackin, F.L., Passaglia, E., Stromberg, R.R., and Steinberg, H.L., J.Res.Nat.Bur.St. **67A**, 363, (1963).

[18] Binks, B.P., Kellay, H., and Meunier, J., Europhys.Lett. **16**, 53, (1991).

[19] Verhoeckx, G.J., de Bruyn, P.L., and Overbeek, J.Th.G., J.Colloid

[20] Aken,G.A.van, Thesis Rijksuniversiteit Utrecht, (1990).
[21] Szleifer, I., Kramer, D., Ben-Shaul, A., Gelbart, W.M. and Safran, S.A., J.Chem.Phys.**92**,6800,(1990)].

CHAPTER 4

THERMODYNAMICS OF WINSOR II MICROEMULSION SYSTEMS: VOLUME FRACTION DEPENDENCE OF THE DROPLET SIZE, INTERFACIAL TENSION AND POLYDISPERSITY.

Willem K.Kegel, Igor Bodnàr and Henk N.W.Lekkerkerker.

Van't Hoff Laboratory, University of Utrecht, Padualaan 8,

3584 CH Utrecht, The Netherlands.

Abstract

A study of droplet type microemulsion systems coexisting with an excess water phase is presented. Experimentally observed volume fraction dependence of the droplet size agrees well with theoretical predictions of Overbeek et al. [J.Th.G.Overbeek, G.J.Verhoeckx, P.L.de Bruyn and H.N.W.Lekkerkerker, J.Coll.Interface Sci.**119**,422,(1987)]. From linear combinations of the bending elastic moduli obtained from this dependence, interfacial tensions of the planar interface between the coexisting phases are calculated being in satisfactory agreement with experiments. From a recent theory droplet size distributions are obtained which are verified by a combination of Small Angle X-ray scattering and the water content of the microemulsion phases.

4.1. Introduction

A mixture of water (with or without salt), oil and one or more surfactants may form a thermodynamically stable dispersion of one of the liquids into the other, with the interface between the two liquids covered by a monolayer of surfactant molecules [1]. The size of the domains of the dispersed phase is determined by the area/volume ratio of the system, expressed by the surfactant concentration. Experimentally, a lower limit for this ratio is found. As soon as the amount of surfactant falls below a certain value, a phase separation into a microemulsion and an excess liquid phase occurs. These systems have been classified by Winsor [2] who described an oil in water (droplets) microemulsion with excess oil (Winsor I), a water in oil (droplets) microemulsion with excess water (Winsor II) and a surfactant rich phase in equilibrium with both excess oil and water (Winsor III).

In this paper a study of Winsor II systems composed of equal volumes of brine (aqueous salt solution) and oil phase (cyclohexane plus pentanol or hexanol as cosurfactant) with Sodium Dodecyl Sulphate (SDS) as surfactant is presented. The total droplet area of these systems is determined by the amount of surfactant but the system is free to choose the dispersed volume and hence the (mean) droplet radius. Moreover the droplet size is expected to be reflected in the interfacial tension of the planar interface between the coexisting phases as this interfacial tension contains the free energy required to unbend the curved droplet interface.

We first describe a somewhat simplified version of a thermodynamic theory of Winsor II microemulsion systems as presented by Overbeek et al.[3]. This theory is combined with a phenomenological expression of the curvature free energy given by Helfrich [4]. From this combination we obtain expressions for the volume fraction dependence of the droplet radius and for the macroscopic interfacial tension as a function of linear combinations of the bending elastic moduli and the preferred radius of curvature. It is shown that the theory describes the experimental observations rather well.

Using parameters obtained from the volume fraction dependence of the (mean) droplet size we deduce the droplet size distribution and the polydispersity from a theory of Overbeek [5]. This size distribution agrees well with the droplet radii obtained with two different techniques (water titration and Small Angle X-ray Scattering) corresponding to different moments of the size distribution.

4.2. Thermodynamics of monodisperse droplet type microemulsions.

Free energy of a droplet type microemulsion.

In order to find the Gibbs free energy of a system of droplets dispersed into a continuous medium we first need the Helmholtz free energy F. The reason is that the pressure in the droplets is expected to be different from the ambient pressure p. We consider N_d droplets in local equilibrium with the continuous medium

$$F=\sum_i N_i\lambda_i - pV_m - (p+\Delta p)V_d + \sigma A + F_{mix} \qquad (1)$$

Here N_i and λ_i are the amounts and the chemical potentials of the components in the system where the droplets are considered seperately, i.e. not (yet) mixed with the continuous medium. V_m and V_d are the volume of the continuous medium and the droplets, σ and A the interfacial tension and the total area of the droplets and F_{mix} the free energy of mixing droplets with the continuous medium. The Gibbs free energy

$$\begin{aligned} G&=F + pV \\ &=\sum_i N_i\lambda_i - \Delta pV_d + \sigma A + G_{mix} \end{aligned} \qquad (2)$$

with $V=V_m+V_d$ and $G_{mix}=F_{mix}$ assuming that no volume changes occur upon mixing the droplets with the continuous medium. As we intend to minimize G we need dG

$$dG=\sum_i N_i d\lambda_i + \sum_i \lambda_i dN_i - \Delta p dV_d - V_d d(\Delta p) + \sigma dA + A d\sigma + dG_{mix} \qquad (3)$$

σ depends on all λ's and on the curvature

$$\begin{aligned} d\sigma&=\sum_i \left(\frac{\partial\sigma}{\partial\lambda_i}\right)_R d\lambda_i + \left(\frac{\partial\sigma}{\partial(2/R)}\right)_{\{\lambda_i\}} d(2/R) \\ &=-\sum_i \Gamma_i d\lambda_i + c\,d(2/R) \end{aligned} \qquad (4)$$

where Γ_i is the adsorption density of component i, R the radius and c the bending stress coefficient

$$c=\left(\frac{\partial\sigma}{\partial(2/R)}\right)_{T,p,\{\lambda_i\}} \tag{5}$$

in which T denotes the temperature. Eq.(5) quantifies the change in free energy upon changing the radius at constant area A. We will relate c to the bending elastic moduli later. Eq.(3) can be simplified considerably by applying the Gibbs-Duhem equations for the continuous medium and the droplets

$$(\sum_i N_{i,m}d\lambda_i - V_m dp)_T=0 \tag{6}$$

$$(\sum_i N_{i,d}d\lambda_i - V_d d(p+\Delta p))_T=0 \tag{7}$$

together with mass conservation

$$N_i=N_{i,m} + N_{i,d} + A\Gamma_i \tag{8}$$

leading to

$$dG_{p,T}=\sum_i \lambda_i dN_i - \Delta p dV_d + \sigma dA + Acd(2/R) + dG_{mix} \tag{9}$$

We can eliminate Δp by using the generalised Laplace equation [6]

$$\Delta p=\frac{2\sigma}{R} - \frac{2c}{R^2} \tag{10}$$

and we express G_{mix} for the moment as

$$G_{mix}=N_d k_B T f(\phi,R) \tag{11}$$

with N_d the number of droplets and k_B Boltzman's constant. ϕ is the droplet volume fraction which we define as the volume fraction of droplet components neglecting the surfactant/cosurfactant layer at the droplet interface thus assuming that the volume occupied by the surfactant is much smaller than the volume occupied by the droplet components. An expression for $f(\phi,R)$ will be derived later. Substituting eqs.(10) and (11) together with $V_d=\frac{4}{3}\pi R^3 N_d$ and

$A=4\pi R^2 N_d$ into eqs.(2) and (9) we have

$$G=\sum_i N_i\lambda_i + \frac{4}{3}\pi R^2 N_d\left(\sigma + \frac{2c}{R} + \frac{3k_BT}{4\pi R^2}f(\phi,R)\right)$$

and

$$dG=\sum_i \lambda_i dN_i + \frac{4}{3}\pi R^2\left(\sigma + \frac{2c}{R} + \frac{3k_BT}{4\pi R^2}f(\phi,R)\right)dN_d + N_d k_B T^* \left\{\left(\frac{\partial f(\phi,R)}{\partial\phi}\right)_R d\phi + \left(\frac{\partial f(\phi,R)}{\partial R}\right)_\phi dR\right\} \qquad (12)$$

From this equation the internal and external equilibrium criteria will be derived.

Internal equilibrium.

From here on we consider a system of water droplets in a continuous oil phase. Water and salt form the aqueous phase and alcohol (cosurfactant) and oil the continuous phase. We require all surfactant to reside at the interface. Together with the assumption that the volume of the surfactant layers can be neglected, our treatment will be less general than that of Overbeek et al.[3]. However the equations will become more transparent and, more important, we found out that the deviations from the 'full' equations are negligible for the kind of systems studied here.

Application of the equilibrium condition, dG=0, to a microemulsion of a given composition (all $dN_i=0$) and neglecting the change in volume due to microemulsion formation (dV=0 and thus $d\phi=0$) to eq.(12) gives

$$\sigma + \frac{2c}{R} + \frac{3k_BT}{4\pi R^2}\left(f(\phi,R) + N_d\left(\frac{\partial f(\phi,R)}{\partial R}\right)_\phi\left(\frac{\partial R}{\partial N_d}\right)_\phi\right) = 0 \qquad (13)$$

since

$$\phi V=\frac{4}{3}\pi R^3 N_d \qquad (14)$$

we find

$$\left(\frac{\partial R}{\partial N_d}\right)_{\phi} = -R/3N_d \qquad (15)$$

Substitution of eq.(15) in eq.(13) leads to the following condition for internal equilibrium

$$\sigma + \frac{2c}{R} + \frac{3k_BT}{4\pi R^2} f(\phi,R) - \frac{k_BT}{4\pi R}\left(\frac{\partial f(\phi,R)}{\partial R}\right)_{\phi} = 0 \qquad (16)$$

External equilibrium: coexistence of a microemulsion and an excess aqueous phase.

We calculate the chemical potentials μ_i of the aqueous components of the microemulsion and find out under which conditions a noncolloidal phase exists with the same chemical potentials. From eq.(12)

$$\mu_i = \left(\frac{\partial G}{\partial N_i}\right)_{T,p,N_{j\neq i}} = \lambda_i + \frac{4}{3}\pi R^2\left(\sigma + \frac{2c}{R} + \frac{3k_BT}{4\pi R^2} f(\phi,R)\right)\left(\frac{\partial N_d}{\partial N_i}\right) +$$

$$+ N_d k_B T\left\{\left(\frac{\partial f(\phi,R)}{\partial \phi}\right)_R\left(\frac{\partial \phi}{\partial N_i}\right) + \left(\frac{\partial f(\phi,R)}{\partial R}\right)_{\phi}\left(\frac{\partial R}{\partial N_i}\right)\right\} \qquad (17)$$

Again neglecting the amount of dissolved surfactant, the adsorption densities of oil and salt and moreover assuming that the aqueous components keep the same molecular volume upon mixing we find

$$\left(\frac{\partial R}{\partial N_i}\right) = \frac{\partial}{\partial N_i}\frac{3V_d}{A} = \frac{3\bar{v}_i}{4\pi R^2 N_d} \qquad (18)$$

$$\left(\frac{\partial\phi}{\partial N_i}\right) = \frac{\bar{v}_i}{V}(1-\phi) = \frac{3\bar{v}_i\phi(1-\phi)}{4\pi R^3 N_d} \qquad (19)$$

$$\left(\frac{\partial N_d}{\partial N_i}\right) = \frac{\partial}{\partial N_i}\frac{A^3}{36\pi V_d^2} = \frac{-3\bar{v}_i}{2\pi R^3} \qquad (20)$$

with $\bar{v}_i$ the molecular volume of component i.
Substituting eqs.(18-20) into (17) and using the criterion for internal equilibrium eq.(16) leads to

$$\mu_i = \lambda_i + \chi\bar{v}_i \qquad (21)$$

with

$$\chi = \frac{3k_BT}{4\pi R^3}\left\{\phi(1-\phi)\left(\frac{\partial f(\phi,R)}{\partial\phi}\right)_R + \frac{R}{3}\left(\frac{\partial f(\phi,R)}{\partial R}\right)_\phi\right\} \qquad (22)$$

Now we derive the external equilibrium condition by stating that the chemical potentials of the components in the (freely translating) droplets and the equilibrium liquid should be equal. We calculate the chemical potential differences of component i between the freely translating droplets, the coexisting aqueous phase and the fixed droplets.

The chemical potentials of the components in the (freely translating) droplets at pressure p+Δp is given by eq.(21). λ_i is the chemical potential of the component i in the fixed droplet with pressure p+Δp. The chemical potential of component i of the fixed droplet at ambient pressure p and the same composition is

$$\mu_i' = \lambda_i + \int_{p+\Delta p}^{p}\left(\frac{\partial\lambda_i}{\partial p}\right)_T dp = \lambda_i - \Delta p\bar{v}_i \qquad (23)$$

Combining this expression with eq.(21) gives

$$\mu_i=\mu_i^{'} + (\Delta p + \chi)\bar{v}_i \qquad (24)$$

the second term in the rhs of eq.(24) represents the work required to bring a unit amount of component i from the freely translating droplets at pressure (p+Δp) to the excess liquid at pressure p. The two phases being in equilibrium, this work is of course zero and therefore we find as the condition for external equilibrium

$$\Delta p + \chi = 0 \qquad (25)$$

Eq. 25 shows that for the droplet components, the rise in chemical potential due to the higher pressure p+Δp is exactly compensated by the decrease caused by the translational freedom of the droplets.

The free energy of mixing.

In Appendix A the free energy of mixing of droplets in a solvent is derived. In the derivation the osmotic pressure Π of the dispersion is given by the Van't Hoff law

$$\Pi=k_BT\rho = k_BT\frac{\phi}{v_d} \qquad (26)$$

with ρ the number density of the droplets and v_d the volume of a droplet. It is assumed that eq.(26) is a good approximation for the low volume fractions of microemulsion droplets we are dealing with in the work presented here. From eq.(26) the chemical potential of the solvent is derived and combined with the chemical potential of the droplets. The final result for G_{mix} is

$$G_{mix}=N_dk_BTf(\phi,R)=N_dk_BT(\ln\phi - 1 - \tfrac{3}{2}\ln(16R^3/\bar{v}_w) \qquad (27)$$

so that, from eq.(11)

$$f(\phi,R)=\ln\phi - 1 - \tfrac{3}{2}\ln(16R^3/\bar{v}_w) \qquad (28)$$

where the last term accounts for the translational fluctuations of the center

of mass of a fixed droplet [7]. In appendix A a thermodynamic argument for such a term is given.

Volume fraction dependence of the droplet radius and interfacial tension of the planar oil-brine interface.

Making use of the internal and the external equilibrium conditions and eq.(28) we will derive an expression for c and σ. Combination with the curvature free energy in terms of the bending elastic moduli then gives an explicit expression for $R(\phi)$. After that we will derive an expression for the interfacial tension of the planar cyclohexane-brine interface in terms of R, ϕ and the bending elastic moduli.

Combining eqs.(10), (22) and (25) we obtain

$$\Delta p = \frac{2\sigma}{R} - \frac{2c}{R^2} = \frac{3k_B T}{8\pi R^3} \qquad (29)$$

using this result and the condition for internal equilibrium, eq.(16), we obtain σ and c separately for a microemulsion in equilibrium with an excess phase

$$\sigma = \frac{k_B T}{4\pi R^2} \left(-\ln\phi + \frac{3}{2}\ln(16R^3/\bar{v}_w)\right) \qquad (30)$$

and

$$c = \frac{k_B T}{4\pi R} \left(-\ln\phi + \frac{3}{2}\ln(16R^3/\bar{v}_w) - 3/4\right) \qquad (31)$$

For a sphere with radius R the curvature free energy F_c in the harmonic approximation is given by [4]

$$F_c = \int \left[2K\left(\frac{1}{R} - \frac{1}{R_0}\right)^2 + \frac{\bar{K}}{R^2}\right] dA \qquad (32)$$

with K the bending elastic modulus, $\bar{K}$ the modulus associated with Gaussian curvature and R_0 the preferred radius of curvature. Now c is immediately obtained by

$$c=\left(\frac{\partial\sigma}{\partial(2/R)}\right)_{T,p,\{\lambda_i\}} = \frac{\partial^2 F_c}{\partial A\,\partial(2/R)} = \frac{1}{\bar{K}}(2K + \bar{K}) - 2K/R_0 \qquad (33)$$

combining eqs.(31) and (33) leads to the volume fraction dependence of the droplet radius $R(\phi)$

$$R(\phi)=R_0\left\{1 + \frac{\bar{K}}{2K} + \frac{k_B T}{8\pi K}\left\{\ln\phi - \frac{3}{2}\ln(16(R(\phi))^3/\bar{v}_w) + \frac{3}{4}\right\}\right\} \qquad (34)$$

$R(\phi)$ depends on two independent linear combinations, $(2K+\bar{K})$ and $2K/R_0$. A negative $\bar{K}$ causes R to be smaller than R_0, as does the ϕ dependent term. Eq.(34) reflects the competition between curvature energy and mixing entropy. The last term tends to lower R thus increasing the number of droplets. Without this term arising from the free energy of mixing, R reduces to the radius obtained by minimizing eq.(32).

The interfacial tension of the planar interface between the coexisting phases, γ, is naturally defined as

$$\gamma=\sigma(R\to\infty,\{\mu_i\}) \qquad (35)$$

This leads to

$$\gamma=\sigma(R,\{\lambda_i\})+\int_{2/R}^{0}\left(\frac{\partial\sigma}{\partial(2/R)}\right)_{T,p,\{\lambda_i\}} d(2/R) + \sum_i \int_{\lambda_i}^{\mu_i}\left(\frac{\partial\sigma}{\partial\mu_i}\right)_{T,p,R\to\infty} d\mu_i \qquad (36)$$

This equation can be simplified using eq.(5) and the Gibbs adsorption equation. The result is

$$\gamma=\sigma(R,\{\lambda_i\})+\int_{2/R}^{0} c\; d(2/R) - \sum_i \Gamma_i(\mu_i-\lambda_i) \qquad (37)$$

where Γ_i denote the surface excess concentration of component i. We will neglect the last term in eq.(37) as it is proportional to the molecular thickness of the surfactant layer.

The integral in eq.(37) is easily calculated by substituting eq.(33) giving

$$\int_{2/R}^{0} c \; d(2/R) = \frac{-1}{R^2}(2K + \bar{K}) + \frac{4K}{R_0 R} \qquad (38)$$

We obtain γ by substituting eq.(34) for R_0 into eq.(38), putting the result in eq.(37) and rearrange it with the expression for σ, eq.(30)

$$\gamma = \frac{1}{R^2}(2K+\bar{K}) + \frac{k_B T}{4\pi R^2}\left\{ \ln\phi - \frac{3}{2}\ln(16R^3/\bar{v}_w) + \frac{3}{2} \right\} \qquad (39)$$

It is interesting to note that upon substituting the relation between R, R_0 and the bending elastic moduli arising from minimising the curvature free energy eq.(32) only, i.e.

$$R = R_0\left(1 + \frac{\bar{K}}{2K}\right) \qquad (40)$$

we get

$$\gamma = \int_{2/R}^{0} c \; d(2/R) = \frac{2K}{R_0 R} \qquad (41)$$

The rhs of this equation is exactly the macroscopic interfacial tension as derived by Robbins [8] and by de Gennes and Taupin [9]. The model used by these authors indeed neglects the free energy of mixing.

In [10,11] expressions for γ are obtained that are different from eq.(39) as well. This will further be discussed in section 6.

4.3. Polydispersity.

The treatment presented here is analogous to the one of Overbeek [5]. Particle categories are defined and their chemical potentials are calculated from the Gibbs free energy of the system. These are compared with the mass action law from which the size distribution follows. We will again use the simplifications as discussed in the previous section. The size distribution function is explicitly expressed in terms of the curvature elastic quantities K, $\bar{K}$ and R_0.

The Gibbs free energy of the droplet type microemulsion system can be written as

$$G=\sum_i N_i\mu_i = \sum_i N_{im}\mu_i + \sum_j N_{dj}\mu_{dj} \qquad (42)$$

where N_{im} are the amounts of components i in the continuous medium and N_{dj} and μ_{dj} are the number of droplets of category j and their chemical potential. We will specify j later. All droplet categories have different R_j, V_{dj}, A_j, Δp_j, σ_j and c_j so that the Gibbs free energy may also be written in analogy with eq.(12)

$$G= \sum_i N_{im}\lambda_{im} + \sum_i \sum_j N_{ij}\lambda_{ij} + \sum_j \frac{4}{3}\pi R_j^2 N_{dj}\left(\sigma_j + \frac{2c_j}{R_j}\right) + k_BT\sum_j N_{dj} f(\phi_j,R_j) \qquad (43)$$

with

$$f(\phi_j,R_j)=\ln\phi_j - 1 - \frac{3}{2}\ln(16R_j^3/\bar{v}_w) \qquad (44)$$

and

$$\phi_j=\frac{4}{3}\pi N_{dj}R_j^3/V \qquad (45)$$

For the components in the continuous medium we now find

$$\mu_i=\left(\frac{\partial G}{\partial N_{im}}\right)_{T,p,N_{jm\neq im}} = \lambda_{im} - k_BT\frac{\sum_j N_{dj}}{V}\bar{v}_i \qquad (46)$$

thus

$$\sum_i N_{im}\mu_i = \sum_i N_{im}\lambda_i - k_B T(1-\phi)\sum_j N_{dj} \qquad (47)$$

From eqs.(43-45) and (47) we have

$$\mu_{dj} = \sum_i \frac{N_{ij}\lambda_{ij}}{N_{dj}} + \frac{4}{3}\pi R_j^2\left(\sigma_j + \frac{2c_j}{R_j}\right) + k_B T\left(\ln\phi_j - \phi - \frac{3}{2}\ln(16R_j^3/\bar{v}_w)\right) \qquad (48)$$

The λ's of the droplet components are related to the chemical potentials

$$\lambda_{ij} = \mu_i + \Delta p_j \bar{v}_i = \mu_i + \left(\frac{2\sigma_j}{R_j} - \frac{2c_j}{R_j^2}\right)\bar{v}_i \qquad (49)$$

in analogy with eqs.(33) and (37), c_j and σ_j can be expressed as

$$c_j = \frac{1}{\bar{R}_j}(2K+\bar{K}) - 2K/R_0 \qquad (50)$$

$$\sigma_j = \sigma_\infty + \frac{(2K+\bar{K})}{R_j^2} - \frac{4K}{R_0 R_j} \qquad (51)$$

σ_∞ depends on the total area and droplet volume fraction. Substituting eqs.(49-51) into (48), using

$$\sum_i \frac{N_{ij}}{N_{dj}}\bar{v}_i = \frac{4}{3}\pi R_j^3 \qquad (52)$$

for the water components, and writing μ_{dj} as the sum of the chemical potentials of the constituent molecular components, known as the law of mass action

$$\mu_{dj} = \sum_i \frac{N_{ij}}{N_{dj}}\mu_i \qquad (53)$$

we arrive at the category distribution

$$\ln \frac{N_{dj}}{V} = \ln \frac{48R_j^{3/2}}{\pi \bar{v}_w^{3/2}} - \frac{4\pi}{k_B T}\left\{(2K+\bar{K}) - \frac{4KR_j}{R_0} + R_j^2 \sigma_\infty\right\} \quad (54)$$

Interestingly, just as the volume fraction dependence of the droplet size, the category distribution is determined by two independent linear combinations of curvature elastic parameters, $(2K+\bar{K})$ and $2K/R_0$.

Taking into account size (and no shape) fluctuations only, a natural choice for the droplet categories j is the number of surfactant molecules per droplet or

$$j=4\pi R_j^2/\sigma_s \quad (55)$$

with σ_s the molecular area occupied by a surfactant molecule.

4.4. Experimental.

Materials

Sodium dodecyl sulfate (SDS) was 'specially pure' grade from BDH. Cyclohexane, 1-pentanol, 1-hexanol and NaCl were Baker 'analyzed' reagents. Deionized water was doubly distilled before use.

Sample preparation

The series of Winsor II equilibria were prepared by carefully pouring 16.00 g initial oil phase on 20.00 g initial water phase. The water phase was composed of 0.20M NaCl and various amounts of SDS. The oil phase consisted of cyclohexane and various amounts of pentanol or hexanol. Equilibrium was attained by gently rolling the samples on a roller bench for several days. Subsequently the samples were permitted to equilibrate at constant temperature ($(25 \pm 0.1)^\circ$C). The amount of alcohol in the oil phase was corrected for the uptake in the SDS-alcohol monolayer at the cyclohexane-brine interface. This correction was determined from dilution titrations [12]. In the pentanol system 3.12 additional alcohol molecules and in the hexanol system 1.77 additional molecules per SDS molecule were added. Apparently the

cosurfactant/surfactant ratios in the curved monolayer are different from the ones in the planar monolayer [13]. This was also observed by van Aken [14] who showed (using synchrotron SAXS) that the molecular area of SDS in the droplet interface remains equal to the one in the planar interface. The 'free' cosurfactant concentrations (i.e. the concentration without SDS) were chosen such as to obtain a mean droplet radius of approximately 15nm corresponding to 18.2% (w/w) pentanol and 8.8% (w/w) hexanol initially in the oil phase.

Determination of the droplet radius from the water content and Small Angle X-ray Scattering.

The droplet radii were determined from the water content in the oil phase using Karl-Fisher titrations and from Small Angle X-Ray Scattering (SAXS). The total area in the system is known from the amount of SDS by $A=N_s\sigma_s$ with N_s the number of surfactant molecules in the system corrected for the cmc [13] so from the water content, V_w, we obtain the radius

$$R_w=3V_w/A=\langle R^3\rangle/\langle R^2\rangle \qquad (56)$$

SAXS measurements were made with an 'Anton Paar' Kratky camera. The apparatus is described in more detail in [15].

In a system of diluted particles, the radius of gyration R_g is obtained from the scattered intensity I(q) measured with SAXS at low scattering vector q [16]

$$I(q\to 0)=I(q=0)\exp(-q^2R_g^2/3) \qquad (57)$$

In case of a (dilute) polydisperse system of spherosymmetrical particles, the scattered intensity is the sum of the intensities scattered by all particle categories. The experimentally determined R_g is an average over all particles but it reflects a different moment of the size distribution compared to the radius R_w. As shown e.g. by Moonen et al.[17] for homogeneous particles

$$R_g^2 = \frac{3}{5}\frac{\langle R^8\rangle}{\langle R^6\rangle} \qquad (58)$$

The microemulsion droplets studied here are not homogeneous but contain a layer of surfactant molecules. Because of the high electron density of the

sulphate groups, these shells contribute significantly to the scattered intensity. In Appendix B we derive R_g of a polydisperse ensemble of particles with a shell. The result is

$$R_g^2=\frac{3}{5}\left(\frac{(\rho_1-\rho_2)^2\langle R_1^8\rangle + (\rho_1-\rho_2)(\rho_2-\rho_s)(\langle R_1^3R_2^5\rangle+\langle R_1^5R_2^3\rangle) + (\rho_2-\rho_s)^2\langle R_2^8\rangle}{(\rho_1-\rho_2)^2\langle R_1^6\rangle + 2(\rho_1-\rho_2)(\rho_2-\rho_s)\langle R_1^3R_2^3\rangle + (\rho_2-\rho_s)^2\langle R_2^6\rangle} \right) \tag{59}$$

where R_1 and R_2 are the radii of the water core and the water core plus coated layer and ρ_1, ρ_2 and ρ_s are the electron densities of the inner (water) core, the surfactant layer and the solvent. The electron densities are calculated from the densities of the constituting molecules and their number of electrons. It is assumed that the electron densities of the hydrocarbon tails of the adsorbed SDS and cosurfactant molecules are not significantly different from the electron density of the oil phase. The electron density ρ_2 of the polar part of the surfactant shell is determined by the molecular area of SDS σ_s and by the shell thickness $d=R_2-R_1$ via

$$\rho_2=\frac{N_e/\sigma_s}{d}+\rho_1 \tag{60}$$

where N_e denotes the number of excess electrons of a sulphate group relative to the number of electrons of water. Eq.(60) implies that increasing d is analogous to diluting the outer layer with water phase. The contribution of the cosurfactant adsorption to the electron density is neglected as in the model used, space is filled with water having about the same electron density as a hydroxy group. Fortunately, performing model calculations it turns out that R_g (and even the full form factor) is hardly affected when d is varied between 0.1 and 1.0 nm (and conservation of matter is taken into account by decreasing R_1 upon increasing d).

4.5. Results

4.5.1 Analysis of the volume fraction dependence of the droplet size and interfacial tensions with monodisperse theory.

It is clear from the different droplet radii obtained from SAXS measurements and from the water content (see section 4.5.2) that the systems studied are polydisperse. In this section we nevertheless analyze our data with the monodisperse theory presented in section 2 thus assuming that the droplet radius R in this theory may be substituted by $R_w=\langle R^3\rangle/\langle R^2\rangle$.

Volume fraction dependence of the droplet size.

The volume fraction dependences of the droplet radius for the pentanol and the hexanol systems are given in fig.1.

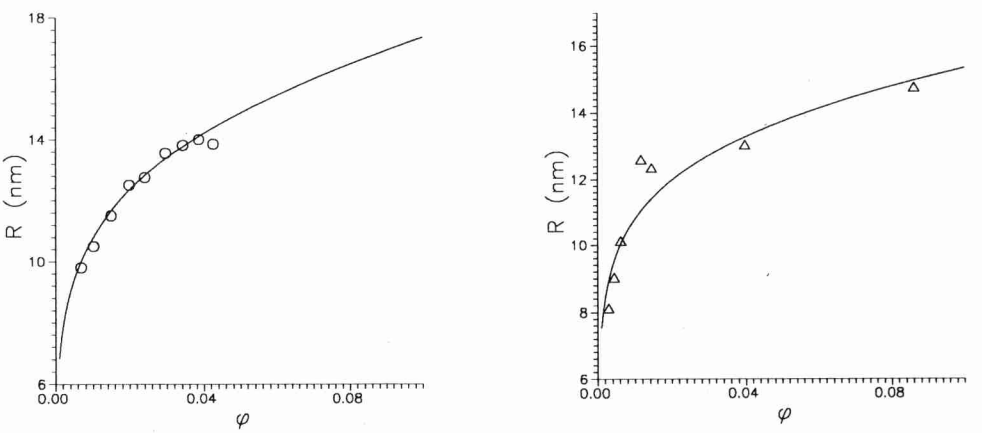

Figure 1. Experimentally determined droplet radius as a function of the droplet volume fraction. Solid lines are best fit lines to eq.(34). Pentanol system (fig.1a, left) and hexanol system (fig.1b, right).

Droplet radii as well as volume fractions are obtained from the water content (Karl-Fisher titration) and the (droplet) area in the system using values of the molecular area of SDS and the critical micel concentration as reported in

[13].

The SAXS measurements were performed using a Cu tube as an X-ray source so that the scattered intensity was too low to permit a reliable determination of the radius of gyration below droplet volume fractions of about 0.02. Consequently the volume fraction dependence of the droplet radius as observed with SAXS is hardly significant.

Best fits to eq.(34) are represented by solid lines in the figures. Best fit results $(2K+\bar{K})$ and $2K/R_0$ are summarized in Table 1. The difference in $(2K+\bar{K})$ for the pentanol and the hexanol system is very small: $(0.14\pm0.08)k_BT$, whereas the values of $2K/R_0$ differ considerably. The errors in these values are however large.

TABLE 1. Values of $(2K+\bar{K})$ and $2K/R_0$ for the pentanol and hexanol systems from best fits to eq.(34).

SYSTEM	$(2K+\bar{K})/k_BT$	$2K/R_0(k_BT/nm)$
pentanol	1.95 ± 0.014	0.0048 ± 0.010
hexanol	2.09 ± 0.069	0.0170 ± 0.025

Interfacial tensions.

Droplet radii and interfacial tensions of the planar oil-brine interface in a similar system with pentanol as cosurfactant are taken from [14]. From this work we also deduced the volume fractions of the droplets and obtained $(2K+\bar{K})$ and $2K/R_0$ being $2.23k_BT$ and $0.053k_BT/nm$, respectively. These values are different from the ones presented in the previous section which may be caused by the higher pentanol concentration as used in [14] (being 0.20 w/w initial in the oil phase which leads to a smaller R_0) and/or the use of a different batch of SDS.

In fig.2 the droplet radii and the (experimental and calculated) interfacial tensions are presented as a function of the droplet volume fraction. The interfacial tensions are calculated from eq.(39) with $(2K+\bar{K})$ obtained by fitting $R(\phi)$ to eq.(34). Although the calculated interfacial tensions are systematically somewhat smaller than the experimental ones the discrepancy can be completely attributed to the experimental uncertainty of the droplet radii (leading to an uncertainty in $(2K+\bar{K})$).

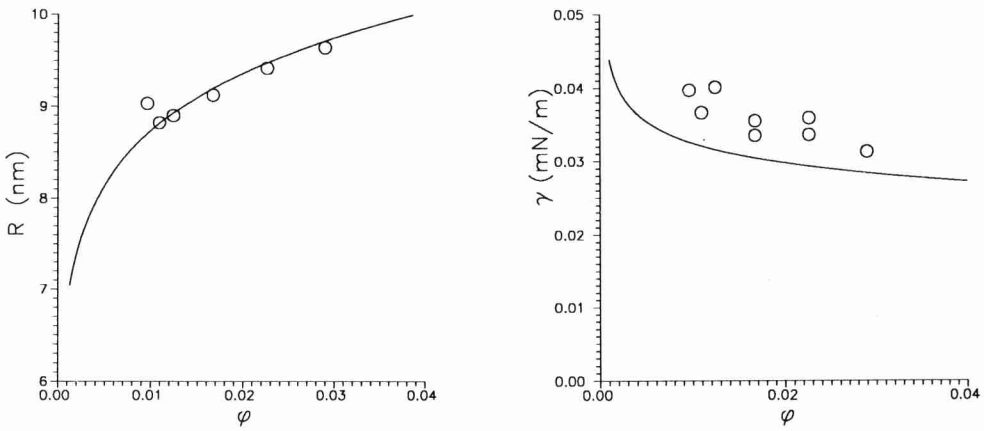

Figure 2. Data obtained from van Aken [14]. The droplet radius as a function of the volume fraction (fig.2a, left) and the interfacial tension as a function of the volume fraction (fig.2b, right). The solid line in fig.2b is calculated from eq.(39) using curvature elastic parameters obtained from fitting the datapoints in fig.2a to eq.(34).

4.5.2 Polydispersity of the droplet size.

From eq.(54) it follows that the droplet size distribution is determined by the 3 parameters $(2K+\bar{K})$, $2K/R_0$ and σ_∞. The first two are obtained from the volume fraction dependence of the droplet radii (see previous section). Then size distributions are generated and σ_∞ is adjusted until both $R_w=\langle R^3\rangle/\langle R^2\rangle$ and $\phi=\sum_j \phi_j$ are as good as possible in agreement with experimentally obtained (R_w,ϕ) pairs. In order to reproduce the experimental results more closely, it appeared to be necessary to slightly adjust the values of $2K/R_0$ and/or $(2K+\bar{K})$. These values are listed in Table 2. Size distributions for the pentanol and the hexanol system are shown in fig.3.

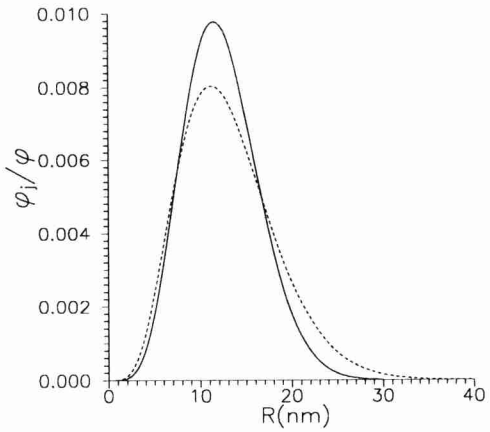

Figure 3. Calculated size distributions (eq.(54)) ϕ_j/ϕ versus R *at* ϕ=0.024 *for the pentanol system (solid line) and the hexanol system (dashed line). Values of* σ_∞ *of* 0.000941 k_BT/nm^2 *(pentanol) and* 0.00018 k_BT/nm^2 *(hexanol) were used. The values of the other parameters (*(2K+$\bar{K}$) and $2K/R_0$*) are listed in Table 2.*

Keeping the values of $2K/R_0$ and (2K+$\bar{K}$) fixed the experimentally observed range of (R_w,ϕ) values could excellently be reproduced by varying σ_∞ only. Moreover R_g was calculated from eq.(59) and the size distributions (eq. (54)). This is shown in figs.4a and 5a. The size distributions corresponding to the calculated radii are obtained by varying σ_∞ in a way as shown in figs. 4b and 5b. The somewhat different values of R_w in figs. 4a and 5a compared to the ones shown in fig.1 is due to the fact that different series of samples were used.

The polydispersity ε, given in Table 2, is calculated from the size distribution via

$$\varepsilon^2 = \frac{\langle R^2 \rangle - \langle R \rangle^2}{\langle R \rangle^2} \qquad (61)$$

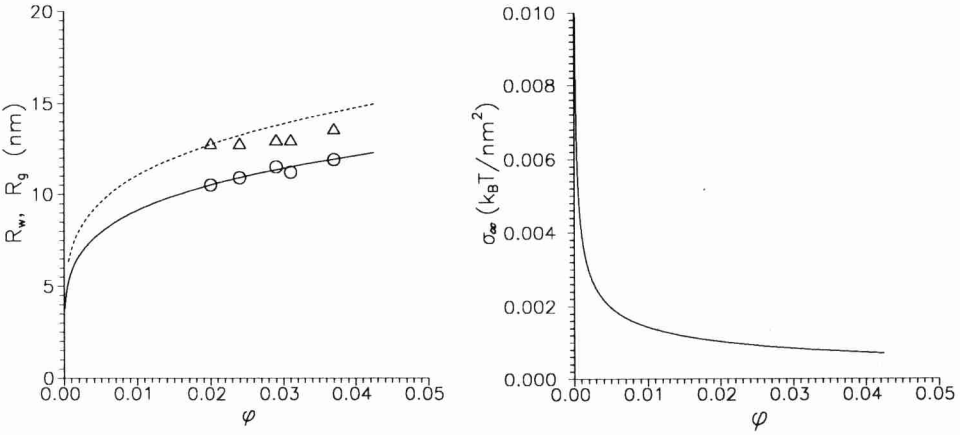

Figure 4a, left. Experimental (points) and calculated (lines) R_w *(circles and solid lines) and* R_g *(triangles and dashed lines) versus* ϕ *for the pentanol system. Experimental* R_w *and* R_g *are obtained from the water content and SAXS. The lines are calculated from the size distribution eq.(54) using eqs. (56) and (59). The size distributions are generated by varying* σ_∞ *in the way as shown in fig.4b, right.*

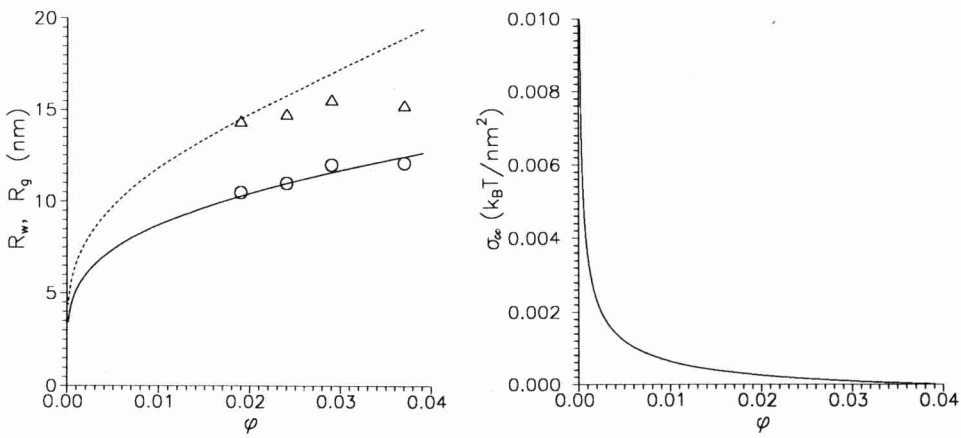

Figure 5. Same as fig.4 but now for the hexanol system.

We also obtained a polydispersity by using a lognormal size distribution which was iteratively generated and made to converge to a distribution satisfying both the experimentally obtained R_w and R_g. This polydispersity appeared to be a slightly decreasing function of the volume fraction. The mean values are listed in Table 2.

TABLE 2. Values of $(2K+\bar{K})$, $2K/R_0$ and the polydispersity ε obtained from adjusting the droplet size distribution eq.(54) to experimental (R_w,ϕ) pairs. The (mean) polydispersity calculated from a lognormal distribution, ε_{ln}, is also given.

SYSTEM	$(2K+\bar{K})/k_BT$	$2K/R_0(k_BT/nm)$	ε	ε_{ln}
pentanol	2.055	0.0048	0.50	0.32
hexanol	1.960	0.0140	0.62	0.41

4.6. Discussion and Conclusions

From figs. 1 and 2a it follows that the droplet size in a Winsor II microemulsion system significantly depends upon the droplet volume fraction. This dependency is correctly described by eq.(34) and is interpreted as a manifestation of the competition between mixing entropy (which tends to increase the number of droplets thus decreasing their size) and curvature energy (preferring a constant radius as described by eq.(40)). When the droplet size dependence is known (or, more specifically, when $(2K+\bar{K})$ is known) the interfacial tension can be calculated leading to satisfactory agreement with experiments.

As the logarithmic term in the mixing free energy eq.(27) is model dependent we consider the absolute values of $(2K+\bar{K})$ and of $2K/R_0$ as presented in Table 1 only approximately correct. We may nevertheless compare the values of $(2K+\bar{K})$ as obtained for the two systems studied here and it follows from table 1 that their difference is very small. By comparing the values of K as obtained by ellipsometry [18] we deduce $\bar{K}$ being $(0.15\pm0.2)k_BT$ for the pentanol system and $(-0.11\pm0.2)k_BT$ for the hexanol system. So apparently $\bar{K}$ decreases upon replacing hexanol for pentanol as a cosurfactant but the errors are large, which is mainly caused by the large errors in K. The positive value for the pentanol system is doubtful from the point of view that the saddle splay

modulus is the negative second moment of the lateral pressure profile which is expected to be for the most part larger than zero [19,20].

In [10,11] $(2K+\bar{K})$ is determined from sets of R, ϕ and γ using an equation equal to eq.(39) up to the first term between the curly brackets. The other terms are absent [10] or different [11] in their analysis leading to a serious difference of $(2K+\bar{K})$ as determined from eq.(39).

The polydispersity was calculated from the size distribution eq.(54) obtained from single sets of experimental (ϕ,R_w) values and (slightly adjusted) parameters obtained from the 'monodisperse analysis'. At the lowest volume fractions, this leads to radii of gyration that are in excellent agreement with the experimental values (figs. 4a and 5a). At higher volume fractions a small but increasing difference between theory and experiments is observed as a function of the volume fraction. Model calculations reveal that this difference may (at least in part) be attributed to the influence of the structure factor upon the experimentally determined radius of gyration. From Table 2 and fig.3 it follows that the polydispersity is large and even larger for the hexanol system. This trend is in agreement with the larger difference between the experimental R_w and R_g for the hexanol system (figs.4a and 5a), and with the polydispersity calculated using a lognormal size distribution.

Acknowledgements.

The authors are grateful to Agnes Peels for performing preliminary work on volume fraction dependence of the droplet size. H.N.W.L and W.K. acknowledge enlightening discussions with Theo Overbeek and W.K. thanks Ger Koper for discussions and correspondence. Gert - Jan Vroege is thanked for a critical reading of the manuscript and for some useful suggestions.

Appendix A. Calculation of the free energy of mixing droplets with a solvent.

In the following we present a very simple derivation of the free energy of mixing assuming ideal behaviour of the droplets instead of using the Carnahan-Starling equation of state [3] being appropriate for the low volume fractions we are dealing with here. After that it is shown that the expression for the free energy of mixing obtained in this way is plausible within the droplet microemulsion model under consideration.

The free energy change G_{mix} of mixing droplets composed of (pseudo)

component 2 with a solvent (component 1), is

$$G_{mix}=N_1(\mu_1-\mu_1^{\circ}) + N_d(\mu_d - n_2\mu_2^{\circ}) \qquad (A1)$$

with N_1 the number of solvent molecules, μ_1 the chemical potential of the solvent, μ_i° the standard chemical potential of component i, N_d the number of droplets, μ_d the chemical potential of a droplet and n_2 the number of molecules of (pseudo) component 2 per droplet.

The relation between the chemical potential μ_1 and the osmotic pressure Π is

$$\mu_1=\mu_1^{\circ} - \Pi\bar{v}_1 \qquad (A2)$$

with $\bar{v}_1$ the molecular volume of the solvent. Π is model dependent. As we are dealing with low volume fractions of droplets we assume the ideal equation of state

$$\Pi=k_BT\rho=k_BT\frac{N_d}{V} \qquad (A3)$$

with ρ the number density of the droplets. Again assuming ideal behaviour, μ_d is

$$\mu_d =\mu_d^0 + k_BT\ln\phi \qquad (A4)$$

where μ_d^0 is the standard chemical potential being different from $n_2\mu_2^{\circ}$:

$$\mu_d^0=n_2\mu_2^{\circ} + \psi \qquad (A5)$$

According to the treatment of Reiss [7] the difference between μ_d^0 and $n_2\mu_2^{\circ}$ can be attributed to the translational freedom of the center of mass of a fixed droplet. His analysis leads to [3]

$$\psi= -\frac{3}{2}\ln(16R^3/\bar{v}_w) \qquad (A6)$$

with $\bar{v}_w$ the molecular volume of water. At low ϕ, $N_1\bar{v}_1/V \cong 1$ and thus

$$G_{mix}=k_BTN_d(\ln\phi - 1 - \frac{3}{2}\ln(16R^3/\bar{v}_w)) \qquad (A7)$$

There is no unanimity about the choice of ψ in the literature. Several choices are discussed in [3]. Our aim is now to compare the expression for G_{mix} as obtained here with the free energy associated with the 'liberation' of droplets from their fixed position to droplets moving in the whole volume V. This free energy is

$$G_{lib}= \sum_i N_i(\mu_i-\lambda_i) \qquad (A8)$$

It is convenient to express G_{mix} as

$$G_{mix}=N_dk_BTf(\phi,R) \qquad (A9)$$

$$f(\phi,R)=\ln\phi -1 + \psi \qquad (A10)$$

Let us leave ψ unspecified for the moment.
With eq.(21) for the aqueous components and for the oil components using

$$\mu_i= \lambda_i - \Pi\bar{v}_i \qquad (A11)$$

we write eq.(A8) as

$$G_{lib}= \chi\sum_{i=NaCl,w} N_i\bar{v}_i - \Pi\sum_{j=co,oil} N_j\bar{v}_j \qquad (A12)$$

$$\text{since } \sum_{i=NaCl,w} N_i\bar{v}_i = N_dv_d \quad \text{and} \qquad (A13)$$

$$\sum_{j=co,oil} N_j\bar{v}_j=V_m=N_d\frac{1-\phi}{\phi}v_d \qquad (A14)$$

working out eq.(A12) by substituting eqs.(A13-A14), χ given by eq.(22) and Π by (A3) using $\rho=\phi/v_d$ gives

$$G_{lib}=k_BTN_d\frac{R}{3}\left(\frac{\partial f(\phi,R)}{\partial R}\right)_{\phi}=k_BTN_d\frac{R}{3}\frac{\partial\psi}{\partial R} \qquad (A15)$$

If $f(\phi,R)$ would be a function of ϕ only, G_{lib} vanishes implying that the Gibbs free energy does not change upon liberating droplets from their fixed positions. This is considered to be unrealistic. In order to obtain an expression of ψ via this approach it is necessary to calculate G_{lib} in another way. At the moment it is not clear to us how to perform such a calculation. Therefore we insert our earlier choice $\psi=-\frac{3}{2}\ln(16R^3/\bar{v}_w)$ into eq.(A15) and obtain

$$G_{lib}=-\frac{3}{2}N_dk_BT \qquad (A16)$$

being physically plausible considering that G_{lib} should be (a) negative and (b) extensive. We conclude from this analysis that in the mixing free energy a term logarithmic in R should be present in order to be consistent with the model presented by Overbeek [3]. The choice of ψ following from the analysis of Reiss [7] meets this requirement.

Appendix B. Calculation of the Guinier Radius of gyration of an ensemble of polydisperse particles with a shell.

At low scattering vector q the radius of gyration R_g for a single particle is conveniently defined by [16]

$$\frac{I(q\to 0)}{I(q=0)}=\exp\left(\frac{-q^2R_g^2}{3}\right) \qquad (B1)$$

with I(q) the scattered intensity at scattering vector q. In dilute systems the normalized scattering intensity of an ensemble of particles is to a good approximation the sum of the intensities scattered by all particle categories [21]

$$I(q)=\sum_i n_i B_i^2(q) \qquad \text{(B2)}$$

where $B_i(q)$ denotes the scattering amplitude of a particle of category i and n_i the number of particles i per unit volume. Now n_i is just the probability to find a particle of category i, p_i, times the number of all particles per unit volume n

$$n_i=p_i n \qquad \text{(B3)}$$

we assume that the particles i only differ in their radius R so $p_i:=p(R_i)$. The scattering amplitude is given by [21]

$$B_i(q)=\int_{particle\ i} d^3r[\rho(\mathbf{r})-\rho_s]e^{i\mathbf{q}.\mathbf{r}} \qquad \text{(B4)}$$

the difference $\rho(\mathbf{r})-\rho_s$ is the local contrast with respect to the solvent. For a spherosymmetrical ensemble of particles with a single shell of thickness $R_{2,i}-R_{1,i}$ with R_1 the radius of the inner core and R_2 the radius of the whole particle it follows from eqs.(B4) and (B2)

$$I(q=0)=\frac{16\pi^2 n}{9}\left((\rho_1-\rho_2)^2\langle R_1^6\rangle+2(\rho_1-\rho_2)(\rho_2-\rho_s)\langle R_1^3R_2^3\rangle+(\rho_2-\rho_s)^2\langle R_2^6\rangle\right) \qquad \text{(B5)}$$

with ρ_1 and ρ_2 the scattering density of the inner core and the outer layer and

$$\langle R^n\rangle=\sum_i p(R_i)R_i^n \qquad \text{(B6)}$$

At finite q we can write

$$I(q)=n\sum_i p(R_i)[4\pi((\rho_1-\rho_2)f(q,R_{1,i}) + (\rho_2-\rho_s)f(q,R_{2,i}))]^2 \qquad \text{(B7)}$$

with

$$f(q,R)=[\sin(qR) - qR\cos(qR)]/q^3 \qquad (B8)$$

at small q, more precisely when qR<1 we may expand eq.(B8)

$$f(qR<1,R)=\frac{1}{3}(R^3 - \frac{1}{10} q^2R^5) \qquad (B9)$$

substituting eqs.(B9) into (B7) and using (B5) we get, after some algebra,

$$\frac{I(q\to 0)}{I(q=0)} = 1 -$$

$$\frac{q^2}{5}\left(\frac{(\rho_1-\rho_2)^2\langle R_1^8\rangle + (\rho_1-\rho_2)(\rho_2-\rho_s)(\langle R_1^3R_2^5\rangle+\langle R_1^5R_2^3\rangle) + (\rho_2-\rho_s)^2\langle R_2^8\rangle}{(\rho_1-\rho_2)^2\langle R_1^6\rangle + 2(\rho_1-\rho_2)(\rho_2-\rho_s)\langle R_1^3R_2^3\rangle + (\rho_2-\rho_s)^2\langle R_2^6\rangle} \right) + \ldots \qquad (B10)$$

Comparing eqs.(B10) and (B1) (and recognizing the Taylor expansion of the exponent) gives

$$R_g^2=\frac{3}{5}\left(\frac{(\rho_1-\rho_2)^2\langle R_1^8\rangle + (\rho_1-\rho_2)(\rho_2-\rho_s)(\langle R_1^3R_2^5\rangle+\langle R_1^5R_2^3\rangle) + (\rho_2-\rho_s)^2\langle R_2^8\rangle}{(\rho_1-\rho_2)^2\langle R_1^6\rangle + 2(\rho_1-\rho_2)(\rho_2-\rho_s)\langle R_1^3R_2^3\rangle + (\rho_2-\rho_s)^2\langle R_2^6\rangle} \right) \qquad (B11)$$

being the radius of gyration of an ensemble of polydisperse particles with a shell.

References.

[1] Hoar,T.P. and Schulman, J.H., Nature **152**, 102, (1943).

[2] Winsor,P.A., Trans.Faraday Soc.**44**, 376, (1948)

[3] Overbeek, J.Th.G., Verhoeckx, G.J., de Bruyn, P.L., and Lekkerkerker, H.N.W., J.Coll.Interface Sci. **119**, 422, (1987).

[4] Helfrich,W., Z.Naturforsch. **c28**, 693, (1973).

[5] Overbeek,J.Th.G., Progr.Colloid Polym.Sci. **83**, 1, (1990).

Overbeek, J.Th.G. in 'Surfactants in solution' Vol.11, K.L.Mittal and D.O.Shah (ed.), Plenum Press New York/London, 1991,p.3.

[6] Rowlinson, J.S. and Widom,B., 'Molecular theory of capillarity', (Oxford 1989).

[7] Reiss, H., J.Coll.Interface Sci.**53**, 61, (1975).

[8] Robbins,M.L. in 'Micellization, Solubilization and Microemulsions', Vol.2, K.L.Mittal (ed.), Plenum Press New York, 1977, p.273.

[9] De Gennes, P.G. and Taupin,C., J.Phys.Chem.**86**, 2294, (1982).

[10] Langevin,D., Adv.Coll.Interface Sci.**34**, 583, (1991).

[11] Kellay,H., Meunier,J. and Binks,B.P., Phys.Rev.Lett.**70**, 1485, (1993).

[12] Verhoeckx, G.J., de Bruyn, P.L., and Overbeek, J.Th.G., J.Coll.Interface Sci.**119**, 409, (1987).

[13] Kegel,W.K., Aken, G.A.van, Bouts,M.N., Lekkerkerker, H.N.W., Overbeek, J.Th.G. and de Bruyn, P.L., Langmuir **8**, 152, (1993); Chapter 2 of this thesis.

[14] Aken, G.A.van, Thesis Rijksuniversiteit Utrecht (1990).

[15] Kegel, W.K. and Lekkerkerker, H.N.W., accepted by J.Phys.Chem. and Chapter 5 of this thesis.

[16] Kerker,M., 'The scattering of light and other electromagnetic radiation' Academic Press, New York, (1969).

[17] Moonen,J., Pathmamanoharan,C. and Vrij,A., J.Coll.Interface Sci. **131**, 349, (1989).

[18] Chapter 3 of this thesis.

[19] Helfrich,W., in Les Houches, Session XXXV, 1980, 'Physics of Defects', R.Balian et.al. eds., North Holland, Amsterdam 1981, p.715.

[20] Szleifer,I., Kramer,D., Ben-Shaul,A., Gelbart,W.M. and Safran,S.A., J.Chem.Phys. **92**, 6800, (1990).

[21] Guinier,A. and Fournet,G., 'Small Angle Scattering of X-rays', Wiley, New York, (1955).

CHAPTER 5

COMPETITION BETWEEN A LAMELLAR AND A MICROEMULSION PHASE IN AN IONIC SURFACTANT SYSTEM.

Willem K.Kegel and Henk N.W.Lekkerkerker.

Van't Hoff Laboratory, University of Utrecht, Padualaan 8, 3584 CH Utrecht, The Netherlands.

Abstract

An experimental study of a microemulsion system consisting of equal volumes of brine (water plus salt) and oil (cyclohexane), sodium dodecyl sulfate (SDS) as surfactant and a mixture of hexanol and pentanol as cosurfactant is presented. Upon increasing the hexanol fraction in the cosurfactant mixture a competition between the (disordered) microemulsion phase and a lamellar phase at vanishing spontaneous curvature is observed culminating in 4 phase brine - lamellar phase - microemulsion phase -oil coexistence. A SAXS study of the lamellar phases is presented. Although a rather high salt concentration was used (0.2M NaCl), several indications for the presence of electrostatic repulsion between the lamellae are found. When the dispersion size ξ of the middle phase microemulsion exceeds the value of approximately 70 nm the lamellar phase becomes stable in the presence of excess oil and water. A similar dispersion size is estimated for a nonionic surfactant system where the lamellar phase is close to the 3 phase body [M.Kahlweit, R.Strey, and P.Firman, J.Phys.Chem.**90**,671,(1986)]. The experimentally observed phase behaviour is compared with a phenomenological theory [D.Andelman, M.E.Cates, D.Roux, and S.A.Safran, J.Chem.Phys. **87**, 7229, (1987)]. It appears that the theory qualitatively correctly describes the competition between the microemulsion and the lamellar phase. However quantitatively there is a difference between theory and experiment which is attributed to the effect of a negative Gaussian bending elastic modulus.

5.1 Introduction

Microemulsions are dispersions of water and oil into one another stabilized by one or more surfactants. They differ markedly from molecular solutions as oil and water are found in domains of order one to ten nanometer in size. This results in an extensive oil-water interface covered with a monolayer of adsorbed surfactant molecules. Commonly observed structures of the oil and water domains range from water droplets in oil or *vice versa* at asymmetric water-oil ratios to bicontinuous and liquid crystalline at comparable volume fractions. The latter are usually found at relatively high amounts of surfactant (more than a few weight percent). In the last few years much work has been done on the phase behaviour of microemulsion systems, experimental (for reviews see refs. [1,2]) as well as theoretical [3-8]. An impressionistic representation of the phase diagram corresponding to equal volumes of water and oil is presented in fig.1.

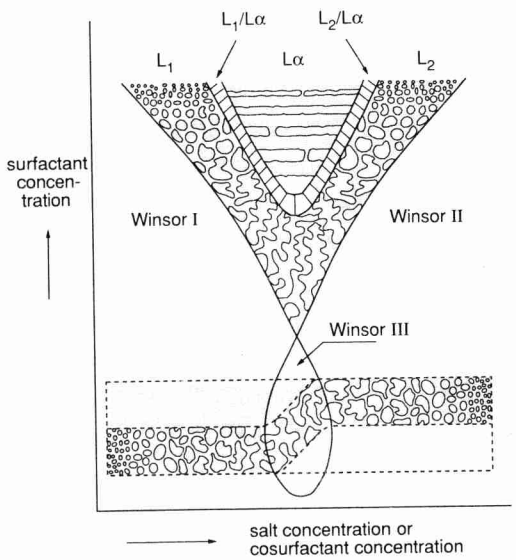

Fig.1. Schematic representation of a typical phase diagram of a microemulsion system at an oil/water ratio equal to 1. After Strey [9] and van Aken [10].

Fig.1 shows the characteristic 'fish' shape. The cosurfactant or salt concentation (in case of ionic surfactants) tunes the curvature of the

surfactant monolayer. At low surfactant concentrations and increasing cosurfactant/salt concentration the (continuous) phase transitions Winsor I (oil droplets in water in equilibrium with excess oil) - Winsor III (present in the 'body of the fish'; a middle phase microemulsion coexisting with both water and oil) - Winsor II (water droplets in oil in equilibrium with excess water) are observed. Increasing the surfactant concentration starting in the body of the fish leads to an increase of the middle phase volume at the expense of the oil and water phases and eventually gives rise to a monophasic microemulsion system. Upon further increase of the surfactant concentration a first order transition to a lamellar phase may occur. In 3 component systems consisting of oil, water and a nonionic surfactant (usually referred to as 'nonionics') the role of salt and/or cosurfactant is replaced by the temperature [1].

One of the thermodynamic models of microemulsion phase behaviour is based upon the 'phenomenological' approach [5,6] which was initiated by Talmon and Prager [3] and further developed by de Gennes and coworkers [4]. In this approach the surfactant monolayer is considered as an incompressible two dimensional fluid separating oil and water regions. The phase behaviour of the system is determined by the curvature energy of the monolayers and the entropy of mixing of the oil and water domains. At an oil water ratio of about one and without any tendency of the surfactant monolayer to curve either towards water or towards oil (i.e. zero spontaneous curvature) these models predict a competition between a microemulsion (bicontinuous) phase and a lamellar liquid crystalline phase.

In this paper we report an experimental study concerning this microemulsion - lamellar phase competition in a system composed of brine (water plus salt), cyclohexane, sodium dodecyl sulfate (SDS), as surfactant and pentanol/hexanol cosurfactant mixtures. Upon increasing the hexanol fraction in the system the lamellar phase becomes stable at increasingly lower surfactant concentration. This trend eventually leads to a penetration of the lamellar phase into the 3 phase body giving rise to an intricate phase behaviour including a 4 phase equilibrium brine, lamellar phase, microemulsion phase, oil [11,12]. The dispersion size ξ and the interlamellar distance D in the microemulsion- and lamellar phases obtained from the compositions and from SAXS measurements are discussed. Interestingly the lengthscale ξ in the microemulsion phase in the 4 phase equilibrium is close to the one in a nonionic system where the lamellar

phase closely approaches the 3 phase body [13]. In the next section we will summarize some aspects of the phenomenological model that are relevant for the interpretation of the work presented here.

5.2 Theory

The characteristic features of the phase behaviour schematically depicted in fig.1 have been successfully explained by a simple phenomenological interfacial model [5,14] In this model the microemulsion phase is described with the help of a cubic lattice of side ξ. The probability of an elemental cell of the lattice to contain water and oil is ϕ and $(1-\phi)$ with ϕ related to the volume fractions water (ϕ_w), oil (ϕ_o) and surfactant (ϕ_s): $\phi=\phi_w+\phi_s/2$ and $(1-\phi)=\phi_o+\phi_s/2$. The incompressible surfactant monolayer of thickness a is constrained to reside in between the oil and water domains. Using a random mixing approximation (i.e. the probability of a cell side to be covered with a surfactant layer is just $\phi(1-\phi)$) the lattice size ξ is determined by the composition of the microemulsion phase

$$\xi/a = 6\phi(1-\phi)/\phi_s \qquad (1)$$

Interestingly in a variety of microemulsion systems Langevin and coworkers [15] found a convincing agreement between ξ as determined from (1) and the lengthscale π/q_{max} obtained from a correlation peak at $q=q_{max}$ determined by SAXS and SANS [15]. The free energy density of the microemulsion phase $F_{\mu E}$ can be written as the sum of the entropy of mixing per unit volume S and the curvature energy density F_c

$$F_{\mu E}=F_c - TS \qquad (2)$$

with

$$S = -k_B(\phi\ln\phi + (1-\phi)\ln(1-\phi))/\xi^3 \qquad (3)$$

and F_c in case of vanishing spontaneous curvature

$$F_c = 8\pi\phi(1-\phi)K(\xi)/\xi^3 \qquad (4)$$

The last equation is based on the association of a bend in the cubic lattice

with a section of a sphere of diameter ξ. $K(\xi)$ is the renormalized bending elastic modulus. The renormalization takes into account the thermal fluctuations of the surfactant monolayer at lengthscales smaller than ξ

$$K(\xi)=K_0 - \frac{\alpha k_B T}{4\pi} \ln(\xi/a) \qquad (5)$$

with α a constant for which values of 1 [16] and 3 [17] have been predicted and K_0 the bending elastic modulus at the molecular lengthscale a. At constant ϕ it follows from eqs.(1) to (5) that the free energy of the microemulsion phase is essentially of the form

$$F_{\mu E}= [A+ B\ln\phi_s]\phi_s^3 \qquad (6)$$

with at equal volumes of brine and oil i.e. $\phi=1/2$

$$A= \frac{8}{27a^3}\left(2\pi K_0 + k_B T[\ln(1/2) - \frac{\alpha}{2}\ln(3/2)]\right) \text{ and}$$

$$B= \frac{4\alpha k_B T}{27a^3}$$

The free energy density of the lamellar phase $F_{L\alpha}$ is estimated by generalising Helfrich's result [18] concerning the confinement free energy of a symmetric fluctuating membrane in a stack of other membranes. The result is

$$F_{L\alpha} = c \frac{(k_B T)^2}{K_0 a^3}[\phi^{-2} + (1-\phi)^{-2}]\phi_s^3 \qquad (7)$$

with c of order 1/100 [18]. At constant ϕ the free energy of the lamellar phase essentially scales as ϕ_s^3. The phase diagram is calculated by double tangent constructions on eqs.(6) and (7) (the 3 phase coexistence was found by first minimizing eq.(6) with respect to ϕ and then with respect to ϕ_s). The result in the $\kappa=4\pi K_0/k_B T$ - ϕ_s plane is shown in fig.2 (taken from Cates et al. [14]) where $\alpha=1$ and $c=0.15/4\pi$ was used.

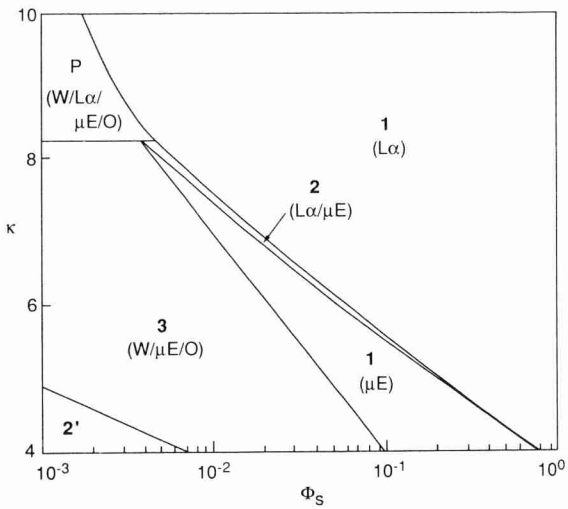

Fig.2. Phase boundaries in the $\kappa=4\pi K_0/k_BT$ - ϕ_s *plane at equal volumes of brine and oil and vanishing spontaneous curvature from Cates et al. [14]. The regions denoted 2, 3, and 1 correspond to almost pure water and oil, Winsor III equilibrium and a single phase microemulsion. 2 and 'P' are a 2 phase lamellar - microemulsion coexistence region and a region corresponding to 'complex polyphasic equilibria between water, oil, lamellar phase and microemulsion phases with a water/oil ratio different from 1.'*

From eqs.(6) and (7) it follows that in this model the phase transition microemulsion - lamellar is determined by the value of K_0. The link between theory and experiment in the case of nonionic surfactant systems is established by assuming that K_0 increases with increasing surfactant chainlength. As a consequence of the logarithmic renormalization of the bending elastic modulus K (eq.5) the phase boundaries are nearly linear in the semilogarithmic representation of fig.2. In fact the theory predicts a strictly linear relation between the logarithm of the dispersion size ξ in the microemulsion phase and the bending elastic modulus K_0 which is reflected in the straight boundary between the Winsor III equilibrium and the 1 phase microemulsion in the representatation of fig.2. This has been verified by Langevin [15] who showed that for various surfactant systems $\ln\xi$ indeed seems to be linearly proportional to K_0. The above analysis only involves the

bending elastic modulus K but neglects the Gaussian bending elastic modulus $\bar{K}$. This quantity is of importance in phase transitions where the genus of the surface is changed which is indeed the case in the microemulsion - lamellar transition. The free energy contribution F_g associated with the Gaussian bending elastic modulus has been estimated within the random mixing model for $\phi=1/2$ as [19]

$$F_g = -\pi\bar{K}/\xi^3 \qquad (8)$$

Including this contribution to the free energy density of the microemusion phase $F_{\mu E}=F_c+F_g-TS$ leaves the form of eq.(6) unchanged but the coefficient A is now given by the expression

$$A = \frac{8}{27a^3}\left[\pi(2K_0-\bar{K}) + k_BT[\ln(1/2) - \frac{\alpha}{2}\ln(3/2)]\right] \qquad (9)$$

from which it follows that both a positive K_0 and a negative $\bar{K}$ destabilizes the microemulsion phase. Using the above expression for A the influence of $\bar{K}$ on the phase boundaries between the microemulsion and the lamellar phase can now be calculated by double tangent constructions on eqs.(6) and (7). The results are presented in fig.3.

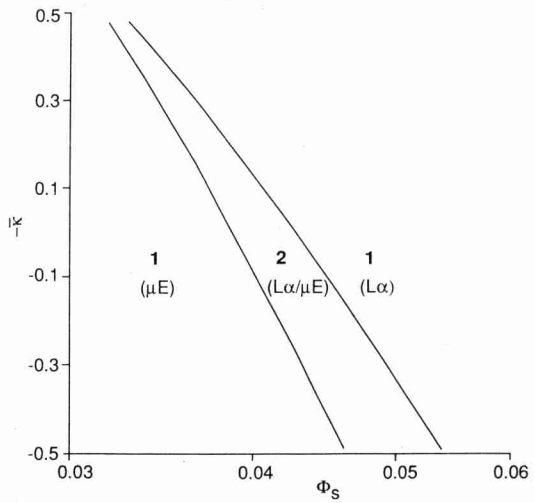

Fig.3. Phase boundaries in the $\bar{\kappa}=4\pi\bar{K}/k_BT$-$\phi_s$ plane at constant $\kappa=4\pi K_0/k_BT=6.28$, equal volumes of brine and oil and vanishing spontaneous curvature.

From figs.2 and 3 it is clear that both a decreasing $\bar{K}$ and an increasing K_0 may cause the phase transition microemulsion - lamellar.

5.3 Experimental

Materials

Sodium dodecyl sulphate (SDS) was 'specially pure' grade purchased from BDH. Cyclohexane, n-pentanol, n-hexanol and NaCl (Baker) were 'analyzed' grade. All chemicals were used without further purification. Deionized water was doubly distilled before use.

Preparation of the samples

8.00 g (and in a number of cases 4.00 g) initial oil phase was carefully poured on 10.00 g (or 5.00 g) of initial water phase in glass tubes with teflon-sealed screw caps. The initial oil phase consisted of cyclohexane and various amounts of n-pentanol plus n-hexanol. The water phase was composed of 0.20 M NaCl and various concentrations of SDS. Equilibrium was attained by gently rolling the samples on a roller bench (ca.1 rev/min.) for several days. Subsequently the samples were permitted to equilibrate at constant temperature ($25 \pm 0.1\ ^{\circ}C$) until no change in phase volumes was observed. Depending on the alcohol mixture used the time necessary to obtain complete phase separation varied from less than a week (pure pentanol) to several months (pure hexanol).

In the single phase lamellar systems in which the interlamellar spacing as a function of the SDS concentration was measured, repartition of cosurfactant between water, oil and monolayers was prevented by the addition of two alcohol molecules with every SDS molecule [22].

Polarization microscopy.

Birefringent phases were characterized using polarization microscopy. The observations were made with a Leitz Metallux 3 optical microscope equiped with a Linkam THMS 600 hot stage element. The qualification 'lamellar phase' is reserved for birefringent phases showing a focal conics texture [20].

Determination of sample compositions.

The volume fraction of oil ϕ_0 (cyclohexane plus pentanol or hexanol) was determined by a Packard Model 433 gas chromatograph equipped with a flame ionization detector and a glass column packed with cross-linked polystyrene

resin. The weightfraction of SDS x_s was obtained by evaporating the liquid components of a (weighted) sample. Correction for the amount of NaCl was carried out. From ϕ_o, x_s and the density of SDS (being 1.45 g cm^{-3}) the volume fraction of water ϕ_w was calculated.

Small Angle X-ray Scattering.

SAXS measurements were made with an 'Anton Paar' Kratky camera. The radiation source is a Philips broadfocus Cu X-ray tube (type PW2253/11) emitting Cu-Kα radiation (wavelength 0.1542nm). The scattered intensity is determined by 2 NaI scintillation counters (type ST-61-I/B) coupled to Photomultipliers (EG&G Ortec model 276) equiped with (EG&G Ortec) amplifiers. One detector is attached to the rear end of the vacuum chamber and measures the scattering curve at a distance of 170mm from the sample. The other detector is mounted above the collimation block and simultaneously monitors the stray-radiation occuring there. By dividing the SAXS intensities through the corresponding signals of the monitor counter they are normalized for the measuring time and corrected for fluctuations in the beam intensity. A constant temperature of 25.0 ^{o}C in the sample holder was maintained using a (Julabo) thermostatic bath coupled to a Pt-100 resistor element. Samples were measured in Mark-Röhrchen capillaries with a pathlength of 2mm.

5.4 Results

Phase behaviour.

The phase diagrams at different pentanol/hexanol ratios in the cosurfactant mixture are given in fig.4a-e. Equal volumes of water phase (0.2M NaCl plus SDS) and oil phase (cyclohexane plus cosurfactant mixture) were used. SDS concentrations are given in weightfractions in the total system and alcohol mixture concentrations are given in weightfractions in the initial oil phase. Fig.4a-e correspond to hexanol fractions x_h in the cosurfactant mixture pentanol plus hexanol of x_h= 0.00, 0.25, 0.50, 0.75 and 1.00, respectively, with $x_h = m_h/(m_p + m_h)$ in which m_h and m_p denote the mass of hexanol and pentanol.

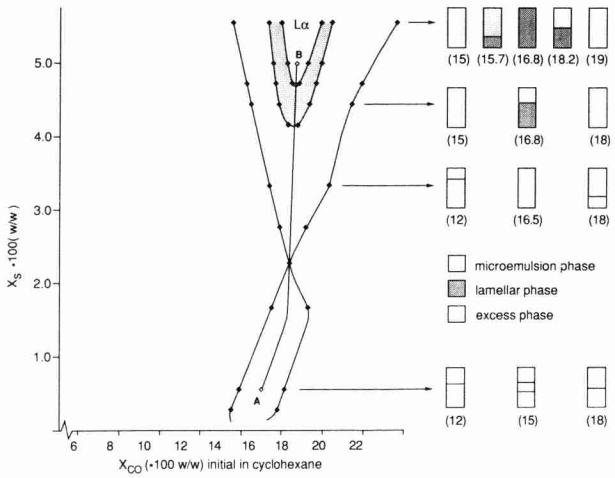
Lα
B
A
5.0
4.0
3.0
2.0
1.0
X_s •100(w/w)
6 8 10 12 14 16 18 20 22
X_{CO} (•100 w/w) initial in cyclohexane
(15) (15.7) (16.8) (18.2) (19)
(15) (16.8) (18)
(12) (16.5) (18)
(12) (15) (18)
microemulsion phase
lamellar phase
excess phase

4a

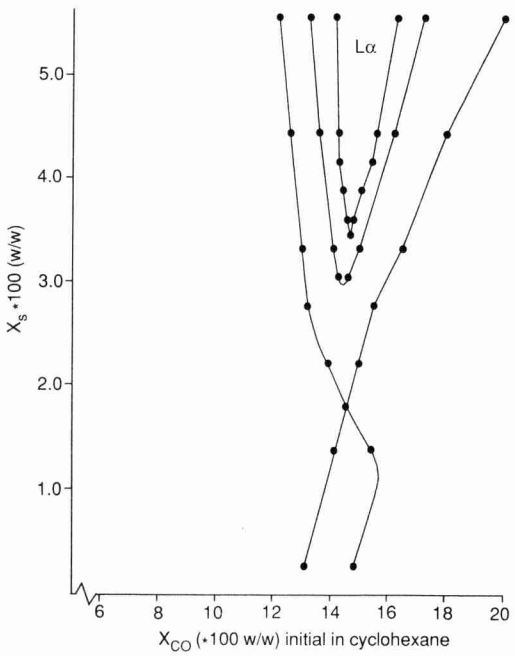
Lα
5.0
4.0
3.0
2.0
1.0
X_s •100 (w/w)
6 8 10 12 14 16 18 20
X_{CO} (•100 w/w) initial in cyclohexane

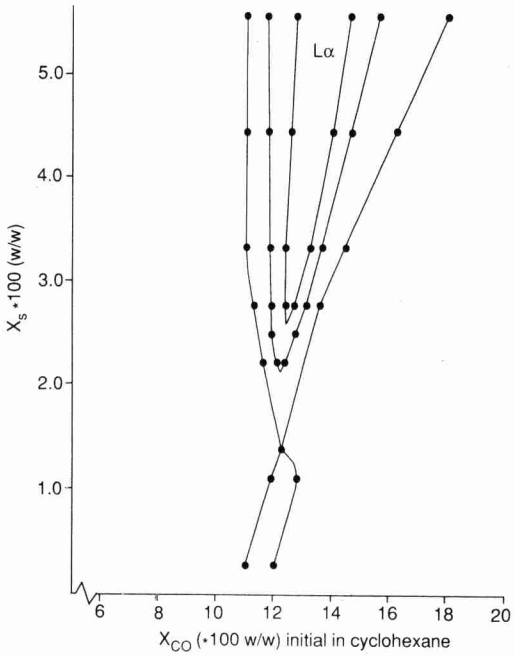
Lα
5.0
4.0
3.0
2.0
1.0
X_s •100 (w/w)
6 8 10 12 14 16 18 20
X_{CO} (•100 w/w) initial in cyclohexane

4c

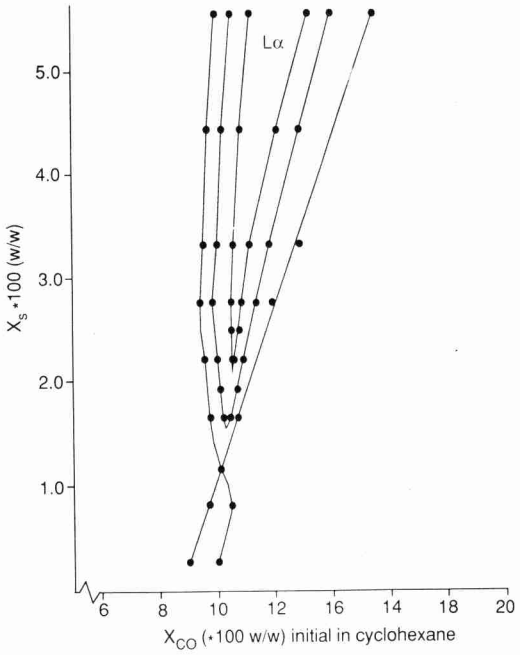

4d

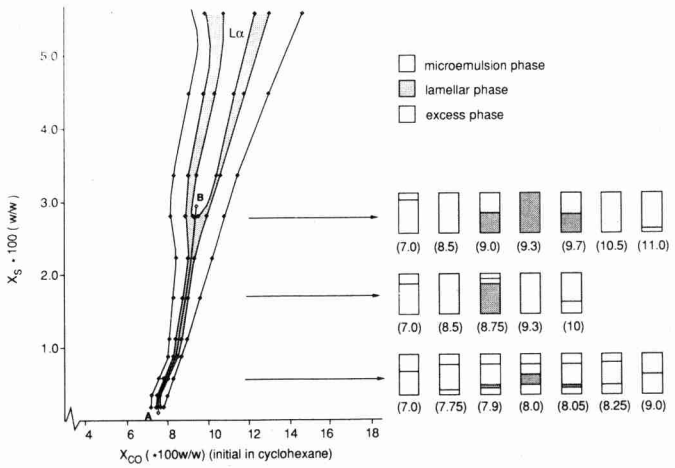

4e

Fig.4. Phase behaviour of brine (0.2M NaCl), cyclohexane, SDS and cosurfactant in the SDS -cosurfactant concentration (i.e. the initial weight fraction of

the cosurfactant mixture in the oil phase) plane with equal volumes of brine and oil phases as a function of the hexanol weight fraction x_h in the cosurfactant mixture pentanol plus hexanol: x_h=0.00 (pure Pentanol) (fig.4a), x_h=0.25 (fig.4b), x_h=0.50 (fig.4c), x_h=0.75 (fig.4d) and x_h=1.00 (pure hexanol) (fig.4e). Shaded regions in the phase diagrams correspond to a lamellar phase in equilibrium with one or more isotropic phases.
The pictograms are on scale representations of the relative volumes of the coexisting phases. The cosurfactant concentrations are indicated between brackets.

For x_h=0, 0.25, 0.50 and 0.75 the well known progression of phase equilibria Winsor I, Winsor III, Winsor II is observed with increasing cosurfactant concentration at low SDS concentration (which depends on x_h: x_s<0.023 for x_h=0, x_s<0.018 for x_h=0.25, x_s<0.014 for x_h=0.50 and x_s<0.012 for x_h=0.75). Increasing the SDS concentration starting from the Winsor III region along the path A-B as indicated in fig.4a (corresponding to a 'balanced microemulsion' i.e. c_0=0) leads to a single phase microemulsion system at increasingly lower surfactant concentration upon increasing x_h. At still higher surfactant concentrations a first order phase transition to a lamellar phase takes place (the dashed regions indicated in figs.4a to 4d). Finally the system is monophasic lamellar. On decreasing or increasing the cosurfactant concentration in the lamellar system, first order phase transitions to the L_1 phase (oil droplets in water) and the L_2 phase (water droplets in oil) are observed, respectively. Going from x_h=0.00 to x_h=0.75 we observe that at low SDS concentrations the amount of cosurfactant in the system necessary to reach the middle phase region (i.e. the region in between Winsor I and Winsor II phase equilibria) is lowered and the concentration range over which it is stable becomes significantly smaller. Moreover the surfactant concentration at which the middle phase swells up to a 1 phase microemulsion system decreases and the lamellar phase becomes stable at increasingly lower surfactant concentrations in such a way as to approach the body of the fish. Using pure hexanol (fig.4e) this trend is extended resulting in a rather different pattern of phase behaviour. At low SDS concentrations (less than about 0.011 w/w) and increasing hexanol concentration the following sequence of phase equilibria is observed: Winsor I, Winsor III, 4 phase equilibrium (water, lamellar phase, microemulsion phase, oil), Winsor III, Winsor II. In the 4

phase equilibrium region the volume of the lamellar phase first increases, reaches a maximum and then decreases upon increasing the cosurfactant concentration while the total volume of the surfactant rich phases remains approximately constant. Although it took several months to obtain a 4 phase equilibrium the system showed birefringence immediately after the addition of the components (for this purpose a 2mm cuvet was used because of the high turbidity of the system). This is a clear indication that the lamellar phase is not a 'pseudo lamellar phase' induced by gravity which has been observed in nonionic systems with a large dispersion size in the middle phase region [21].

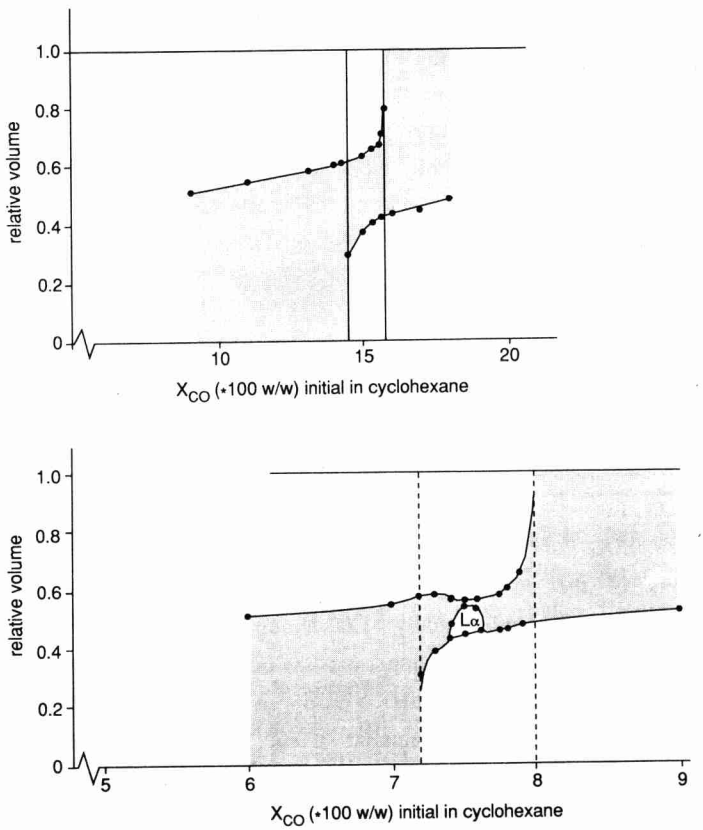

Fig.5. Relative volumes of the surfactant rich phase(s) (indicated as shaded regions) as a function of the cosurfactant concentration in a system with x_h=0.00 (pure pentanol) with an initial SDS weightfraction of 0.006 (a, top) and a system with x_h=1.00 (pure hexanol) with an initial SDS weightfraction of 0.0014 (b, bottom).

In fig.5 the relative volumes of the microemulsion phase and the lamellar phase as a function of the cosurfactant concentration at low SDS concentrations are given for x_h=0.00 (fig.5a, only a microemulsion middle phase present) and x_h=1.00 (fig.5b). The figure illustrates that in the pentanol system the phase volumes vary continuously going from Winsor I to Winsor II upon increasing the cosurfactant concentration. For the hexanol system there seem to be small jumps at the hexanol concentrations at which the lamellar phase appears. These 'jumps' in total surfactant rich phase volume are only small indicating that the lengthscales in the microemulsion and in the lamellar phase are comparable. Looking at fig.5b it follows that in between hexanol concentrations of 7.50 (%w/w) and 7.56 (%w/w) the volume of the microemulsion phase is reduced to about 10% of the total surfactant rich phase. This suggests that a small range of hexanol concentrations could exist for which a triphasic brine-lamellar-oil equilibrium occurs. In view of the large number of samples closely spaced in surfactant and cosurfactant concentration we have studied we think this is rather unlikely unless this triphasic system is stable over a very narrow cosurfactant concentration range of about 0.01% (w/w).

Increasing the SDS concentration in the hexanol system starting from the middle of the middle phase region along the path A-B as indicated in fig.4e, the volumes of the surfactant rich phases increase at the expense of the excess phases. However, while the middle phase volumes increase linearly with the amount of SDS in the systems with $x_h \leq 0.75$, this is not the case in the hexanol systems for SDS concentrations above about 0.006w/w. This is reflected in the compositions of the coexisting phases which is discussed in the next section. The lamellar phase preferentially takes up water resulting in a 3 phase equilibrium (lamellar -microemulsion- excess oil) somewhat above 0.011 (w/w) SDS. At about 0.020 (w/w) SDS a 2 phase equilibrium (lamellar-microemulsion) and a single lamellar phase above 0.027 (w/w) SDS. Interestingly this latter value is significantly higher than the minimum surfactant concentration of 0.021 w/w required for the formation of a single lamellar phase in the system with x_h=0.75.

In fig. 6 the phase boundaries at $c_0 \cong 0$ between Winsor III -1 phase microemulsion (further referred to as the 3-1 line) - 2 phase microemulsion/lamellar (the 1-2 line) and 1 phase lamellar systems (the 2-1 line) as a function of the weightfraction of SDS for systems with different

hexanol mass fractions are shown.

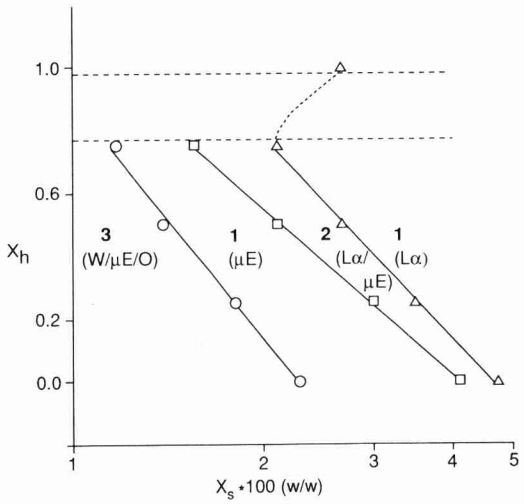

Fig.6. Phase boundaries at $c_0 \cong 0$. Symbols (o), (□) and (Δ) represent boundaries between Winsor III/1 phase microemulsion, 1 phase microemulsion/microemulsion-lamellar phase coexistence and microemulsion-lamellar phase/single lamellar phase. In between the boundaries indicated by the dashed lines a 4 phase equilibrium appears.

Looking at Fig.6 it follows that up to a hexanol mass fraction x_h=0.75 the boundaries between the phases are almost linear in this semilogarithmic representation but the extrapolated 3-1 and 1-2 lines do not intersect at $x_h \leq 1$ as it should be. We will come back to this point in the discussion section.

Compositions of the coexisting phases.

In Table 1 the compositions of the equilibrated phases in the pentanol (x^h=0.00) and hexanol (x^h=1.00) systems at several SDS concentrations along the path A-B corresponding to a 'balanced system' as indicated in figs.4a and 4e are given.

TABLE 1. Composition of the phases with pure pentanol and hexanol as a cosurfactant. x_s is the determined weightfraction in the coexisting phases and B, L_α, μE and O denote excess aquous phase, lamellar phase, microemulsion phase and excess oil.

Pentanol system

total SDS concentration (g/g)	Coexisting Phases	Composition Phases			
		Phase	x_s	ϕ_o	ϕ_w
0.0431	L_α/μE	Lα	0.047	0.468	0.509
		μE	0.041	0.500	0.480
0.0472	L_α/μE	L_α	0.047	0.485	0.492
		μE	0.041	0.510	0.470

Hexanol system

total SDS concentration (g/g)	Coexisting Phases	Composition Phases			
		Phase	x_s	ϕ_o	ϕ_w
0.0028	B/L_α/μE/O	Lα	0.015	0.369	0.621
		μE	0.012	0.564	0.425
0.0056	B/L_α/μE/O	L_α	0.015	0.341	0.647
		μE	0.012	0.560	0.429
0.0083	B/L_α/μE/O	Lα	0.019	0.312	0.681
		μE	-	-	-
0.0111	B/L_α/μE/O	Lα	0.022	0.320	0.669
		μE	0.020	0.524	0.465
0.0167	L_α/μE/O	Lα	0.025	0.334	0.653
		μE	0.022	0.546	0.443
0.0250	L_α/μE	Lα	0.027	0.485	0.512
		μE	0.025	0.522	0.461

In case of pentanol the SDS concentrations in the coexisting lamellar and microemulsion phases (in between SDS concentrations of 0.043 and 0.047 (w/w)) correspond to the values at the boundaries of the coexisting region as it should be in a first order phase transition. From gas chromatography measurements it was found that the pentanol concentration in the lamellar phases is somewhat higher than the pentanol concentration in the microemulsion phases (not given in Table 1). The total recovered amount is smaller than the initial amount which is probably caused by adsorption effects in combination with SDS in the column. Although hardly measurable, the lamellar phase seems to contain slightly more brine.

In the hexanol system the lamellar and the microemulsion phases in the 2 phase microemulsion/lamellar, the 3 phase lamellar/microemulsion/oil and the 4 phase brine/lamellar/microemulsion/oil equilibria were analysed. It appears that in the two phase system the oil/brine ratio is approximately equal to 1 for both phases but in the 3- and 4 phase systems the lamellar phase contains almost twice as much brine as oil while the microemulsion phase contains slightly more oil. From gas chromatography measurements it was found that the lamellar phase contains a little more hexanol than the microemulsion phase. From the results presented in Table 1 it is clear that upon increasing the amount of surfactant in the system the SDS concentration in both the lamellar and microemulsion phase in the 4 phase equilibrium increases. This phenomenon accounts for the observation that the volume of the surfactant rich phases does not increase linearly with the surfactant concentration. This change in surfactant concentration in the lamellar and the microemulsion phase might be caused by the negative adsorption of salt at the large charged oil/brine interface leading to an increasingly higher 'effective' salt concentration as a function of the amount of SDS in the system which in turn influences the interlamellar spacing. We will return to this issue in the discussion section.

Small Angle X-ray Scattering.

In Fig.7 scattering curves of a typical microemulsion phase and a lamellar phase are shown.

From a study of single phase lamellar systems it is found that the bump in the scattering curve corresponding to the lamellar phase reflects approximately the q value q_{max} at which a Bragg peak is expected. The peak position $D = 2\pi/q_{max}$ as a function of $1/x_s$ (with x_s the SDS concentration (w/w)

in the lamellar phase in single- and multiphase systems is given in Fig.8.

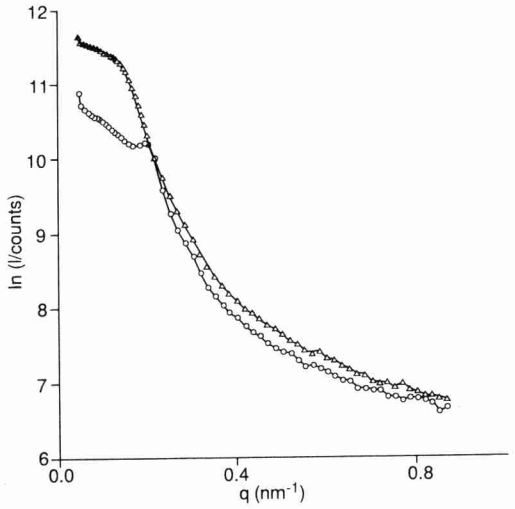

Fig.7. Scattering curves of a typical (coexisting) microemulsion phase (triangles) and a lamellar phase (circles). x_h*=0.00. The lines are guides to the eye.*

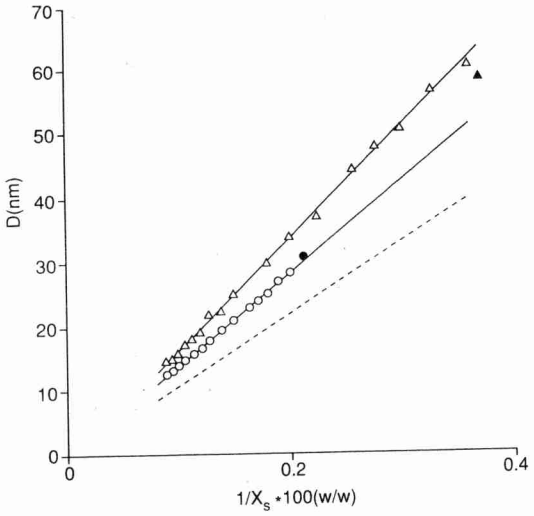

Fig.8. Bragg peak positions $2\pi/q_{max}$ *versus* $1/x_s$ *with* x_s *the SDS weightfraction*

in the lamellar phase. Single phase lamellar systems for x_h=0.00 (circles) and x_h=1.00 (triangles) (empty symbols). Peak positions obtained from lamellar phases coexisting with a microemulsion phase are indicated by the corresponding filled symbols. Solid lines are best-fit lines to the points corresponding to single lamellar phases. The dashed line is calculated from the adsorption density of SDS at the planar cyclohexane-brine interface [22].

In fig.8 solid lines are best-fit lines to the points corresponding to single lamellar phases. From the slopes of the best fit lines the molecular areas of SDS are deduced to be (0.73 $\pm$0.01)nm^2 in the pentanol system and (0.63 $\pm$0.01)nm^2 in the hexanol system, significantly lower than the molecular area obtained from interfacial tension measurements at the planar cyclohexane-brine interface being 0.93nm^2 for both pentanol and hexanol systems [22]. The line corresponding to this value is also given in Fig.8. So from the interlamellar spacing an apparent total area smaller by a factor 0.78 (pentanol) and 0.68 (hexanol) is found. We will return to this point in the discussion section.

In Table 2 the values of D of the lamellar phases in the multiphasic lamellar systems are given, to be compared to D_c calculated from the compositions given in Table 1 using

$$D_c = \frac{2 M_s}{x_s \, N_A \, \rho_{L_\alpha} \, \sigma_{s,app.}} \qquad (10)$$

where M_s, x_s, N_A, $\rho_{L\alpha}$ and $\sigma_{s,app.}$ are the molecular weight of SDS, the mass fraction of SDS (given in Table 1), Avogadro's number, the density of the lamellar phase (being 0.90g/cm^3 for systems with an oil/brine ratio of approximately 1 and 0.95g/cm^3 otherwise) and the apparent molecular area of SDS obtained from SAXS.

TABLE 2.

Comparison of lamellar spacings obtained from Bragg-peak positions in the small angle X-ray scattering curves and D_c calculated from the compositions given in TABLE 1 using the apparent molecular areas deduced from fig.8.

Pentanol system

Total SDS Concentration (g/g)	Coexisting Phases	SAXS D (nm)	composition D_c (nm)
0.0431	$L_\alpha/\mu E$	29	31
0.0472	$L_\alpha/\mu E$	29	31

Hexanol system

Total SDS Concentration (g/g)	Coexisting Phases	SAXS D (nm)	composition D_c (nm)
0.0028	$B/L_\alpha/\mu E/O$	110	104
0.0056	$B/L_\alpha/\mu E/O$	96	105
0.0083	$B/L_\alpha/\mu E/O$	89	86
0.0111	$B/L_\alpha/\mu E/O$ (top)[a]	72	72
	(middle)	81	-
	(down)	90	-
0.0167	$L_\alpha/\mu E/O$	61	63
0.0250	$L_\alpha/\mu E$	59	63

(a). '(top)', '(middle)' and '(down)' refer to the height positions where the samples were taken.

Determination of Dispersion Sizes

The dispersion size ξ in the microemulsion phase defined by eq.(1) is easily obtained from the microemulsion volume $V_{\mu E}$ and the total area in the system $A = N_s\sigma_s$ with N_s and σ_s the number of SDS molecules and the area per molecule using

$$\xi = \frac{3V_{\mu E}}{2A} \qquad (11)$$

where it is assumed that all the surfactant resides in the microemulsion phase. In case of the system with pure hexanol as cosurfactant a lamellar

phase is present and therefore we calculated ξ from the composition of the microemulsion phase by

$$\xi = \frac{6\,\phi_o\phi_w M_s}{N_A\, x_s\, \rho_{\mu E}\, \sigma_s} \qquad (12)$$

in which $\rho_{\mu E}$ denotes the mass density of the microemulsion phase being 0.90 (g/cm^3). The dispersion sizes are presented in Table 3 where we used σ_s=0.93nm^2 [22] and not $\sigma_{s,app}$ as the latter reflects properties of the lamellar phase and is not necessarily the real molecular area of SDS.

TABLE 3. Dispersion size ξ in middle phase microemulsions as a function of the hexanol mass fraction x_h in the cosurfactant mixture pentanol plus hexanol.

x_h	ξ(nm)
0.00	35.8
0.25	44.4
0.50	57.3
0.75	68.5
1.00	72.0*

*Lamellar phase present.

As shown in Table 3, the dispersion size ξ in the microemulsion (middle) phase increases steeply as a function of the hexanol fraction in the cosurfactant mixture. This is directly related to the observation that the middle phase is swollen up to a 1 phase microemulsion at the expence of the excess phases at increasingly lower surfactant concentrations.

5.5 Discussion

Phase behaviour and lengthscales

The almost linear behaviour of the phase boundaries as presented in Fig.6 is qualitatively in agreement with the theoretical results depicted in fig.2. A similar agreement was reported in [14] where theory and experiment on nonionic C_iE_j microemulsion systems (with i the chainlength and j the headsize) were compared. Therefore we conclude that increasing the hexanol fraction x_h in the cosurfactant mixture in our ionic surfactant system has the same effect on the

phase diagram as an increase of (i+j) in a nonionic system and both variations seem to increase K. One expects that a 4 phase equilibrium water - lamellar - microemulsion - oil is reached as soon as the 3-1 and 1-2 phase boundaries intersect as is indeed predicted theoretically [5,6,14]. Extrapolating the 3-1 and 1-2 phase boundaries (fig.6) results in an intersection point higher than x_h= 1.0 where a lamellar phase in equilibrium with a microemulsion phase and two excess phases is observed experimentally. This suggests that the 3-1 and the 1-2 phase boundaries approach each other much more rapidly than is expected from the linear extrapolation of these lines. However the relation between x_h and K is not *a priori* a linear one but as mentioned in the theory section, in [15] experimental evidence is presented that $\ln\xi$ increases linearly with K. A more direct comparison with fig.2 is therefore obtained by presenting the phase lines in the $\ln\xi$ - x_s plane rather than in a x_h - x_s representation. This is shown in Fig.9.

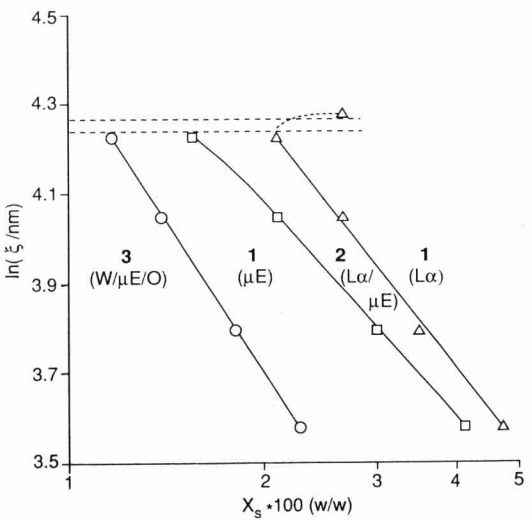

Fig.9. Phase boundaries in the $\ln\xi$-x_s plane. Symbols are the same as in fig. 6. Here again the 4 phase equilibrium appears in between the boundaries indicated by dashed lines.

If we leave out of consideration the point corresponding to x_h=1.00 the phase boundaries in this double logarithmic representation again behave almost

linearly. The 3-1 line is strictly linear as it is based on eq.(11). However the 1-2 line curves differently than predicted by theory. As mentioned above the 3-1 line and the 1-2 line should intersect in between $\xi \cong 69$nm and $\xi \cong 72$nm (where the four phase equilibrium appears) which can only be accomplished if the 1-2 line strongly curves towards the 3-1 line. Such a strong curvature of the 1-2 line towards the 3-1 line is not found in the theory of Andelman et.al [14] nor in the theory of Golubovic and Lubensky [6]. From inspection of fig.3 where we plotted the 1-2 and the 2-1 lines in the $\bar{\kappa}$ - $\log(\phi_s)$ plane we observe that the 1-2 line has the appropriate curvature. This implies that an increasingly negative $\bar{K}$ as a function of the hexanol fraction in the cosurfactant mixture might be responsible for the experimentally observed curvature of the 1-2 line towards the 3-1 line. As pointed out in [12] it is indeed expected that $\bar{K}$ is negative for a surfactant monolayer and that it will decrease with the (co)surfactant chainlength [23,24]. Therefore our results indicate that (within the model under consideration) a simultaneously increasing K and a more negative $\bar{K}$ are responsible for the increasing stability of the lamellar phase compared to the microemulsion phase as a function of the hexanol fraction in the system studied here. In general it is expected that both K and $\bar{K}$ will change with the fraction of cosurfactant (mixture) as well. However as shown by us recently [22] the monolayer composition is the same for both pentanol and hexanol as cosurfactant and it does not change above a cosurfactant weight fraction of 0.05 initial in oil. Therefore we expect K and $\bar{K}$ to remain effectively constant for weight fraction of cosurfactant (mixture) above this value.

From table 3 and fig.4 it follows that the increasing stability of the lamellar phase upon increasing x_h is accompanied by an increase of the dispersion size in the microemulsion phase. Above $\xi \cong 70$ nm the lamellar phase even becomes stable in the body of the fish. We wonder whether a similar limiting value can also be found in other surfactant systems. Lee et al.[25] reported the dispersion sizes in the nonionic systems C_8E_3(in decane) and $C_{10}E_4$ (in octane) being 5.8nm and 18.7nm, respectively, much lower than the lengthscales observed in our system. In the $C_{10}E_4$ system the lamellar phase is still relatively far away from the body of the fish but it is much closer in the $C_{12}E_4$ system [13]. Now the lamellar phase almost touches the body of the fish. Assuming that the adsorption densities of $C_{10}E_4$ and $C_{12}E_4$ at the octane-water interface are equal we can write

$$\xi_{C_{12}E_4} = \frac{c^*_{s,C_{10}E_4}}{c^*_{s,C_{12}E_4}} \xi_{C_{10}E_4} \qquad (13)$$

where c^*_s is the molar surfactant concentration necessary to take up the excess water and oil phases (corrected for the critical micelle concentration). Using this relation we estimate $\xi_{C_{12}E_4} \cong 75$nm which is close to the value of ξ=72nm as found for the hexanol system. Apparently $\xi \cong 70$-80 nm is an indication for the proximity of a lamellar phase to the middle phase region in two different systems. *A priori* one would expect that as soon as the lamellar phase is stable at a surfactant concentration at which the middle phase in the 3 phase system is swollen up to a one phase microemulsion, ξ and D will be of comparable size since $\xi \cong 3V/2A$, $D=2V/A$ and $V/A \propto 1/x_s$ in a system with equal volumes of water and oil but there is no necessity for an 'absolute' lengthscale or an upper limit for ξ. This limit may follow from model considerations comparing the free energies of the microemulsion phase and the lamellar phase. Here an indication is found that such a limit exists by comparing two completely different systems.

The lamellar phase in the presence of isotropic phases.

From the data presented in Table 2 it follows that the agreement between D and D_c is satisfactory which provides additional evidence that the birefringent phase in the 3 and 4 phase equilibria in the hexanol system has indeed a lamellar structure. Taking into account the volume fractions of oil and water given in Table 1, it follows that in the two phase coexistence region lamellar - microemulsion the oil and water interlamellar spacings $D_o=\phi_o D$ and $D_w=\phi_w D$ are approximately equal. However as soon as more phases come into play (as is the case in the system containing pure hexanol) the situation becomes rather complicated. First of all in the lamellar phase the oil water symmetry is broken to the extend that $D_w \cong 2D_o$ while at the same time in the microemulsion phase the oil/water ratio remains approximately equal to 1. Furthermore in the four phase region above a surfactant concentration x_s= 0.006 (g/g) the interlamellar spacing decreases with increasing x_s. Whether or not this may be attributed to the effect of a negative adsorption of salt resulting in an

increasing effective salt concentration and therefore a decreasing electrostatic repulsion between the lamellae as a function of the SDS concentration is still under study. Nevertheless the combination of this observation with the larger interlamellar water spacing compared to the oil spacing leads us to the conclusion that in spite of the rather high salt concentration we used, electrostatic effects still seem to play a role. Evans and Parsegian [26] directed attention to the possibility that thermal undulations may lead to a much slower decay of the electrostatic repulsion between charged bilayer membranes than expected from classical double layer theory [27]. This effect was further elaborated by Pincus, Joanny and Andelman [28], Evans and Ipsen [29] and Odijk [30]. The treatment of Evans and Ipsen [29] of the renormalisation of the electric repulsion between membranes leads to the prediction that even for large separations there is still a considerable enhancement of the electrostatic repulsion. Whether this enhancement is sufficient to explain the experimentally observed asymmetry of the water and oil spacings requires detailed calculations which we hope to address in a future publication.

A complicating factor is that in the four phase system with x_s=0.011 (somewhat lower than the surfactant concentration at which the water phase disappears) a gradient in interlamellar spacing seems to be present (Table 1) and a slight increase of ϕ_w with increasing lamellar distance is observed (not shown). It is expected that the gradient in interlamellar spacing will be proportional to the gravity constant times the osmotic compressibility. The latter will increase upon increasing interlamellar spacing and since the interlamellar spacing is quite high, the gradient apparently becomes considerable.

Variation of the interlamellar spacing with the SDS concentration in single phase lamellar systems.

The smaller total area obtained from the interlamellar spacing compared to the one obtained using the Gibbs adsorption equation [22] is rather puzzling. Strey et al. [32] found a comparable discrepancy in a $C_{12}E_5$/octane/water system. As pointed out in [31] this difference may be attributed to a combination of strongly undulating monolayers and area consuming defects. The influence of the first possibility will now be investigated. A logarithmic deviation from the linear (ideal) dilution law of the lamellar phase

$$D = \frac{\delta}{\phi_s} \qquad (14)$$

with δ the thickness of the surfactant layer which can be written as $\delta = \bar{v}_s/\sigma_s$ where $\bar{v}_s$ is the surfactant molecular volume and ϕ_s the surfactant volume fraction was first described by Strey et.al. [32] for a nonionic bilayer in water system. We will apply a similar analysis for the mixed monolayer system here.

In a fluctuating membrane system thermal undulations tend to decrease the projected area while the total area A is conserved. A first order correction to the projected area $A_{proj.}$ of a membrane caused by thermal undulations is [33]

$$\frac{A}{A_{proj.}} = 1 + \frac{k_B T}{4\pi K} \ln\left[\frac{q_{max}}{q_{min}}\right] \qquad (15)$$

where q_{max} and q_{min} are the upper and lower wavenumber cutoffs

$$q_{max} = 2\pi/a \quad ; \quad q_{min} = 2\pi/\lambda \qquad (16)$$

with a again a molecular lengthscale and λ the deflection length

$$\lambda = c' u (K/k_B T)^{1/2} \qquad (17)$$

where c' is a model dependent constant of order unity [33,34] and u is the root mean square of the amplitude of the undulations. In a lamellar phase with only short range steric repulsions between the membranes the deflection length is directly proportional to the interlamellar distance D as in that situation $u \propto D/2$ (recall that D is defined here as the sum of the water and oil spacing). Using eqs.(14) - (17) then leads to a dilution law of the form [32,36]

$$D\phi_s/2 = A - B\ln(\phi_s) \qquad (18)$$

in which

$$A = \delta\left(1 + \frac{k_B T}{4\pi K}\ln\left(\frac{c''\delta}{a}(K/k_B T)^{1/2}\right)\right) \qquad (19)$$

and

$$B = \delta k_B T/4\pi K \qquad (20)$$

with c'' a constant of order unity.

In fig.10 we plot $D\phi_s/2$ against $\ln(\phi_s)$. According to eq.(18) the slope of the line is a measure for the 'hidden' area caused by thermal undulations of the monolayers.

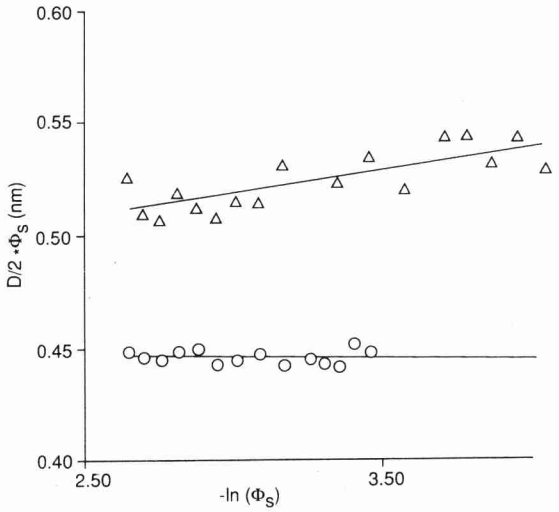

Fig.10. Data from Fig.8 plotted as $(D/2)\phi_s$ versus $-ln(\phi_s)$. Straight lines correspond to a best fit of the data to eq.18.

If undulation repulsion would indeed dominate in our system, which is to be expected for a salt concentration of 0.2M (in that case the Debije length is approximately 0.7nm being of the same order of magnitude as in [35] where no indications for electrostatic repulsions are found), we would expect B≅ 0.05-1.2 nm (δ varied between 0.5 and 1.5 nm and K between 0.1 and 1 $k_B T$). However we found values for B that are much lower: close to zero for the

pentanol system and B= (0.020 $\pm$ 0.004)nm for the hexanol system. This implies that undulation repulsion does *not* dominate and that electrostatic repulsion plays an important role. In that case the deflection length is given by (17) but now u depends in a complicated way on D. In principle the value of u can be determined from self consistent mean field theories of charged multimembrane systems [29,30]. However the situation is complicated by the fact that in a system containing an extensive charged surface a substantial amount of co-ions will be negative adsorbed leading to a larger effective salt concentration. We calculated the effective salt concentration from the co-ion adsorption using the Poisson-Boltzmann equation. We found a steep increase as a function of the SDS concentration ranging from 0.25M at x_s=0.055 to 0.33M at x_s=0.11. At constant interlamellar spacing it is expected that an increasing salt concentration will increase u (the amplitude of the undulations will increase since the Debije length decreases). Therefore, although the interlamellar spacing decreases as a function of the SDS concentration which tends to decrease u, this may be more or less compensated by the concomitant change in the effective salt concentration having the opposite effect on u. This effectively results in a lower $\ln\phi_s$ dependence of the interlamellar spacing compared to what may be expected for systems without electrostatic interactions. In this light we would like to note that Roux et al. [36] performing the same analysis (i.e. eqs.(18)- (20)) on several bilayer systems found indications that at a salt concentration of 0.2M undulation repulsion dominates. For the pseudo-ternary monolayer systems studied here, however, indirect evidence is presented that even at salt concentrations higher than 0.2M electrostatic interactions are still present. A possible explanation for this difference is that in our system K might be lower leading to more pronounced electrostatic repulsion enhancement.

The larger slope in fig.8 implies that the hexanol system 'hides' more surface than the pentanol system, presumably caused by the relatively large interlamellar spacing. Indeed fitting the data in fig.8 for the hexanol system up to x_s= 0.067 (w/w) reveals a molecular area of (0.71 $\pm$ 0.03) nm^2, approximately equal to the one obtained for the pentanol system. This however does not explain the discrepancy with the area obtained with an other method [22]. As our analysis of the thermal undulations is obscured by some complicating electric double layer effects it is at this stage not possible to distinguish the separate contributions from thermal undulations and defects.

5.6 Concluding Remarks.

From this work some interesting conclusions can be drawn. First of all it is shown that the competition between the lamellar and the microemulsion phase at vanishing spontaneous curvature can be tuned by the variation of the hexanol fraction in a cosurfactant mixture consisting of pentanol and hexanol. Upon increasing the hexanol fraction in the cosurfactant mixture the lamellar phase becomes stable at increasingly lower surfactant concentration. At the same time the dispersion size in the microemulsion (middle) phase increases. Above a certain value of the dispersion size (approximately 70 nm) the lamellar phase becomes stable in the body of the fish leading to a different and rather complicated pattern of phase behaviour. This value of the dispersion size is comparable to the one estimated for a nonionic system [13] where the lamellar phase is close to the body of the fish. A speculative explanation for this observation may be that this is the lengthscale at which the entropy of mixing oil and water domains becomes too small to compensate for the curvature free energy of the microemusion phase.

The comparison of our experimental results with a phenomenological theory [5] reveals that the competition between the lamellar and the microemulsion phase is qualitatively correctly described by theory. A more quantitative comparison points to the necessity to include $\bar{K}$.

From the study of the lamellar phase in the systems with pure pentanol and with pure hexanol as cosurfactant several indications are found for the presence of fluctuations enhanced electrostatic repulsion. These indications are:

(a). The larger interlamellar water spacing compared to the oil spacing ($D_w \cong 2D_o$) in the lamellar phase coexisting with a microemulsion phase and one or more excess phases;

(b). The decreasing interlamellar distance in the lamellar phase upon increasing x_s in the 4 phase (hexanol) systems above $x_s \cong 0.006$ (g/g);

(c). The much lower slope of $D\phi_s/2$ versus $\ln\phi_s$ in the single phase lamellar systems (fig.10) compared to what may be expected [36].

As far as point (a) is concerned it was pointed out to us by an anonymous referee that also in nonionic surfactant systems the lamellar phase appears to be more stable on the aqueous than on the oleic side. Therefore the observation described under point (a) by itself does not necessarily indicate the existence of enhanced electrostatic repulsion.

Acknowledgements. The authors thank Mr. M.H.Tollenaar for drawing the figures, Bonny Kuipers for his help with the SAXS equipment, Theo Odijk for enlightening discussions and an anonymous referee for pointing out to us the last remark in the conclusion section. The investigation was supported by the Netherlands Foundation of Chemical Research (SON) with financial aid from the Netherlands Organization for Scientific Research (NWO).

Literature

[1] Kahlweit,M.,Strey,R., and Busse,G.J.Phys.Chem.**94**, 3881 (1990).

[2] Bellocq,A.M., Biais,J., Bothorel,P., Clin,B., Fourche,G., Lalanne,P., Lemaire,B., Lemanceau,B. and Roux,D., Adv.Coll.Interface Sci. **20**, 167, (1984).

[3] Talmon,Y. and Prager,S., J.Chem.Phys.**69**, 2984, (1978).

[4] Jouffroy,J., Levinson,P. and de Gennes,P.G., J.Physique (France) **43,** 1241, (1982).

[5] Andelman.,D., Cates,M.E., Roux,D. and Safran,S.A., J.Chem.Phys. **87**, 7229, (1987).

[6] Golubovic,L., and Lubensky,T.C., Phys.Rev.A **41**, 4343, (1990).

[7] Widom,B., Langmuir **3**, 12, (1987).

[8] Gompper,G. and Schick,M., Phys.Rev.B. **41**, 9148, (1990).

[9] Strey,R., Habilitationsschrift, Göttingen (1992).

[10] van Aken, G.A., Thesis Rijksuniversiteit Utrecht (1990).

[11] Hackett,J.L. and Miller,C.A., S.P.E. Res.Eng.**3**, 791, (1988)

[12] Kegel,W.K. and Lekkerkerker,H.N.W. Colloids Surfaces **A76**, 241, (1993).

[13] Kahlweit,M., Strey,R., and Firman,P., J.Phys.Chem.**90**, 671, (1986).

[14] Cates,M.E., Andelman,D., Safran,S.A., and Roux,D., Langmuir **4**, 802, (1988).

[15] Langevin,D. Adv.Coll.Int.Sci. **34**, 583, (1991).

[16] Helfrich,W., J.Physique (France) **46**, 1263, (1985).

[17] Peliti,L. and Leibler,S., Phys.Rev.Lett.**54**, 1960, (1985).

[18] Helfrich,W., Z.Naturforsch. **33a**, 305, (1978).

[19] Roux,D., Coulon,C. and Cates,M.E., J.Phys.Chem.**96**, 4147, (1992).

[20] Hartshorne,N.H. and Stuart,A., 'Crystals and the Polarizing Microscope', Edward Arnold, London, (1970).

[21] Strey,R., personal communication.

[22] Kegel,W.K., Aken,G.A. van, Bouts,M.N., Lekkerkerker,H.N.W., Overbeek,J.Th.G and de Bruyn,P.L. Langmuir **9**, 252, (1993); Chapter 2 of this

thesis.
[23] Helfrich,W., in Les Houches, Session XXXV, 1980, 'Physics of Defects', R.Balian et.al. eds., Nort-Holland, Amsterdam (1981), p.715.
[24] Szleifer,I, Kramer,D., Ben-Shaul,A., Gelbart, W.M., and Safran,S.A., J.Chem.Phys. **92**, 6800, (1990).
[25] Lee,L.T., Langevin,D., Meunier,J., Wong,W., and Cabane,B., Progr.Colloid Polym. Sci. **81**, 209, (1990).
[26] Evans,E.A. and Parsegian,V.A.,Proc.Natl.Acad.Sci.U.S.A. **83**, 7132, (1986).
[27] Verwey,E.J.W. and Overbeek,J.Th.G., *Theory of Stability of Lyophobic Colloids*, Elsevier, Amsterdam.
[28] Pincus,F., Joanny,J.F., and Andelman,D., Europhys. Lett. **11**, 763, (1990).
[29] Evans,E. and Ipsen,J., Electroch.Acta **36**, 1735, (1991).
[30] Odijk,T., Langmuir **8**, 1690, (1992).
[31] Strey,R., Winkler,J., and Magid,L., J.Phys.Chem. **95**, 7502, (1991).
[32] Strey,R., Schomäcker,R., Roux,D., Nallet,F. and Olsson,U., J.Chem.Soc.Faraday Trans. **86**, 2253, (1990).
[33] Helfrich,W. and Servuss,R.M., Nuovo Cimento **3D**, 137, (1984).
[34] Golubovic,L. and Lubenski,T.C., Phys.Rev.B **39**, 12110, (1989).
[35] Nallet,F., Roux,D. and Prost,J., Phys.Rev.Lett.**62**, 276, (1989); Roux,D. and Safinya,C.R., J.Physique (France) **49**, 307, (1988).
[36] Roux,D., Nallet,F., Freyssingeas,E., Porte,G., Bassereau,P., Skouri,M. and Marignan,J., Europhys.Lett. **17**, 575, (1992).

CHAPTER 6

EVIDENCE FOR ENHANCED ELECTROSTATIC INTERACTIONS IN LAMELLAR MONOLAYER SYSTEMS.

Willem K.Kegel and Henk N.W.Lekkerkerker.

Van't Hoff Laboratory, University of Utrecht, Padualaan 8, 3584 CH Utrecht, The Netherlands.

Abstract

The influence of salt on the interlamellar spacing is investigated in charged single- and multiphase lamellar oil - water systems. It is demonstrated that even at rather high salt concentrations (at least up to 0.3M) electrostatic repulsion still plays a significant role which is attributed to a coupling with monolayer undulations.

Under certain conditions systems consisting of water, oil and one or more amphiphiles may order themselves into a stack of undulating monolayers or bilayers. Over the last decade it has become clear that undulations may strongly renormalize direct interactions arising from intermolecular forces [1-4]. Thermal undulations are predicted to lead to a much slower decay of the electrostatic repulsion between charged bilayer membranes than expected from classical double layer theory [5-8]. Supporting experimental evidence for such an effect can be obtained from the distance dependence of the interaction between charged membranes [9]. Moreover Odijk [10] deduced from his self consistent theory of undulation enhanced interactions a melting rule for a lamellar phase coexisting with an isotropic phase which is in semi - quantitative agreement with recent experimental results of Dubois and Zemb [11].

The aim of the work presented here is to provide experimental evidence for enhanced electrostatic repulsion in fluctuating monolayer systems. We first present a study of the interlamellar spacing as a function of the salt concentration (0.1 - 0.4M) in a lamellar phase coexisting with excess oil and brine and a microemulsion phase. After that we turn to single phase lamellar systems in which the interlamellar spacing is measured as a function of the monolayer volume fraction. The effective salt concentration in these systems is shown to depend upon the total area of the charged monolayer at the oil-brine interface. We present a simple method to control the effective salt concentration independent of the monolayer volume fraction. Making use of this method we confirm our earlier conclusion that even at relatively high effective salt concentrations (up to 0.3M) electrostatic repulsion still plays a significant role.

The system in which we studied the spacing in a lamellar phase coexisting with a brine, oil and microemulsion phase as a function of the salt concentration consists of SDS as surfactant, hexanol as cosurfactant and equal volumes of brine and oil (cyclohexane plus hexanol). The 4 phase coexistence region was determined in the salt concentration - cosurfactant concentration plane at constant surfactant concentration (0.005 w/w initial in brine). Because of the low surfactant concentration in this system a large reservoir of brine is present and the effective salt concentration is therefore about equal to the initial concentration which is varied.

We studied this system with salt concentrations ranging from 0.10M up to

0.40M and hexanol concentrations in between 5% and 18% (w/w) initially in the oil phase. The interlamellar spacings D obtained from the Bragg peak positions $2\pi/q_{max}$ measured by Small Angle X ray Scattering (using an Anton Paar Kratky camera) are presented in fig.1 as a function of the salt concentration. We also measured the water volume fraction in the lamellar phase which is presented in Table 1.

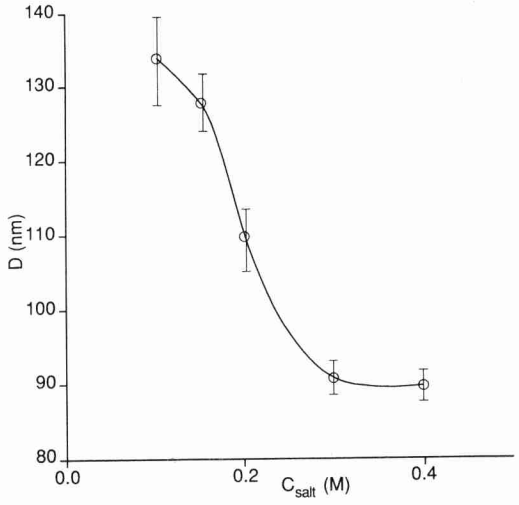

Fig.1. The interlamellar spacing D obtained from SAXS in the 4 phase systems as a function of the salt concentration C_{salt}.

TABLE 1. Water volume fraction in the lamellar phase as a function of the salt concentration in 4 phase systems.

Salt concentration (M)	water volume fraction
0.10	0.699
0.15	0.699
0.20	0.687
0.30	0.660
0.40	-

It is clear from fig.1 and Table 1 that upon increasing the salt concentration up to 0.3M the interlamellar spacing decreases and the oil/water ratio becomes less asymmetric. This variation in D cannot be explained by the variation of

the molecular area of SDS as a function of the salt concentration [12] or the hexanol concentration [13]. These results therefore provide direct evidence that at relatively high salt concentrations electrostatic repulsion still plays a role. Since the water spacings (75nm at 0.2M NaCl) are much larger than the Debye lengths (0.7 nm at 0.2M) in these systems the electrostatic repulsion appears to be strongly enhanced by thermal undulations.

Before presenting our results concerning the single phase lamellar systems we summarize some theoretical aspects of charged undulating membrane systems that are relevant for the work presented here. In a fluctuating membrane system thermal undulations tend to decrease the projected area while the total area A is conserved. The first order correction to the projected area $A_{proj.}$ of a membrane caused by thermal undulations is [14]

$$\frac{A}{A_{proj.}} = 1 + \frac{k_B T}{4\pi K} \ln\left[\frac{q_{max}}{q_{min}}\right] \qquad (1)$$

Where K denotes the bending elastic modulus. The upper and lower wavenumber cutoffs q_{max} and q_{min} that appear in the expression above are given by

$$q_{max}=2\pi/a \quad ; \; q_{min}=2\pi/\lambda \qquad (2)$$

in which a is a molecular lengthscale and λ the deflection length

$$\lambda=c'u(K/k_B T)^{1/2} \qquad (3)$$

where c' is a model dependent constant of order unity [14,15] and u is the root mean square of the amplitude of the undulations. If the interaction between the membranes is dominated by long range electrostatic repulsion the membranes are essentially flat. Then the interlamellar (oil plus water) spacing D varies according to the ideal dilution law

$$D/2= \frac{\delta}{\phi_s} \qquad (4)$$

where δ is the thickness of the surfactant layer and ϕ_s is the membrane volume fraction. On the other hand if the electric potential is screened by a large

salt concentration the membranes behave as if they are uncharged at interlamellar spacings larger than a certain (small) boundary layer thickness. In that case u is proportional to D and therfore the deflection length is directly proportional to D as well. This leads to a dilution law of the form [16,17]

$$D\phi_s/2 = A-B\ln(\phi_s) \tag{5}$$

in which

$$A= \delta\left(1 + \frac{k_B T}{4\pi K}\ln\left(\frac{c''\delta}{a}(K/k_B T)^{1/2}\right)\right) \tag{6}$$

and

$$B=\delta k_B T/4\pi K \tag{7}$$

where c" is a constant of order unity.

At intermediate salt concentration the situation is less simple. Here theories predict rather complicated relations between u, D and the Debije length $1/\kappa$ [7,8]. Furthermore, as already indicated, the Debije length being determined by the effective salt concentration is in turn a function of the amount of charged membranes in the system. Therefore it is imperative to know the effective salt concentration in order to unravel consequences of dilution (i.e. of varying D) and of varying salt concentration.

To calculate the effective salt concentration c as a function of the initial salt concentration c_{init} and the amount of (charged) surfactant in the system we use the relation

$$c=c_{init} - \Gamma_{co\text{-}ion}\frac{A}{V} \tag{8}$$

with A the total charged surface, V the volume of brine in the system and $\Gamma_{co\text{-}ion}$ the surface excess concentration of co-ions. Using Gouy-Chapman double layer theory one can show that for a 1:1 electrolyte [18]

$$\Gamma_{co\text{-}ion}=-2c\kappa^{-1}(p-q+1) \tag{9}$$

where κ is the inverse Debije length,

$$p= \frac{|\sigma|}{(8\varepsilon_0\varepsilon_r RTc)^{1/2}} \quad ; \quad q=(p^2+1)^{1/2} \tag{10}$$

in which σ is the surface charge density, F denotes Faraday's constant, $\varepsilon_0\varepsilon_r$ is the dielectric constant of the medium and R is the gas constant. The effective salt concentration can now be calculated iteratively from (8)-(10) using

$$\frac{A}{V}=c_s N_A \sigma_s \tag{11}$$

where c_s denotes the initial (molar) surfactant concentration in brine, N_A Avogadro's number, σ_s the surfactant molecular area and

$$\sigma=-F/(N_A\sigma_s) \tag{12}$$

Although σ_s is known to depend somewhat on the salt concentration, this dependence is neglegible in the concentration range studied here [12] and a constant SDS molecular area of $0.94nm^2$ was used [13]. We moreover introduced an essentially salt free volume equal to $A\delta_s$ with δ_s=0.2nm being the thickness of the Stern layer [19,20]. The effective salt concentration as a function of the SDS mass fraction in the system with an initial salt concentration of 0.2M is presented in fig.2. The limiting value $\Gamma_{co\text{-}ion}=-2c\kappa^{-1}$ corresponding to a very high charge density (eq.(9)) is also indicated in the figure. We measured the salt concentration in the excess water phase in systems where the lamellar phase coexists with excess brine and oil and a microemulsion phase (as in the previous section, but now with 0.2M NaCl and more SDS). The results are indicated by the points in fig.2. It seems that the experimentally determined salt concentration is systematically somewhat higher than the calculated concentrations which might be caused by curvature effects in the (coexisting) microemulsion phase [20]. However the experimentally observed trend can be regarded to be in good agreement with the calculated results.

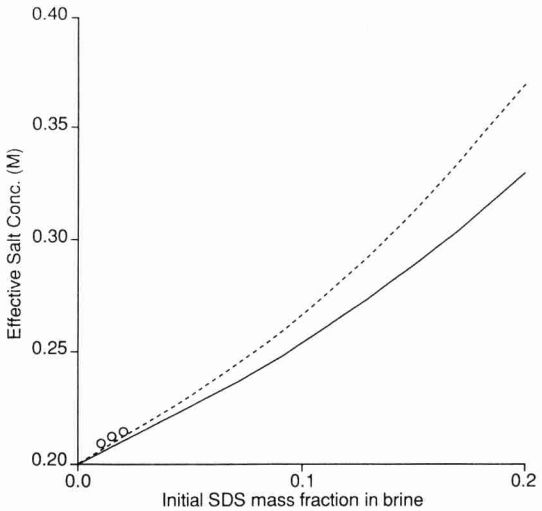

Fig.2. The effective salt concentration as a function of the initial mass fraction SDS in brine with an initial concentration of 0.20M. Surface charge density calculated according to eq.(12) (Solid line) and the upper bound corresponding to an infinite charge density (dashed line). A Stern layer thickness of 0.2nm was used. Points indicate experimental results (see text).

As long as $A\delta_s/V<<1$ the initial salt concentration necessary to obtain a constant effective salt concentration as a function of the charged area/volume ratio is easily shown to be given by eq.(8) with V replaced by $(V-A\delta_s)$

$$c_{init} = c + \Gamma_{co\text{-}ion} c_s N_A \sigma_s (1 + \delta_s c_s N_A \sigma_s) \qquad (13)$$

We studied two kinds of single phase lamellar systems. In the first system the initial salt concentration was constant and in the other one it was varied in such a way as to keep the effective salt concentration constant as a function of the SDS concentration. The systems studied consisted of equal volumes of brine and oil. The latter was a mixture of cyclohexane and pentanol. The initial mass fraction of pentanol in the oil phase varied from 0.16 to 0.20 and was chosen such that the spontaneous curvature of the surfactant film is about zero (i.e. the pentanol concentration corresponds to

a symmetrical position in between two demixing regions in the phase diagram).

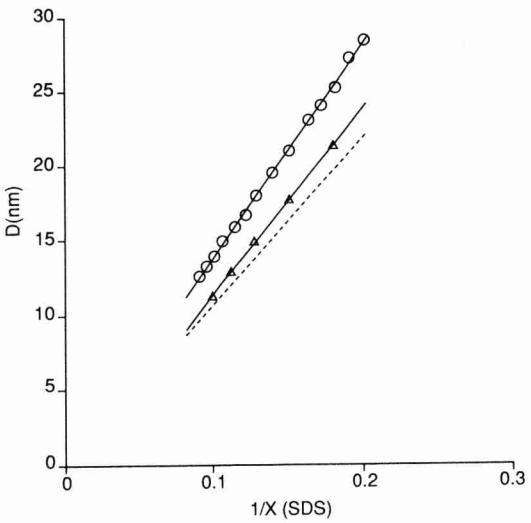

Fig.3. Bragg peak positions $D=2\pi/q_{max}$ versus 1/x(SDS) with x(SDS) the SDS weightfraction (in percent) in the lamellar phase. Single phase lamellar systems with constant initial salt concentration (circles) and constant effective salt concentration (triangles). The dashed line is calculated from the SDS molecular area obtained from interfacial tension measurements and application of the Gibbs adsorption equation [14].

In fig.3 the peak positions $D=2\pi/q_{max}$ as a function of the inverse surfactant weight fraction in the system is given for the systems with constant initial salt concentration (0.2M) and constant effective salt concentration (0.2M). The solid lines are linear best fit lines. Two features are apparent from fig.3. First from the slopes of the best fit lines the molecular areas of SDS can be calculated being $(0.73\pm0.01)nm^2$ for the system with constant initial salt concentration and $(0.84\pm0.02)nm^2$ for the system with constant effective salt concentration. The latter value is closer to the one obtained from interfacial tension measurements and applying the Gibbs adsorption equation being 0.94 nm^2 [13]. The line corresponding to this value is also given in fig.3. Second the systems with a constant effective salt concentration all have a lower interlamellar spacing compared to the ones with

a constant initial salt concentration at equal SDS concentrations. These features are first indications that electrostatic repulsion still plays a role in the system studied here as area is recovered (or the undulation amplitude is reduced i.e. the monolayers are 'flattened') upon decreasing the salt concentration.

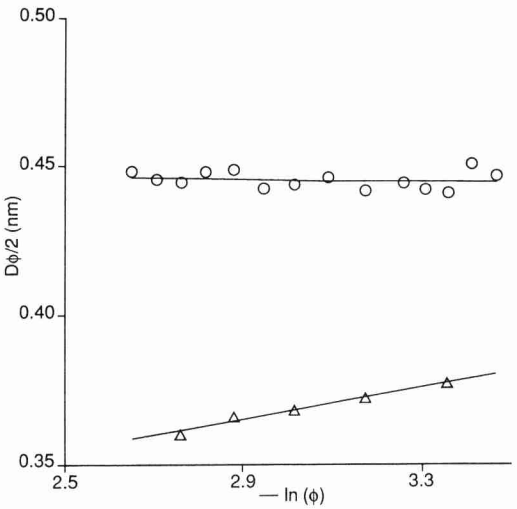

Fig.4. Data from Fig.3 plotted as $D\phi_s/2$ versus $-ln(\phi_s)$. Straight lines correspond to a best fit of the data to eq.5.

Plotting $D\phi_s/2$ versus $-\ln(\phi_s)$ (fig.4) it is apparent that the system with constant initial salt concentration very nearly follows the 'ideal dilution' law eq.(4) while the system with constant effective salt concentration has a noticable deviation from this ideal swelling and can be described by eq.(5) (B=0.026nm). Apparently, the interlamellar spacing in the system with a constant initial salt concentration has no measurable $\ln\phi_s$ dependence eventhough the amount of lost area is large. On the contrary, the interlamellar spacing in the system with constant effective salt concentration has a significant $\ln\phi_s$ dependence eventhough its lost area is smaller. This points to the important role of electrostatic repulsion and the confounding influence of salt partitioning. Upon diluting the interlamellar spacing D is increased which tends to increase the root mean square amplitude of the undulations u. This is clear from the results on the system with constant

effective salt concentration. In the system with constant initial salt concentration, this trend is apparently compensated by the concomitant change in the effective salt concentration having the opposite effect on u. This results in an apparent ideal dilution behaviour caused by two compensating effects. The undulation amplitude is however larger than in the system with constant effective salt concentration leading to a difference in projected area of about 15%.

A combination of the results concerning the multiphase lamellar systems together with the ones presented in fig.2 allow us to explain at least in part a feature of the lamellar phase as encountered in a previous study [21]. Here it was observed that the interlamellar spacing in a 4 phase system decreases upon increasing surfactant concentration from 110nm at 0.005 (w/w) SDS initial in brine down to 89nm at 0.015 (w/w) SDS. The initial salt concentration was kept constant at 0.20M. From fig.2 it is seen that the effective salt concentration is then increased from about 0.20M up to about 0.215M. Looking at fig.1 it follows that this difference in salt concentration explains a part of the observed difference in D but an unexplained difference still remains.

To conclude the experimental results presented provide strong evidence that electrostatic repulsion plays a significant role in both single- and multiphase lamellar monolayer systems even at salt concentrations up to 0.3M and interlamellar spacings of order 10 to 100 nm. In multiphase lamellar systems the electrostatic repulsion is manifested by an increasing interlamellar spacing upon decreasing the salt concentration. On the other hand in single phasic systems a decreasing salt concentration tends to 'flatten' the monolayers leading to a decreasing (mean) interlamellar spacing.

By compensating for the negative adsorption of salt it is shown that an apparent ideal behaviour of a lamellar system upon dilution is caused by two compensating effects on the undulation amplitude of the monolayers.

Acknowledgements. One of us (HL) thanks Theo Odijk for extensive discussions and correspondence on undulation enhanced electrostatic repulsion. The investigation was supported by the Netherlands Foundation of Chemical Research (SON) with financial aid from the Netherlands Organization for Scientific Research (NWO).

Literature

[1] Lipowski,R. and Leibler,S., Phys.Rev.Lett.**56**, 2541, (1986).

[2] Leibler,S. and Lipowski,R., Phys.Rev.Lett.**58**, 1796, (1987).

[3] Larche,F.C., Appell,J., Porte,G., Bassereau,P. and Marignan,J., Phys.Rev.Lett.**56**, 1700, (1986).

[4] Evans,E., Langmuir**7**, 1900, (1991).

[5] Evans,E.A. and Parsegian,V.A., Proc.Natl.Acad.Sci.U.S.A. **83**, 7132, (1986).

[6] Pincus,F., Joanny,J.F., and Andelman,D., Europhys. Lett. **11**, 763, (1990).

[7] Evans,E. and Ipsen,J., Electroch.Acta **36**, 1735, (1991).

[8] Odijk,T., Langmuir **8**, 1690, (1992).

[9] Loosely-Millman,M., Rand,R.P. and Parsegian,V.A., Biophys.J.**40**, 221, (1982).

[10] Odijk,T., submitted to Europhys.Lett.

[11] Dubois,M. and Zemb,T., Langmuir **7**, 1352, (1991).

[12] Verhoeckx,G.J., De Bruyn,P.L. and Overbeek,J.Th.G., J.Coll.Interface Sci.**119**, 409, (1986).

[13] Kegel,W.K., Aken,G.A. van, Bouts,M.N., Lekkerkerker,H.N.W., Overbeek,J.Th.G and de Bruyn,P.L. Langmuir **9**, 252, (1993); Chapter 2 of this thesis.

[14] Helfrich,W. and Servuss,R.M., Nuovo Cimento **3D**, 137, (1984).

[15] Golubovic,L. and Lubenski,T.C., Phys.Rev.B.**39**, 12110, (1989).

[16] Strey,R., Schomäcker,R., Roux,D., Nallet,F. and Olsson,U., J.Chem.Soc.Faraday Trans. **86**, 2253, (1990).

[17] Roux,D., Nallet,F., Freyssingeas,E., Porte,G., Bassereau,P., Skouri,M. and Marignan,J., Europhys.Lett. **17**, 575, (1992).

[18] Overbeek,J.Th.G., Prog.Biophysics and Biophysical Chem.**6**, 57, (1956).

[19] Biais,J., Barthe,M., Bourrel,M., Clin,B., and Lalanne,P., J.Colloid Interface Sci. **109**, 576, (1986).

[20] Aken,G.A. van, Overbeek,J.Th.G., De Bruyn,P.L. and Lekkerkerker,H.N.W., J.Colloid Interface Sci.**157**, 235 (1993).

[21] Kegel,W.K. and Lekkerkerker,H.N.W. Accepted for publication in J.Phys.Chem.; Chapter 5 of this thesis.

SUMMARY

This thesis reports a study of a microemulsion model system composed of the ionic surfactant SDS (Sodium Dodecyl Sulfate), the cosurfactant pentanol and/or hexanol, water, salt and cyclohexane. Depending on the concentrations of the constituent parts, this system may form microemulsion phases and liquid crystals. The investigation aims to understand this phase behaviour in terms of so-called phenomenological theories. These theories predict global phase behaviour and detailed properties of droplet type microemulsions as a function of physical properties of the surfactant(s) monolayer at the oil-water interface.

Chapter 2 and 3 deal with the mixed surfactant/cosurfactant monolayer at the planar cyclohexane - brine (water plus salt) interface. The adsorption densities of SDS and cosurfactant are obtained by measuring interfacial tensions and applying the Gibbs Adsorption Equation. This is described in Chapter 2. A thorough data analysis reveals that in the neighborhood of the critical micelle concentration the assumption of saturation adsorption is a good approximation. Replacing pentanol by hexanol does not lead to measurable differences of the molecular areas and of the surfactant/cosurfactant ratio in the mixed monolayer. From relatively low cosurfactant concentrations on, this ratio is moreover practically independent of the cosurfactant concentration. The bending elastic modulus was measured by Polarization Modulation Ellipsometry (Chapter 3). Although the uncertainty of the absolute values is large, it is shown that the bending elastic modulus of the mixed monolayer increases with order $0.1k_BT$ upon replacing pentanol by hexanol. The difference is explained qualitatively by an increased (integrated) lateral pressure at the chain side of the monolayer.

In Chapter 4 a study of Winsor II systems (water in oil microemulsions coexisting with excess water) is presented. A simplified version of the theory of Overbeek et al. [1] is combined with the expression of the curvature free energy given by Helfrich [2] leading to explicit expressions of the volume fraction dependence of the droplet size and the interfacial tension of the planar interface between the coexisting phases. These expressions describe experimental observations rather well. The size distribution of the droplets was calculated [3] from the bending elastic parameters obtained from the volume fraction dependence of the droplet radius. This size distribution is in good agreement with droplet radii obtained by two different techniques (water

titration and Small Angle X-ray Scattering), measuring effectively different moments of the size distribution. Combining some results with those of Chapter 3 reveals that the Gaussian bending elastic modulus of the droplet interface decreases with order $0.1k_BT$ upon replacing pentanol by hexanol.

From the previous chapters it appears that interchanging pentanol and hexanol as cosurfactants does not give rise to dramatic differences of the monolayer properties and of the behaviour of Winsor II microemulsions. A rather different picture arises from a study of the global phase behaviour (Chapter 5). In the case of pentanol, at low surfactant concentrations and increasing alcohol concentration, the well known progression of phase equilibria Winsor I (oil in water microemulsion coexisting with excess oil) - Winsor III (middle phase microemulsion in equilibrium with excess water and oil) - Winsor II is observed. The use of hexanol however leads to the sequence Winsor I - Winsor III - 4 phase equilibrium water, lamellar phase, microemulsion phase, oil - Winsor III - Winsor II. By using mixtures of different ratios of pentanol and hexanol as cosurfactant it is shown that this behaviour can be understood in terms of a competition between a (disordered) microemulsion and a lamellar liquid crystal: increasing the hexanol fraction in the cosurfactant mixture reduces the surfactant concentration at which the (first order) phase transition microemulsion - lamellar occurs. This trend culminates in a region of 4 phase coexistence. By performing a lengthscale analysis of the microemulsion phases this behaviour is compared with a phenomenological theory [4]. It appears that the theory qualitatively correctly describes the competition between the microemulsion and the lamellar phase. However a quantitative understanding requires not only to consider changes in the bending elastic modulus K but to include also variations of the Gaussian bending elastic modulus $\bar{K}$. In that case the free energy of the microemulsion (in the most simple case) contains a term proportional to $(2K-\bar{K})$. This might explain the enormous influence of the cosurfactant chainlength upon the lamellar- microemulsion competition. As shown before, K increases and $\bar{K}$ decreases with order $0.1k_BT$ upon replacing pentanol by hexanol. The volume fraction dependence of the droplet radius in Winsor II systems, on the other hand, depends upon the linear combinations $(2K+\bar{K})$ and $2K/R_0$ (R_0 being the spontaneous radius of curvature of the interface). The variation of these combinations apparently is too small to give rise to dramatic differences.

In Chapter 6 a SAXS (Small Angle X-ray Scattering) study of lamellar

systems is presented. From the interlamellar spacings as a function of the surfactant concentration and of the salt concentration it is concluded that electrostatic interactions up to large interlamellar spacings (order 10-100nm) and high salt concentrations (0.3M) still play a role. This effect is attributed to a coupling of classical electrostatic interactions with monolayer undulations.

References

[1] Overbeek,J.Th.G., Verhoeckx,G.J., De Bruyn,P,L., and Lekkerkerker,H.N.W., J.Colloid Interface Sci. **119**, 422, (1987).

[2] Helfrich,W., Z.Naturforsch.**28c**, 693, (1973).

[3] Overbeek,J.Th.G., Progr.Colloid Polym.Sci. **83**, 1, (1990).

[4] Andelman,D., Cates,M.E., Roux,D. and Safran,S.A., J.Chem.Phys. **87**, 7229, (1987).

SAMENVATTING

In dit proefschrift is een onderzoek beschreven aan een model mikro-emulsie systeem bestaande uit de oppervlakte aktieve stoffen SDS (Natrium Dodecyl Sulfaat) en de alkohol(en) pentanol en/of hexanol, water, zout en cyklohexaan. Dit systeem vormt, afhankelijk van de konsentraties van de samenstellende delen, mikro-emulsie fasen en vloeibare kristallen. Het onderzoek is gestart met als doel dit fasegedrag te begrijpen in termen van zgn. fenomenologische theorieën. Deze theorieën voorspellen het globale fasegedrag en gedetailleerde eigenschappen van mikro-emulsies met een druppelstruktuur als funktie van fysische eigenschappen van de monolaag van oppervlakte aktieve stof(fen) aan het olie-water grensvlak.

Hoofdstuk 2 en 3 gaan over de gemengde SDS/alkohol monolaag aan het vlakke cyklohexaan- water (met zout) grensvlak. De adsorptie dichtheden van SDS en alkohol zijn verkregen uit grensvlakspannings metingen gebruikmakend van de Gibbs adsorptie vergelijking. Dit is beschreven in Hoofdstuk 2. Uit een grondige data analyse volgt dat in de buurt van de kritische micel konsentratie het grensvlak in goede benadering als verzadigd mag worden beschouwd. Vervanging van pentanol door hexanol heeft geen (meetbare) invloed op de molekulaire oppervlakken en ook niet op de verhouding SDS/alkohol in de gemengde monolaag. Vanaf relatief lage alkohol konsentraties blijkt deze verhouding bovendien praktisch onafhankelijk te zijn van de alkohol konsentratie. De buigingselasticiteits modulus van de gemengde monolaag is gemeten met behulp van polarisatie modulatie ellipsometrie (Hoofdstuk 3). Hoewel de onzekerheid in de absolute waarden groot is blijkt dat de buigings elasticiteits modulus met orde $0.1k_BT$ toeneemt wanneer pentanol wordt vervangen door hexanol. Het verschil kan kwalitatief worden verklaard door een toegenomen (geintegreerde) laterale druk aan de ketenzijde van de gemengde monolaag.

In Hoofdstuk 4 is een studie beschreven aan Winsor II systemen. Dit zijn water in olie mikro-emulsies in evenwicht met een waterfase. Kombinatie van een vereenvoudigde theorie van Overbeek en medewerkers [1] met de uitdrukking voor de buigings vrije energie gegeven door Helfrich [2] levert expliciete uitdrukkingen voor de volume fraktie afhankelijkheid van de druppelstraal en de grensvlakspanning van het vlakke grensvlak tussen de koëxisterende fasen. Deze uitdrukkingen geven een goede beschrijving van de experimentele resultaten. Uit de buigingselasticiteits parameters verkregen uit de volume

fraktie afhankelijkheid van de druppelstraal is de deeltjesgrootte verdeling berekend [3]. De deeltjesgrootte verdeling is in goede overeenstemming met druppelstralen die zijn verkregen met behulp van twee verschillende technieken (water titratie en kleine hoek Röntgen verstrooiing). Deze technieken meten effektief verschillende momenten van de deeltjesgrootte verdeling. Een kombinatie van de resultaten met die beschreven in Hoofdstuk 3 levert dat de Gaussische buigingselasticiteits modulus van het druppelgrensvlak met orde $0.1k_BT$ afneemt wanneer van pentanol wordt vervangen door hexanol.

Uit de voorgaande hoofdstukken blijkt dat vervanging van pentanol door hexanol slechts aanleiding geeft tot marginale verschillen in de eigenschappen van de monolaag en het gedrag van Winsor II mikro-emulsies. Een studie van het globale fasegedrag (Hoofdstuk 5) geeft een geheel ander beeld. In geval van pentanol is bij lage SDS konsentraties als funktie van de alkohol konsentratie het 'klassieke' verloop Winsor I (olie in water mikro-emulsie in evenwicht met olie) - Winsor III (een bikontinue mikro-emulsie in evenwicht met olie en water) - Winsor II gevonden. Vervanging door hexanol geeft Winsor I - Winsor III - 4 fasen evenwicht water, lamellaire fase, mikro-emulsie, olie - Winsor III - Winsor II. Door systemen met verschillende verhoudingen pentanol en hexanol te onderzoeken is aangetoond dat dit gedrag begrepen kan worden in termen van een kompetitie tussen een (wanordelijke) mikro-emulsie fase en een lamellaire vloeibaar kristallijne fase. Toename van de relatieve hoeveelheid hexanol in het systeem drijft de (eerste orde) fase overgang mikro-emulsie-lamellair naar steeds lagere SDS konsentraties. Deze trend kulmineert in een 4 fasen evenwicht. Met behulp van een lengteschaal analyse van de mikro-emulsie fasen is dit gedrag vergeleken met de voorspellingen van een fenomenologische theorie [4]. Het blijkt dat het experimenteel gevonden gedrag kwalitatief goed beschreven wordt door deze theorie. Echter voor een kwantitatief begrip is het noodzakelijk niet alleen de buigingselasticiteits modulus K te beschouwen maar bovendien variaties in de Gaussische buigingselasticiteits modulus $\bar{K}$ mee te nemen. Het resultaat is dat de vrije energie van de mikro-emulsie (in het eenvoudigste geval) een term bevat die evenredig is met $(2K-\bar{K})$. Dit is waarschijnlijk de reden dat de mikro-emulsie- lamellair kompetitie zo gevoelig is voor de alkohol ketenlengte: K neemt toe en $\bar{K}$ neemt af met orde $0.1k_BT$ bij vervanging van pentanol door hexanol. De volumefraktie afhankelijkheid van de druppelstraal in Winsor II systemen is een funktie van de lineaire kombinaties $(2K+\bar{K})$ en $2K/R_0$ (met R_0 de spontane kromtestraal van het grensvlak). Deze kombinaties varieren blijkbaar onvoldoende om aanleiding te geven tot

dramatische verschillen.

In Hoofdstuk 6 is een SAXS (Small Angle X-ray Scattering of Kleine Hoek Röntgen Verstrooiing) studie gepresenteerd aan lamellaire systemen. Op grond van de interlamel afstand als funktie van de SDS konsentratie en van de zout konsentratie is gekonkludeerd dat elektrostatische interakties tot op grote lamelafstanden (orde 10-100nm) en hoge zoutkonsentraties (tot 0.3M) nog steeds een rol spelen. Dit effekt is toegeschreven aan een koppeling van klassieke elektrostatische interakties aan fluktuaties rond de gemiddelde posities van de monolagen.

Referenties

[1] Overbeek,J.Th.G., Verhoeckx,G.J., De Bruyn,P,L., and Lekkerkerker,H.N.W., J.Colloid Interface Sci. **119**, 422, (1987).

[2] Helfrich,W., Z.Naturforsch.**28c**, 693, (1973).

[3] Overbeek,J.Th.G., Progr.Colloid Polym.Sci. **83**, 1, (1990).

[4] Andelman,D., Cates,M.E., Roux,D. and Safran,S.A., J.Chem.Phys. **87**, 7229, (1987).

CURRICULUM VITAE

De schrijver van dit proefschrift werd geboren op 17 januari 1961 te Hilversum. In 1978 behaalde hij het diploma MAVO IV en begon een MBO laboratorium opleiding aan het Van't Hoff Instituut te Rotterdam. In 1980 stapte hij over op de HBO opleiding aan hetzelfde instituut. De stage periode werd doorgebracht bij de vakgroep Biochemie van de Technische Universiteit Delft en het diploma HBO-B werd behaald in 1983. Vervolgens was hij van 1983 tot 1985 werkzaam als docent aan het opleidings instituut voor dokters assistenten 'Leni Mooldijk' te Rotterdam en van 1984 tot 1986 als research analist bij de vakgroep Molekulaire Plantkunde aan de Rijksuniversiteit Leiden. In 1985 werd begonnen aan de deeltijd studie scheikunde aan de Universiteit Utrecht. In 1986 werd de propedeuse behaald en volgde inschrijving als voltijdstudent. Het doktoraal examen werd afgelegd in 1989 met als hoofdvak Chemische Thermodynamika en keuzevakken Anorganische Chemie en Fysische Chemie. Tijdens zijn studie was hij enige tijd werkzaam als student assistent en tussen 1988 en 1992 was hij vrijwilliger bij de Chemie Winkel Utrecht. Sinds november 1989 is hij werkzaam bij de vakgroep Fysische en Colloïdchemie (Van't Hoff laboratorium). Het promotie onderzoek werd verricht in dienst van de Nederlandse organisatie voor Wetenschappelijk Onderzoek (NWO). Resultaten van het onderzoek zijn gepresenteerd op konferenties in Compiègne (juli 1991), Lund (juli 1992) en York (september 1993). Op 1 maart 1994 treedt hij als 'postdoctoral fellow' in dienst van de University of California, Los Angeles.

NAWOORD

In dit waarschijnlijk een van de meest gelezen onderdelen wil ik een aantal mensen noemen die tijdens het bewerken van dit proefschrift een belangrijke rol hebben gespeeld.

Allereerst mijn promotor Henk Lekkerkerker van wie ik heb geleerd immer aan uitgangspunten te twijfelen, vooral als ze vanzelfsprekend schijnen. Ik bewaar zeer goede herinneringen aan onze diskussies. In dit verband dank ik ook Theo Overbeek die regelmatig de moeite heeft genomen zijn werk te verhelderen en het mijne van opbouwende kritiek te voorzien. George van Aken heeft mij begeleid op mijn eerste wankele schreden op dit vakgebied en hem dank ik voor de handige experimentele trukjes die hij mij heeft geleerd. Met Ger Koper (RU Leiden) verbaas ik mij nog steeds dat een varkensdoder SDS-kosurfaktant mikroemulsies doet fasenscheiden. Ik heb veel plezier beleefd aan onze diskussies over de thermodynamika van druppeltjes.

De studenten (in volgorde van binnenkomst) Marcel Bouts, Patrick van der Hofstad, Agnes Peels en Igor Bodnàr hebben ieder op een eigen manier een bijdrage geleverd aan het onderzoek en de sfeer op het van't Hoff lab.

I am grateful to Jacques Meunier and Hamid Kellay for teaching me the art of ellipsometry during my visit at the Ecole Normale Supérieure, Paris, and to Bob Aveyard for his kind permission to perform Spinning Drop measurements at the University of Hull.

Veel leden van het technisch personeel waren behulpzaam bij het blootstellen van mijn monsters aan diverse vormen van fysisch geweld. Ik dank Gerard Harder en Marco van Amerongen voor het op indrukwekkende wijze bouwen van de eerste vertikale Polarisatie Modulatie Ellipsometer van de Benelux en Carel van der Werf voor het uitvoeren van de komputer interfacing. Bonny Kuipers dank ik voor zijn hulp met de Röntgen verstrooiings apparatuur en het oplossen van een aantal elektronische problemen, Jacques Suurmond voor het uitvoeren van Spinning Drop metingen, Igno Dur voor het vervaardigen van glaswerk en Ed Vlietstra (Vg.Fysisch-Organische Chemie) voor zijn hulp bij polarisatie mikroskopie.

Een groot aantal figuren in dit proefschrift, inklusief dat op de voorkant, zijn het resultaat van de kreatieve inspanningen van Jan den Boesterd, Ingrid van Rooyen en M.Tollenaar.

Leuke kamergenoten zijn de krenten in de wetenschappelijke pap. De aktiviteiten op het Ministry of Silly Jumps varieerden van verbale

geweldpleging tot serieuze studie van de statistische fysika.

Tenslotte dank ik mijn vrienden, en in het bijzonder mijn levensgezellin Marianne, die zonder daar altijd expliciet op te wijzen mij doen beseffen dat er op deze wereld nog veel meer te beleven is dan fysische chemie.